Ultrasonic Guided Wave Propagation in Pipes Coated with Viscoelastic Materials

A thesis submitted for the degree of

Doctor of Philosophy

by

Zahari Zlatev

School of Engineering and Design

Brunel University

September 2014

Abstract

This work studies guided wave propagation in pipes coated with thick highly viscoelastic coating materials. The main motivation for this study is the problems associated with Long Range Ultrasonic Testing (LRUT) of coated pipelines. The results reported in the literature show that the proper determination of the optimum LRUT parameters depends strongly on the bulk acoustic properties of the coating materials. The bulk acoustic properties of coating materials reported in the literature show that they could vary significantly depending on the coating material age, temperature and bonding level. The methods for acoustic characterisation of coating materials reported by other researchers, have been studied and it was found that they do not take into account the temperature changes and bonding level variation.

In this work, the bulk acoustic properties of two highly viscoelastic bitumen based coating materials are investigated. The conventional methods for acoustic characterisation are studied and a new method for independent measurement of bulk shear properties of bitumen is developed. The bulk acoustic properties of bitumen based coating materials are also studied by two new characterisation methods. The first method derives the bulk coating material properties from experimental data on guided wave reflection coefficients. The second method derives the coating material bulk properties from experimentally measured guided wave attenuation data. It is demonstrated that these new methods deliver much more accurate values for the bulk acoustic properties when compared to the data measured by conventional methods. The second method is used to study the temperature effect on the bulk acoustic properties and it is demonstrated that temperature has a significant effect. The validity of the acoustic properties for the two bitumen materials is investigated through comparison between numerical predictions and experimental data measured for guided wave reflection coefficients and attenuation of the torsional T(0,1) and longitudinal L(0,2) guided wave modes. Good agreement is achieved in the frequency range between 20 kHz and 100 kHz, which is typical for LRUT of pipes.

Acknowledgments

I would like to express my gratitude to Dr. R. Kirby and Prof. P. Mudge for their supervision, guidance and professionalism. This also extends to all staff members in TWI Ltd and Brunel University, for their kind support.

I would like to thank my family and friends for their encouragement and constant support.

For the project funding, I would like to thank TWI Ltd., without whom the research reported here would not have been possible.

Contents

List of Figures

List of Tables

Nomenclature

A	signal amplitude
A_s	bulk shear attenuation
$A_{(w)}$	frequency dependent attenuation
A_{gw}	guided wave attenuation
$A_{n,m}$	guided wave mode
Att_n	attenuation between two points
Att_f	average attenuation
a_1, a_2	pipe diameter
$\tilde{a}_c$	bulk longitudinal speed of the coating material
b_1, b_2	coating material diameter
C_L	longitudinal acoustic speed
C_S	shear acoustic speed
$C_{L,S}$	bulk acoustic speed
$C_{aL,S}$	bulk acoustic speed, real part
C_{gw}	guided wave phase speed
$\tilde{c}_c$	bulk shear speed of the coating material
D_{1-n}	distance between points
e	Euler's number
$\vec{e}$	unit vector
f	frequency
G	shear modulus of elasticity
h	coating material thickness
I	incident wave
$Im\{\}$	imaginary part of the quantity

i	$\sqrt{-1}$
$K_{(\omega)}$	transfer function
k	wave number
L_n	defect length
N	number of points
$\vec{n}$	displacement vector
n, m	mode order
p	direction
$\vec{p}$	propagation vector
R	reflected wave
$Re\{\}$	real part of the quantity
$r_{(s,c)}$	coated pipe geometry
r, θ, z	cylindrical coordinate system
T	transmitted wave
t	time
$\boldsymbol{u}$	displacement vector
$\overrightarrow{u}$	polarization vector
U_{R1}	reflected pulse amplitude
U_{T3}	transmitted pulse amplitude
α_c	bulk shear attenuation constant
α_L	bulk longitudinal constant
$\alpha_{L,S}$	bulk acoustic attenuation constant
λ	Lame's constant
μ	Lame's constant
ρ	density
ω	angular frequency
Λ	reflection coefficient

Chapter 1

Introduction

Pipeline transport plays an important role in many industries. For example the pipeline network used for natural gas transportation in USA alone consists of more than three hundred thousand miles of pipes [1]. However, most pipelines have been in use for many years and the formation and growth of defects caused by metal corrosion and erosion can lead to pipes fracturing [2]. Damage of pipelines is an ongoing problem requiring inspection and subsequent maintenance decisions to ensure safe and reliable performance. Most conventional non-destructive testing (NDT) methods are suitable only for local inspection and their application for inspecting long lengths of pipes is not time and cost effective [3]. Long Range Ultrasonic Testing (LRUT) [4] is an NDT technique employing ultrasonic mechanical waves guided by the boundaries of the pipe (guided waves) in a way that allows many meters of the pipeline to be inspected for defects from a single test position [3-9]. LRUT also offers full volumetric coverage and has the potential to decrease maintenance costs and inspection time [9-12]. However, the presence of relatively thick viscoelastic bitumen coatings can severely reduce the LRUT inspection range or even make LRUT impossible [13-16]. This thesis investigates the influence of viscoelastic coating materials and their acoustic properties on the ability of LRUT technology to detect defects in coated pipes. The bulk properties of two types of bitumen based coating materials are investigated by novel acoustic characterisation methods and it is also demonstrated that the acoustic properties of these coating materials are strongly temperature dependent.

1.1 Aims and Objectives

The main scope of this thesis is to investigate methods for studying guided wave attenuation and reflection coefficients from defects in pipes coated with viscoelastic materials and to develop new methods capable of determining the bulk acoustic properties of an unknown viscoelastic material over a range of different temperatures. The objectives of this work are:

- To develop new methods for the determination of the bulk shear properties of a bitumen based material used to coat pipes over the frequency range 20 kHz to 100 kHz.
- To obtain new data on the bulk acoustic properties of bitumen used for pipeline corrosion protection.
- To develop new methods to determine the bulk acoustic properties of viscoelastic materials at different temperatures.
- To generate new data for the bulk acoustic properties of coating materials at different temperatures and to use them in a theoretical model.
- To compare measured data against predictions generated by theoretical methods for the attenuation and reflection of guided waves.
- To obtain coating material properties suitable for future theoretical investigations into the scattering of elastic waves from defects in coated pipelines.

The development of methods for measuring and/or predicting the attenuation and reflection coefficients for guided waves scattered by defects in coated pipes is of great practical interest. This is mostly because such methods would allow predicting which mode at which frequency will ensure the maximum test range in a specific coated pipe with respect to the defect of interest. It was mentioned before that some of the problems associated with LRUT of coated pipes have been investigated by other researchers. Unfortunately the ratio between the methods for studying coated pipes reported in the literature and those which could be used on-site is relatively low. The motivation for this work is to go beyond the

current knowledge on methods for studying coated pipes by investigating and suggesting new and better methods. Therefore, even though the current study is focused on guided wave propagation and reflection coefficients in bitumen coated pipes, the findings described in this work are applicable in many other areas associated with the characterisation of the dynamic behaviour of viscoelastic materials, including guided wave propagation in waveguides with attenuation, and guided wave interaction with defects.

1.2 Thesis outline

The thesis is divided into seven chapters:

Chapter 2 provides a general overview of the theory of bulk waves that forms the basis of the following section on guided waves and their application in LRUT. Chapter 2 also reviews the theoretical and experimental methods on viscoelastic wave propagation and associated problems reported in the literature

Chapter 3 deals with experimental methods for the independent measurement of the bulk acoustic properties of coating materials and also presents a new method for the experimental measurement of the bulk shear properties of viscoelastic bitumen.

Guided wave attenuation in coated pipes is studied in Chapter 4 by a new method which does not rely on measuring a reflected signal and which can measure guided wave attenuation in a continuous coated pipe. The method is also used for studying guided wave attenuation in coated pipes at specific temperatures.

Chapter 5 presents a novel method for the acoustic characterisation of a viscoelastic coating material. The method derives the coating material properties by comparing prediction with experimental data for the reflection coefficient from a discontinuity with known geometry located in a coated pipe.

Chapter 6 deals with the practical application of the findings reported in the previous chapters. It shows that the bulk acoustic properties for a bitumen coating material measured by the independent methods investigated in Chapter 2 do not give good correlation for those measurements reported in Chapter 4. The chapter then presents a new method to

determine the bulk acoustic properties from measured guided wave attenuation data. The method is used to study the temperature dependence of the bulk acoustic properties of bitumen and good agreement is achieved between numerical predictions based on the values provided by the new method, and experimental data on attenuation at specific temperatures for torsional T(0,1) and longitudinal L(0,2) guided wave modes.

Chapter 7 summarises the main conclusions of the thesis and discusses potential future applications.

Chapter 2

Literature review

The main scope of this chapter is to provide a background to the following chapters and to investigate the current knowledge on theoretical and experimental methods allowing determination of guided wave characteristics in pipes coated with viscoelastic materials. The chapter starts with conventional bulk wave theory and this forms the basis of the following sections on guided waves and their application in LRUT. The last two sections provide a review of the theoretical and experimental methods on guided wave propagation in coated pipe and associated problems reported in the literature. The literature review also deals with methods for the characterisation of the bulk acoustic properties of coating materials as these are needed as input parameters for theoretical models.

2.1 Ultrasonic bulk waves

Bulk stress waves are mechanical waves propagating through a medium. When used in NDT they are quite frequently referred as ultrasonic waves. This is because their frequency is above the human audible range, which is typically above 20 kHz. Following [17, 18] the bulk wave speed c in m/s, wavelength λ in m and frequency f in Hz are related by

$$c = \lambda f. \tag{2.1}$$

Bulk waves exist in unbounded media or in materials where the boundaries do not affect wave propagation and their acoustic properties depend on the bulk mechanical properties of the medium [17, 18, 19]. Depending on how the material's particles move with respect to the bulk wave propagation vector $\vec{p}$, three types of bulk waves are possible. These are associated with the direction, d, of the three particle displacement vectors $\vec{u}^{(d)}$ ($d = 1,2,3$). These can be referred to as having different polarizations. Pure modes can be defined in different ways, and Auld defines them in [18] as modes where either $\overrightarrow{u} \parallel \vec{p}$ or $\overrightarrow{u} \perp \vec{p}$. Where, $\overrightarrow{u} \parallel \vec{p}$ we say that the mode is longitudinal, and where $\overrightarrow{u} \perp \vec{p}$ we can say

that the mode is shear as shown in Figure 2.1. Following [20], when a bulk wave propagates in a linear, viscoelastic and unbounded medium, the particles displacement $\boldsymbol{u}$ are described by Navier's equation [18]

$$\mu(i\omega)\nabla^2\boldsymbol{u} + \big(\lambda(i\omega) + \mu(i\omega)\big)\nabla(\nabla.\boldsymbol{u}) = \rho\frac{\partial^2\boldsymbol{u}}{\partial t^2}, \tag{2.2}$$

where $\lambda(i\omega)$ and $\mu(i\omega)$ are the complex frequency dependent Lamé constants and ρ is the density of the medium.

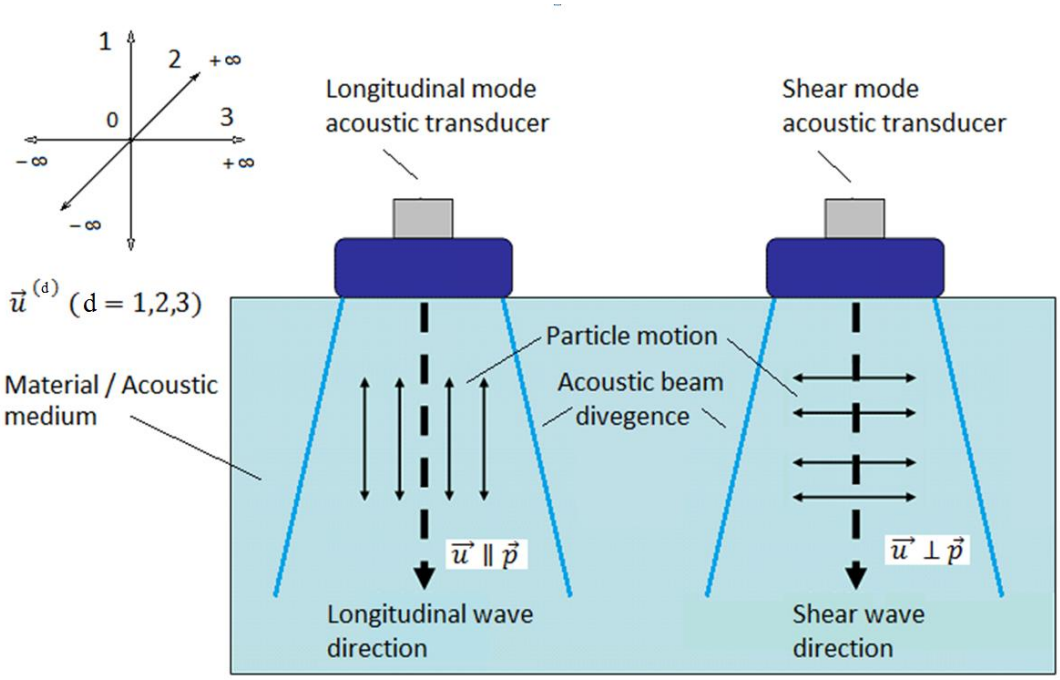

Figure 2.1: Longitudinal and shear bulk wave.

Accordingly, the velocities of the bulk wave depend on the bulk mechanical properties of the viscoelastic medium and these are described by:

$$C_L(i\omega) = \sqrt{\frac{\lambda+2\mu-i(\lambda'+2\mu')}{\rho}}, \tag{2.3}$$

$$C_S(i\omega) = \sqrt{\frac{\mu-i(\mu')}{\rho}}. \tag{2.4}$$

Following [20], the terms C_L and C_S are the wave velocities of the longitudinal and shear bulk waves respectively. They are specified as complex and frequency dependent $(i\omega)$ in the case of a viscoelastic material. The terms λ and λ' are the real and imaginary parts of the first Lamé constant, and μ and μ' are the real and imaginary parts of the second Lamé constant. The Lamé constants are material properties that are related to the elastic modulus and Poisson ratio [21]. The second Lamé constant is identical to the shear modulus of elasticity G. The term ρ is the density of the media. The constants C_L and C_S are real and exactly equal to the bulk velocities of longitudinal and shear waves respectively if the media is perfectly elastic and the damping parameters [primed terms in Eqs. (2.3) and (2.4)] are zero, [20,21]. In reality materials are not perfectly elastic and bulk wave amplitude attenuates with distance. Following [20-23], in case of attenuating waves the longitudinal and shear acoustic speed are complex and frequency dependent and are given as

$$C_{L,S}(i\omega) = \left[\frac{1}{C_{aL,S}(\omega)} + i\frac{\alpha_{L,S(\omega)}}{\omega}\right]^{-1}, \tag{2.5}$$

where $C_{aL,S}$ represents the bulk acoustic speed in meters per second (the rate at which the stress propagates through the medium, which is always real) and $\alpha_{L,S(\omega)}$ is the attenuation in Nepers per meter, such that a wave of unit amplitude is reduced to an amplitude of $e^{-\alpha}$ after traveling one meter.

Following [20-23], the acoustic velocity $C_{a\,L,S}$ and attenuation constant $\alpha_{L,S(\omega)}$ can be defined from the complex wave velocity $C_{L,S}(i\omega)$ by

$$C_{aL,S}(\omega) = \left[Re\left(\frac{1}{C_{L,S}(i\omega)}\right)\right]^{-1}, \tag{2.6}$$

$$\alpha_{\,L,S}(\omega) = \omega Im\left[\frac{1}{C_{L,S}(i\omega)}\right]^{-1}. \tag{2.7}$$

2.2 Ultrasonic guided waves

In contrast to the bulk waves, guided waves refer to mechanical waves guided by a surrounding medium such as pipe, plate, rod or rail [17, 18, 24]. The wave is termed "guided" because it travels along the bounded medium guided by its geometric boundaries. Since the wave is guided by the geometric boundaries of the medium, the geometry has a strong influence on the wave propagation characteristics. In contrast to the longitudinal and shear ultrasonic bulk waves, where acoustic speed and attenuation depends on the bulk mechanical properties of the medium, the guided wave phase speed and attenuation can vary significantly with frequency, as well as the waveguide geometry. In addition, at a given frequency, guided waves propagate in different wave modes and orders [17-19].

Following [25], a guided wave propagating in the positive z (axial) direction along cylindrical waveguide can be assumed time harmonic and described as

$$\vec{u}(r,\theta,z;t) = \vec{u}(r)e^{in\theta}e^{i(\omega t - kz)}. \tag{2.8}$$

Where $\vec{u} = u_r\vec{e}_r + u_\theta\vec{e}_\theta + u_z\vec{e}_z$ is the displacement vector in cylindrical coordinates $(r,\theta,z,)$, and $\vec{e}_r, \vec{e}_\theta, \vec{e}_z$ are the unit vectors associated with each direction; ω is the angular frequency and k is the wavenumber. The circumferential order n is an integer that describes the symmetry of the waveform around the z axis. Depending on the circumferential order n and type of displacement the guided wave modes are divided into several types, as shown in Figure 2.2. When $n = 0$, the guided wave modes are referred as axisymmetric and they have identical displacement vectors around the circumference. When $n > 0$ the guided wave modes are referred as non-axisymmetric and the amplitude of the displacement vector varies around the circumference. The axisymmetric guided wave modes can be decoupled in two families: torsional $\mathrm{T}(0,\mathrm{m})$, and longitudinal, $\mathrm{L}(0,\mathrm{m})$. The torsional modes have only circumferential displacement, u_θ, whereas the longitudinal modes have both axial u_z and radial u_r displacements. The modes without axial symmetry, $n \geq 1$, are termed flexural modes $\mathrm{F}(\mathrm{n},\mathrm{m})$ and these have displacements in all three directions u_θ, u_r and u_z, as shown in Figure 2.2.

The torsional and longitudinal guided wave modes with order $n = 0$ have displacements similar to guided wave modes in plates [14]. For example the T(0,1) mode in pipes is analogous to the shear horizontal mode SH_0 in plates because both modes display shear motion when they propagate. Both L(0,1) and L(0,2) have displacements parallel and normal to the pipe surface, with displacements in the axial u_z, and radial, u_r direction, respectively. The difference between these two modes is in their dominant displacement: L(0,1) has greater displacement normal to the pipe surface and it is analogues to A_0 mode in plates. L(0,2) mode has greater displacement parallel to the pipe surface and it is analogous to the S_0 mode in plates.

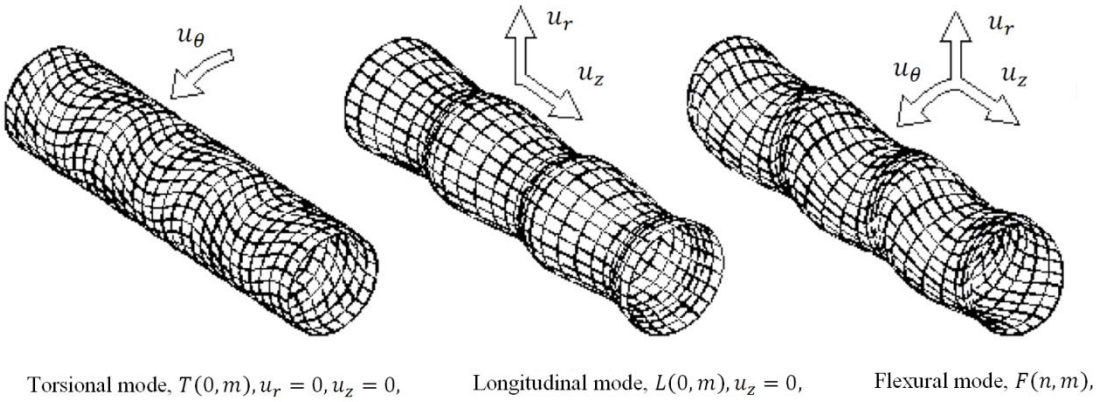

Figure 2.2: Guided wave modes in a cylindrical waveguide, [25].

If we assume that the waveguide's material is perfectly elastic, following Eq. (2.8) the guided wave mode will propagate in the z direction without decreasing in amplitude. In reality materials are not perfectly elastic and they exhibit a certain level of viscoelasticity [26, 27]. When the waveguide is made of a viscoelastic material part of the energy carried by the guided wave mode is absorbed by the material and its amplitude decays with distance. If the material is viscoelastic then the wavenumber k becomes complex and the real part of the wavenumber provides information about the guided wave phase speed, and the imaginary part of the wavenumber provides information on the attenuation. Following [25], the guided wave phase speed is described as

$$C_{ph} = \frac{\omega}{\mathrm{Re}(k)}. \tag{2.9}$$

The phase speed is frequency dependent except for the fundamental torsional mode T(0,1). Figure 2.3 shows the phase speeds for a pipe made of stainless steel with outside diameter of 56 mm and wall thickness of 3 mm [28]. This figure shows the guided wave speed at a particular frequency and it is applicable when a continuous wave at a single frequency is excited.

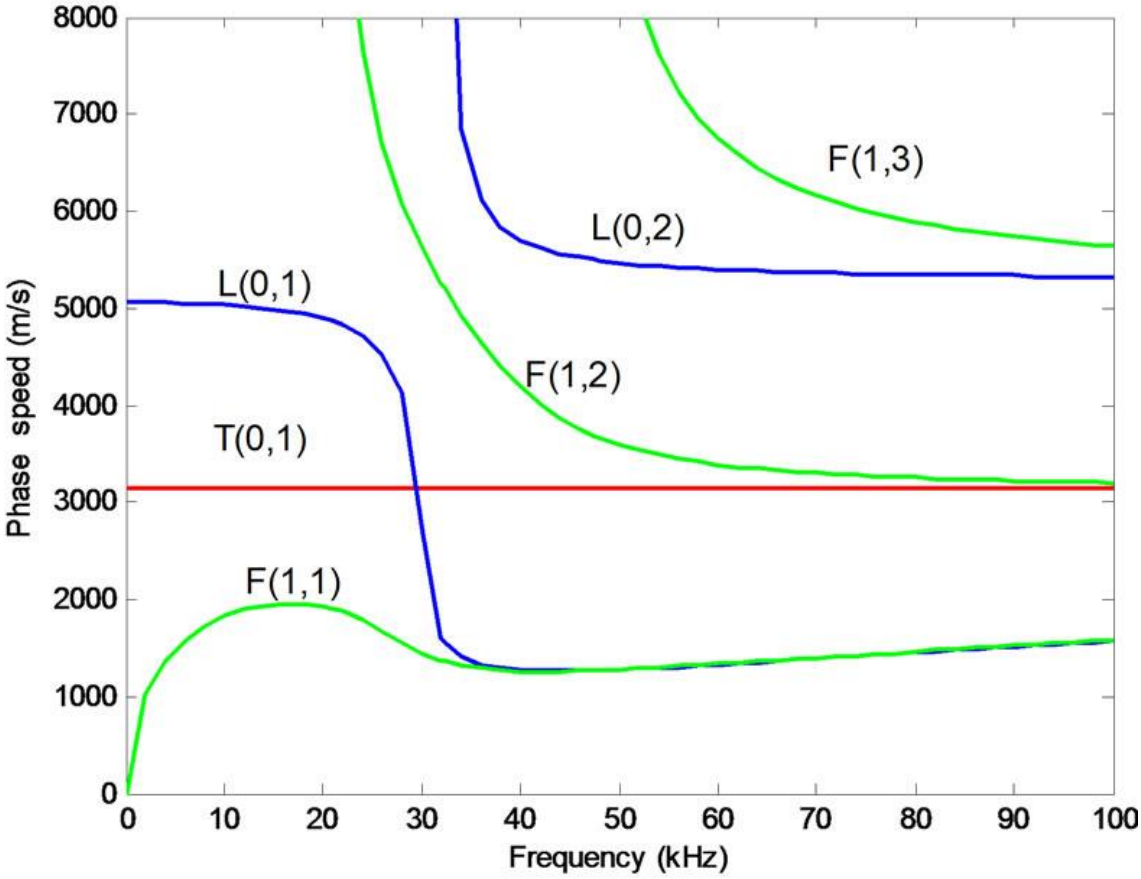

Figure 2.3: Phase speed dispersion curves, taken from [28].

The guided waves used in long range ultrasonic testing are usually excited by a tone burst signal consisting of several cycles of a particular frequency [29], see Fig. 2.4. The tone burst signal is usually modulated by a windowing function, such as a Hanning window [30], in order to reduce the bandwidth of the pulse. However, the pulse still has a certain bandwidth and so it will propagate with its own velocity, known as its group speed. Following [25], the group speed is defined mathematically as

$$C_{gr} = \frac{d\omega}{dk}, \tag{2.10}$$

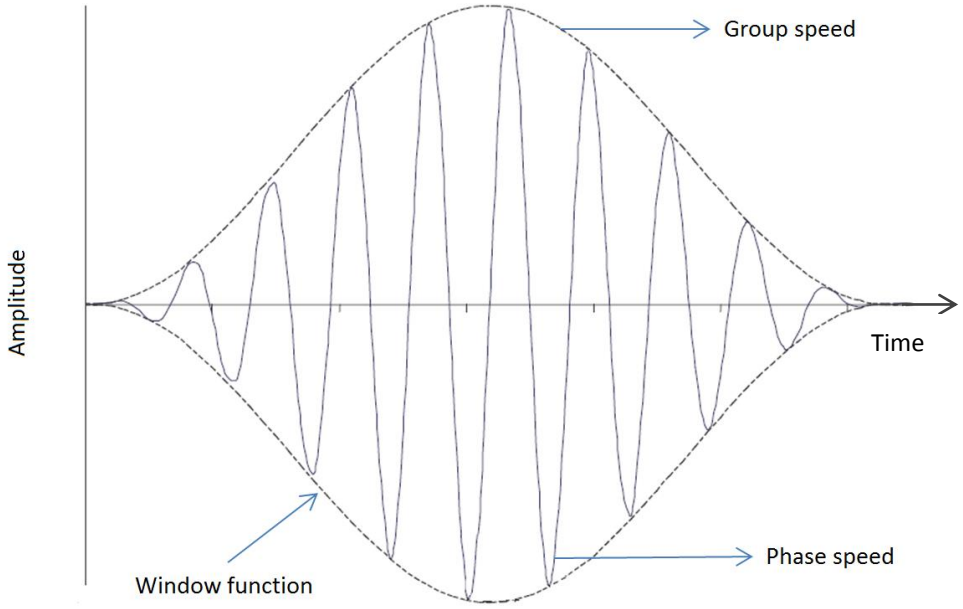

Figure 2.4: Phase speed vs. group speed.

Figure 2.5 shows the group speed for the same pipe size/material as that used to calculate the phase speed dispersion curves in Fig. 2.3. Dispersion refers to the different frequency components traveling with different phase speeds as the signal propagates through the medium. As result of this, the signal elongates and lowers its maximum amplitude as it travels. When the group speed is equal to the phase speed the wave is non-dispersive. Those guided wave modes with low dispersion, such as L(0,2), and no dispersion T(0,1) are the most commonly used for LRUT in pipes [9, 31]. This is because dispersion complicates the LRUT of pipes by deteriorating the signal to noise ratio and making the determination of the time of flight of each reflected signal difficult [32].

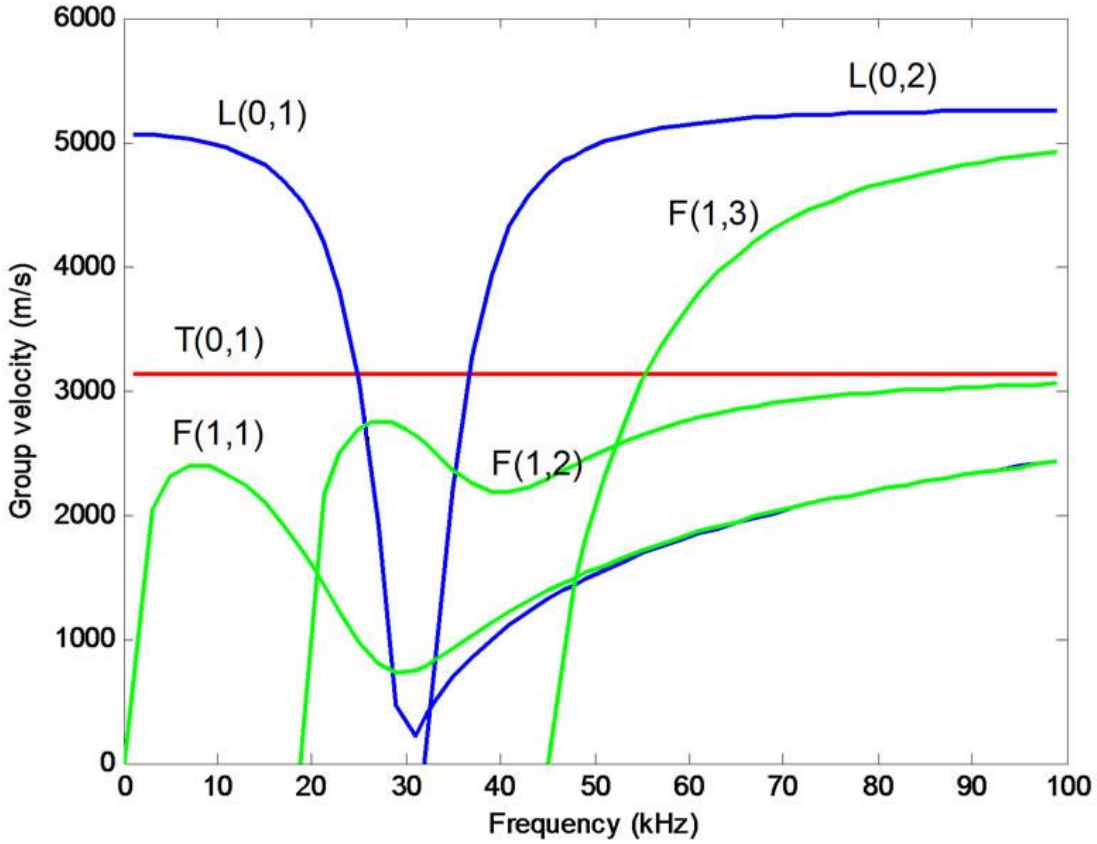

Figure 2.5: Phase speed dispersion curves [28].

Another complication is the presence of number of guided wave modes over certain frequencies as these have different modal shapes and propagation characteristics. In comparison with the bulk waves, the guided waves speed and attenuation depends on number of parameters. The problem becomes even more complicated when we want to study the propagation characteristics of guided waves in multilayered structures such coated pipes. In this case the guided wave phase speed and attenuation depends on the bulk acoustic properties of the metal substrate (pipe wall), as well as the bulk acoustic properties of the coating material and its geometry. This dependence is summarised as

$$A_{n,m}\left(C_{gw}(\omega), A_{gw}(\omega)\right) = f(C_{L(s,c),}\, C_{S(s,c),}\, \alpha_{L,S(c),}\rho_{(s,c)}, r_{(s,c)}) \qquad (2.11)$$

where the frequency dependent phase speed $C_{gw}(\omega)$ in $\mathrm{m/s}$, and attenuation $A_{gw}(\omega)$ in $\mathrm{dB/m}$ of the $A_{n,m}$ guided wave mode is a function of the bulk longitudinal speed $C_{L(s,c)}$ in

m/s, bulk shear speed $C_{S(s,c)}$ in m/s, density $\rho_{(s,c)}$ in kg/m^3 and the radius $r_{(s,c)}$ in m of the steel pipe and coating material, respectively. The constant $\alpha_{L,S(c)}$ represents the bulk longitudinal and shear attenuation constants of the coating material in s/m. The attenuation in the coating materials investigated is considered to be not stress dependent. The steel material for the pipe is considered to be perfectly elastic in this study, so no attenuation values are considered for the steel pipe wall.

2.3 Long Range Ultrasonic Testing

The principle of LRUT is based on an ultrasonic guided wave being sent along the pipe wall and recording and processing the signals reflected back from features/defects located along the pipe [4-11]. Changes in the pipe wall thickness cause a disruption to the guided wave and produce both reflections and changes to the transmitted wave. Because of the excitation around the whole circumference, there is no geometric spreading of the wave front and so there is low attenuation of the sound travelling along the pipe walls. The typical frequency range for the use of ultrasonic guided waves is between 20 kHz and 100 kHz. The successful commercial application of LRUT technology has been achieved by developing specialised multi-channel pulse/receiver units that use cylindrical multi-ring arrays of ultrasonic transducers. More details about those ultrasonic transducers used in these systems can be found in [32-34]. There are several guided wave inspection systems available commercially including Plant Integrity Ltd. [35], Guided Ultrasonics Ltd. [36], M.K.C. Korea [37], and Olympus Corporation [38]. The author was working for TWI Ltd. during the development of the work in this thesis and so the majority of the experimental work reported here was conducted with the Teletest® LRUT equipment, which is commercially available through Plant Integrity Ltd. [35]. The Teletest® system is sensitive to pipe wall cross section loss, which makes it suitable for detection of internal and external corrosion. Normally it can reliably detect down to about 9% of wall loss but its sensitivity can be improved by using focusing techniques [39-42]. The use of a focusing technique then allows detection of defects up to an equivalent 3% wall cross section area loss. A typical LRUT field setup is shown in Figure 2.6.

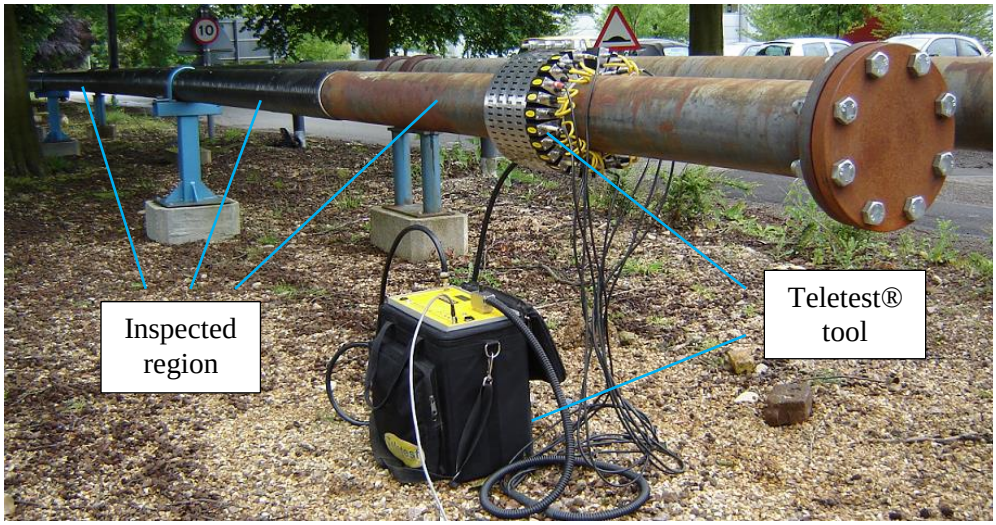

Figure 2.6: Typical LRUT field setup.

Teletest® detects the presence of defects by the generation of a few cycles of a guided wave mode with known propagation characteristics (phase/group speed and attenuation), which is launched along the pipe wall and the signals reflected back from defects located along the pipeline are then recorded back at the Teletest® equipment. The desired guided wave mode is generated using several rings of dry coupled piezoelectric shear mode transducers [32, 33]. The transducers are placed into modules, each of them containing five transducers, as shown in Fig. 2.7. The modules cover the whole circumference of the pipe and they are coupled to the pipe by applying pressure generated by a cylindrical inflatable collar surrounding each module. The shear mode transducers are designed to generate in-plane displacements parallel to the pipe surface and orientated along the longer dimension of the transducer's faceplate.

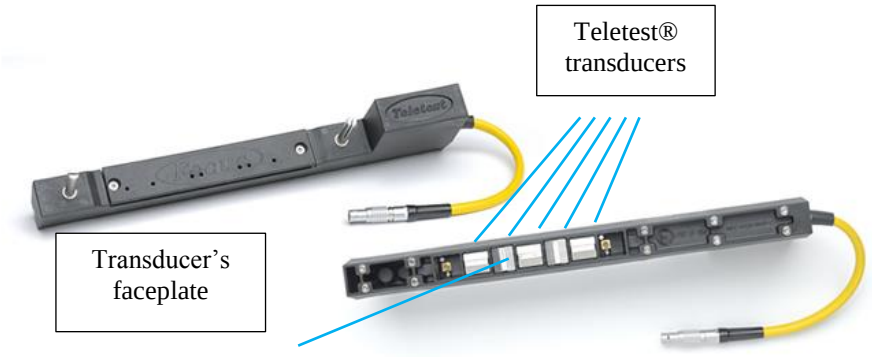

Figure 2.7: Teletest® module with transducers, [35].

The transducers in ring two and four are orientated along the circumference of the pipe, in the θ direction. These rings are designed to generate T(0,1) guided wave mode. The transducers in the other three rings, (one, three and five) are orientated in such a way that they generate displacements in the axial direction. These three rings are designed to generate the L(0,2) guided wave mode. The rings are designed to generate a single mode by applying appropriate phase delays between each ring. However, the fixed ring spacing means that the backwards going signal cannot be cancelled at every possible frequency. In order to minimize the amplitude of the backwards going signal the ring spacing is selected in such way so most of the energy is directed in forward direction in the frequency range of interest. Using this technique, a T(0,1) guided wave mode can be generated in one direction using two rings of transducers because it is the only axisymmetric torsional mode having identical displacement u_θ around the circumference of the pipe. Unfortunately, two rings are not enough to generate L(0,2) because there is another guided wave mode, L(0,1), that also has axial, u_z and radial, u_r displacements. The generation of L(0,1) mode may only be cancelled when L(0,2) mode is generated by adding an additional ring and applying the appropriate phase delays between the electrical signals for three rings.

The electrical signal used to excite each ring of transducers consists of several cycles of a periodic sine wave with a centre frequency between 20 kHz and 100 kHz. The amplitude is modulated using a Hanning window in order to reduce the bandwidth of the signal. It is defined by the Hanning function [30] as

$$A(x) = \frac{1}{2}(1 - cos\frac{\pi x}{a}) \tag{2.12}$$

Figure 2.8 shows ten cycles of a Hanning modulated signal which is used as an excitation signal.

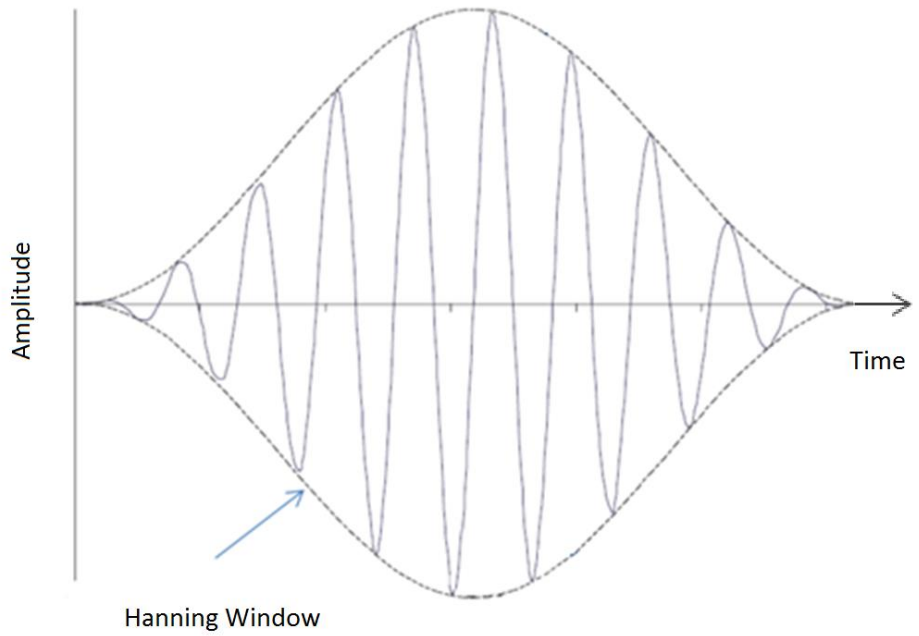

Figure 2.8: Ten cycles of Hanning modulated signal.

Once the guided wave is generated it travels along the pipe wall until it reaches an area with a different acoustic impedance. A change in the acoustic impedance can be caused by a change in pipe wall thickness or a pipe wall discontinuity. A change in pipe wall thickness can be caused by internal or external erosion/corrosion, which makes the LRUT suitable for the detection of this type of defect. Pipe wall thickness change can also be caused by adding material to the pipe wall. This means that the LRUT is also sensitive to features commonly found on pipes like welds, flanges and branches [9, 11, 31]. The girth welds used to join pipes usually reflect approximately 20% of the incoming wave [9]. Pipe wall discontinuity also can be caused by a through thickness crack which could be located along the circumference of the pipe or along the pipe axis. In most cases axial cracks cannot be successfully detected because they have a small cross section in the guided wave propagation direction. The signals reflected from the features located along the pipe are recorded in the time domain. The position and size of the defects and features of interest are determined by processing and analysing the recorded signal. Usually, the processed data is presented as an A-scan, shown in Figure 2.9.

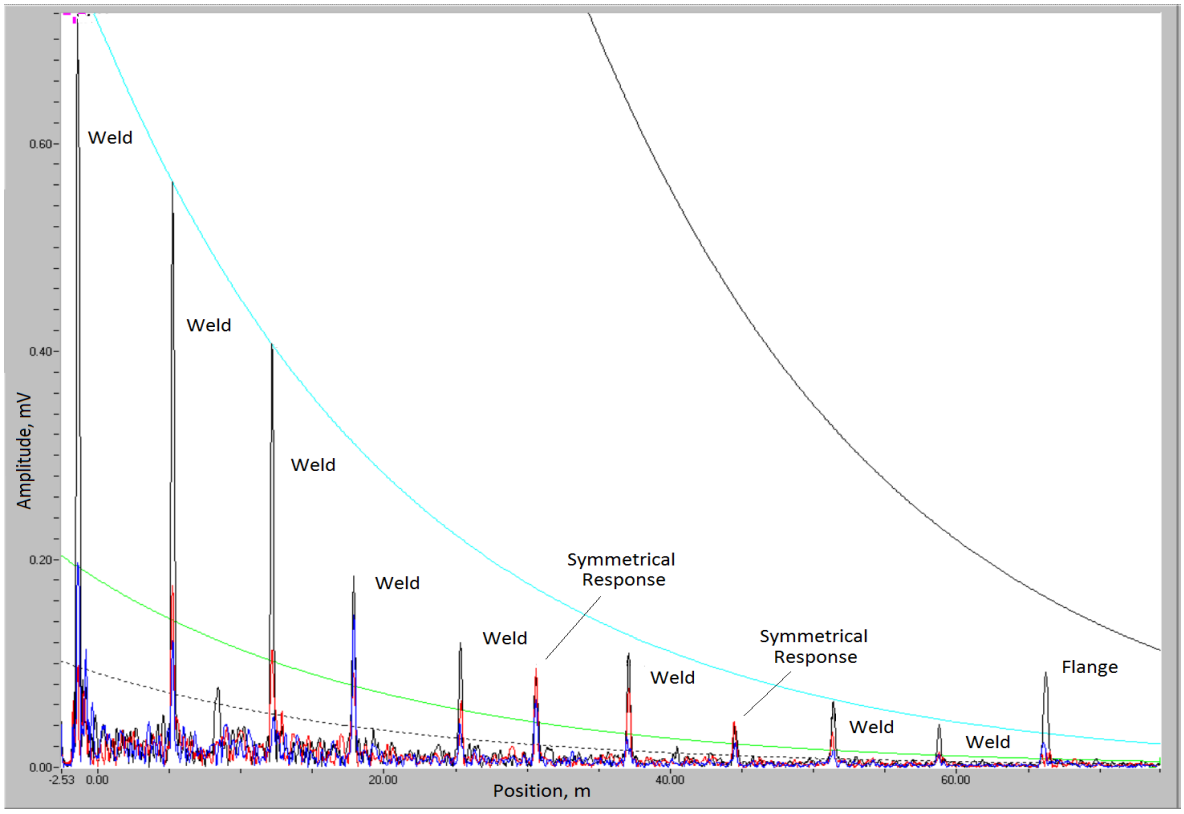

Figure 2.9: Processed guided wave data. Teletest®, [35].

Each curve is superimposed by the user onto to the time domain plot. The curves are movable so that the user can line them up with a particular signal on the chart. For example, the light blue curve is lined up with the reflected signal from the first known weld in the diagram. The light blue curve then corresponds to the expected amplitude of all other signals with the same strength as the first weld, which indicates that all signals lining up with this light blue curve are also welds. This process may be repeated for other known defects and this enables the operator to eliminate signals that are from a known source so that it is possible to focus on defects. The amplitude of the signals reflected depend on the change in the acoustic impedance and the axial and circumferential extent of the defect, [43-45]. When an axisymmetric mode like T(0,1) or L(0,2) interacts with defect that has a non-axisymmetric geometry (like local patch of corrosion), the defect reflects part of the axisymmetric mode but the reflection also generates non-axisymmetric (flexural) modes [12]. By processing the set of modes reflected the operator can try and determine the geometry of the defect and its location around the pipe. The detection and processing of

flexural modes is also possible as result of the Teletest® equipment design, which can record and process signals from different sections of the cylindrical array of transducers clamped around the pipe.

If the pipe is in good condition, uncoated and installed above ground then the LRUT inspection range is more than 100m from a single test position [9]. When the pipe is painted or coated with a relatively thin viscoelastic material then the typical practical range of use is usually between 20 m and 40 m in each direction [9-11]. In case of a pipe coated with a relatively thick layer of viscoelastic bitumen (>0.5mm) then the LRUT inspection range may be limited to few metres or may even be practically impossible [9, 13-16]. The presence of a bitumen coating material reduces the inspection range by introducing additional attenuation along the pipeline, reducing the energy of the incident and reflected waves and making responses from defects difficult to detect. The energy reflected back to the LRUT tool depends simultaneously on the guided wave attenuation along the coated pipeline and the energy reflected from the defect. The first part of that problem, associated with the increased attenuation along the pipeline by the presence of the viscoelastic coating material, is not new. It has been studied by other researchers [9, 13-16, 46, 47] and they show that certain guided wave modes operating at certain frequencies could ensure longer propagation distance in coated pipes, and also that the attenuation spectra of each mode strongly depends on the bulk acoustic properties of the viscoelastic coating material. This has led to the development of several methods for acoustic characterisation of liquid and solid viscoelastic materials, see for example [13-16, 22, 48, 49]. The second part of the problem associated with the energy reflected back from defects located in coated pipes is relatively new and it has been studied mostly in pipes without coating material applied [50-53].

2.4 Methods for studying guided waves in coated pipes

The propagation of guided waves in coated pipes is a problem that has occupied researchers for many years. This has been prompted by the fact that this type of wave is widely used in the long range ultrasonic inspection of structures over long distances. Guided wave modes can be described mathematically by a characteristic equation which describes the guided

wave mode displacements as function of frequency, speed, pipe geometry and material properties. The characteristic equation is solved by setting its value to zero and the solutions are determined in an iterative way. Solutions provide information on the guided wave modes available in the frequency range investigated and how their speed changes with frequency. The solutions are most commonly plotted as dispersion curves. There are commercially available programs, such DISPERSE [21], which can generate dispersion curves for cylindrical structures and plates using an iterative approach. DISPERSE uses the global matrix method described in [21, 54] to find the solutions. The global matrix method was also used by Barshinger [20, 22, 23] to determine guided wave characteristics for a coated pipe. His studies show that the global matrix method is not all that computationally efficient when used for studying coated pipes, and it can predict attenuation only for pipes coated with a relatively thin material. However it has the benefits of simplicity and inherent numerical stability that can be difficult to achieve in the transfer matrix method described by Lowe [54].

Simonetti studied the propagation of guided wave in viscoelastic bilayers [14, 55-57], with the aim of determining the modes and frequencies at which attenuation is minimal. The author primarily analyses shear horizontal modes and Lamb modes propagating in elastic plate-like structures coated with viscoelastic layers. He specifies that these waves are analogous to the torsional T(m, n) and longitudinal L(m, n) modes used in LRUT of pipes. The author supports this claim by stating that most insulated pipes are characterized by a large diameter to thickness ratio and in this case the curvature of the pipe does not have a large impact on the characteristics of the guided modes. The propagation of shear horizontal modes investigated in [14, 55], and Lamb modes investigated in [14, 56], has also been analysed by Simonetti with the help of an analytical formulation based on superposition of partial bulk waves (SPBW), which uses the transfer matrix method described in [54]. For this purpose, a comparison is made between the propagation of the modes of interest in a perfectly elastic system and those in a viscoelastic bilayer system. The input parameters used in this analysis are the geometry of the waveguide and the bulk acoustic properties of the viscoelastic material.

Here it should be noted that Simonetti differentiates between the purely theoretical models based upon linear viscoelasticity described in [58, 59] and the actual behaviour of viscoelastic materials, discussed in [60, 61]. For the sake of further theoretical research on the propagation of guided modes, Simonetti accepts constant acoustic speed and attenuation that is linearly proportional to frequency. Based upon the results of the theoretical analysis of shear horizontal and Lamb modes in a viscoelastic bilayer system, Simonetti demonstrates that the attenuation spectra of guided wave modes in elastic waveguides coated with viscoelastic material exhibit minima and maxima, the positions of which are strongly dependent upon the geometric and acoustic characteristics of the viscoelastic layer in question. The author also demonstrates that the position and amplitude of the first attenuation peak strongly depends upon the shear acoustic properties of the viscoelastic layer.

Luo studied in the propagation of L(0,2) in plain and coated pipes [53, 62], and used the commercial finite element package ABAQUS [63] to model coated pipes using wave focusing. More information about the finite element modelling of linear continuous systems using commercial packages can be found in [64-66]. The pipe studied by Luo is made of mild steel with outside diameter of 273 mm and wall thickness of 9.27 mm, and the number of elements used to discretise a 1.6m length is 99,600. The desired wave modes are generated by Luo by applying a narrow-band tone burst excitation (dynamic load) at the end of the pipe. Attenuation was introduced using Rayleigh damping which is embedded into the ABAQUS modelling package. Results presented by Luo show that the focusing technique enhances penetration power in pipe inspection and improves the probability of detection. Although this improves the sensitivity of the approach, results show that the inspection range is still severely reduced by presence of highly viscoelastic coatings.

Luo [53] also investigated the global matrix method as well as the complex root finding algorithm of Barshinger [23]. Luo presented a new improved complex root finding algorithm and this was used to conduct parametric studies by changing the basic material properties and determining the effect on guided wave propagation. The results show that the propagation characteristics of different guided wave modes are strongly affected by the coating material bulk properties.

Guided wave propagation in coated pipes has also been studied experimentally by Luo [53], who measured the attenuation of T(0,1) and L(0,2) in a pipe coated with 2 mm of wax. The desired modes were generated with a tone burst system and an array of transducers firmly clamped around the pipe. Attenuation was measured by comparing the back wall reflection amplitudes for coated and uncoated pipes. Luo shows that the attenuation of T(0,1) is much higher than L(0,2).

Mu and Rose [67] investigated the possibility of using the semi-analytical finite element (SAFE) method to determine the phase speed and attenuation of modes in a coated pipe. They justify the choice of a SAFE formulation by describing the complications associated with the root searching technique of the global and local transfer matrix methods, which makes them computationally inefficient for studying coated pipes. Mu and Rose simplify the problem by reducing the two-dimensional (2D) SAFE method reported by Sun in [68] to one-dimensional (1D) SAFE method. Although such simplification improves the accuracy in the calculation for flexural modes with higher circumferential orders, and reduces computation cost, Mu and Rose report that the difficulties associated with mode differentiation inherent for the SAFE method still exist in their formulation. They address this by utilising modal orthogonality to separate different families of modes. The stability of the SAFE method is investigated by generating numerical predictions for a pipe with an outside diameter of 114.3 mm and a wall thickness of 6.02 mm, coated with 0.5mm of a highly viscoelastic Bitumastic 50 bitumen material. The results of Mu and Rose are shown in Figure 2.10, and this demonstrates that the SAFE method can handle highly viscoelastic materials such bitumen and it can be successfully used to generate numerical predictions up to 1.4MHz, and attenuations of over 100dB/m.

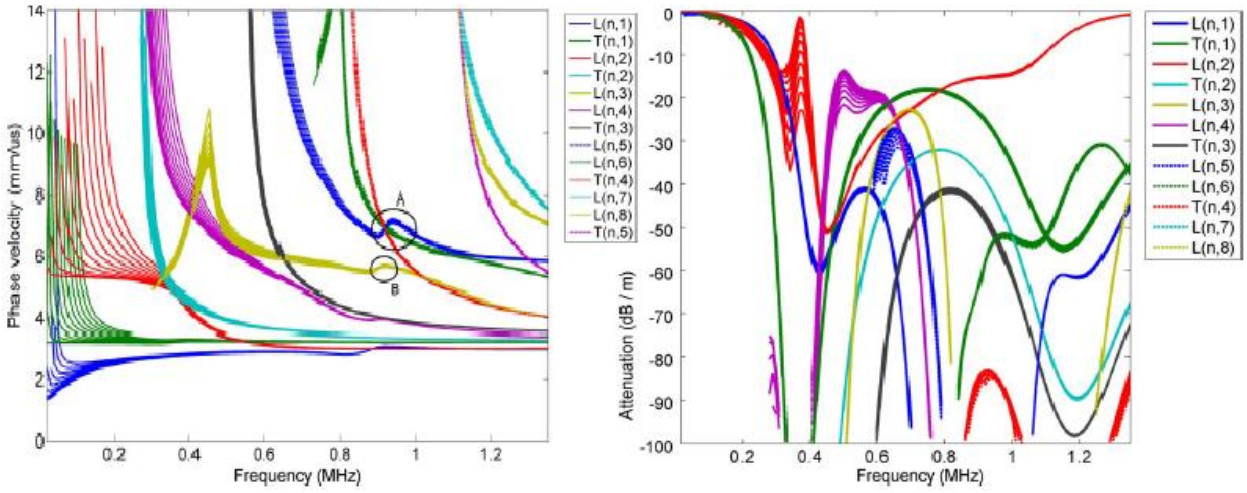

Figure 2.10: Guided wave phase velocity and attenuation, from [67].

The validity of the SAFE formulation reported by Mu and Rose is investigated by Hua and Rose in reference [15]. Here the SAFE method predictions are compared against experimental measurements and FEM based predictions generated by the commercial software ABAQUS. Predictions are presented for a pipe with an outside diameter of 114.3 mm and a wall thickness of 6.02 mm, coated with Bitumastic 50 bitumen material. The predictions were generated for coating thickness varying from 0.5mm to 2.5mm in 0.5mm intervals at frequency of 80kHz. Results presented show good correlation between the SAFE method and FEM ABAQUS predictions. The slight mismatch between the numerical predictions and the experimentally measured data is explained with variations in the coupling between the coating material and the pipe wall.

Kirby et al. simplify the general SAFE method in [69] and [70] by finding the torsional modes and longitudinal modes for a coated pipe separately. This is achieved by separating Navier's equation into its three components and then solving the equation for the circumferential displacement to find the torsional modes, and the radial and axial displacement to find the longitudinal modes. The SAFE method is then used to model scattering from an area discontinuity (or defect) located in coated pipe. For uniform defects the modes in the defect are calculated using the SAFE method, and for non-uniform defects a finite element discretisation is used for the region surrounding the defect [69, 70]. In both cases the modes in the uniform section of the pipe before and after the defect are

determined by modal expansion technique and then these modes are then matched to the solution for the defect using a mode matching technique. This enforces the appropriate continuity conditions over the planes located at the beginning and the end of the defect and so enables the calculation of the modal amplitudes in the pipe. The validity of this approach was investigated by comparing numerical predictions against experimental data for reflection coefficients from defects with uniform and non-uniform geometries in a coated pipe for L(0,2) and T(0,1). Kirby et al. found a significant discrepancy between measurement and prediction if the predictions are obtained using data for bitumen in the literature [20]. This problem is reviewed and addressed in the chapters that follow in this thesis.

The experimental results for guided wave attenuation in coated pipes reported by Cobb et al. [71] also show that attenuation depends not only on the coating material type but also on its temperature. Researchers like Simonetti [14, 55-57], Lakes [26] and others report that the mechanical properties of some viscoelastic materials could strongly depend on temperature and as result of this their bulk acoustic properties are also expected to be temperature dependent. The study of Cobb et al. [71] investigates the temperature dependence of the attenuation of T(0,1) for a pipe with an outside diameter of 168 mm and a wall thickness of 7.01 mm, coated with the following coating materials: enamel TGF-3 coating, coal tar epoxy CTE coating, and a polyethylene coating PRITECs. The attenuation measurements were conducted between 17.8 ºC and 48.9 ºC in 5.6 ºC increments by measuring the amplitude drop of the signal reflected from the pipe ends. The end of the pipe was excited in T(0,1) mode by a pulse/receiver tool using the Magnetostrictive Sensor technology described in [72]. Results covering a frequency range between 10kHz and 60kHz show that the attenuation of the T(0,1) mode in coated pipes is strongly dependent on both temperature and frequency. The guided wave attenuation dependence on frequency was previously numerically and experimentally demonstrated by other researchers, but the data on guided wave attenuation dependence on temperature is something new and interesting. Further investigation of the experimental data presented in [71] show that increasing the frequency and temperature could reduce the attenuation of T(0,1) by more than ten times. This shows that when the optimum parameters for LRUT are selected the temperature should also be taken into account.

2.5 Summary

Most of the results reported in the literature on global and local matrix methods suggest that these methods have limitations when used for studying guided waves in pipes coated with thick viscoelastic materials. These difficulties have been overcome by using conventional finite element modelling packages, although the increased size of the problem caused by the need to discretise the whole 3D structure is still an issue. One possibility to study guided waves in coated pipes in a computationally efficient way is to use the SAFE method. The SAFE formulation reduces the size of the problem by an order of one and so significantly reduces computational expenditure, and can easily be applied to viscoelastic coating materials. Although the SAFE has some problems with the modal differentiation, this can be overcome using modal orthogonality.

The experimental methods available for measuring guided wave attenuation in coated pipe are applicable only to pipes with limited length, where multiple reflections from the pipe ends could be obtained. The coating properties such thickness, density and bulk acoustic properties can have significant effect on guided wave attenuation. The guided wave attenuation results reported in the literature show that the bulk shear properties of the coating play major role on guided wave attenuation spectra in the frequency range of interest. This hypothesis has been also confirmed in Simonetti's work [55-57].

Some studies on coated pipes reported in the literature that look at actual installations of pipework show that the coupling between the coating material and the pipe wall is not always perfect and usually degrades with time. This suggests that guided wave propagation in coated pipes could be more accurately modelled by taking into account the actual coupling between the pipe wall and the coating material, however this is likely to be difficult to quantify.

The guided wave attenuation in coated pipes is not a steady increasing function with frequency. It exhibits minima and maxima. The frequency range over which the attenuation minima occur is of practical interest. The position and the amplitude of the minima and maxima strongly depends on the bulk shear properties of the coating material. The

temperature can also have a significant effect on guided wave attenuation in coated pipes. This is most likely because the temperature affects the bulk mechanical/acoustic properties of the coating material and as result of that the guided wave attenuation is affected too. This assumption needs further investigation in order to clarify the guided wave attenuation temperature dependence and obtain data quantifying its behaviour.

2.6 Acoustic characterisation of coating materials

Although acoustic characterisation of viscoelastic materials is a matter which has occupied researchers for many years, the methods for acoustic characterisation of viscoelastic coating materials used for corrosion protection of pipes have been studied only recently and few methods have been developed.

The method reported by Simonetti in [14, 48] is specifically designed for acoustic characterisation of liquid bitumen based materials.. The material investigated, TML 24515 45/60 is in a liquid state and its bulk properties are measured when added to a thin copper tube as shown in Figure 2.11. The tube was excited in T(0,1) mode by two piezoelectric shear transducers clamped to the copper tube. The amplitude of the torsional mode was measured at several positions by a laser vibrometer [90] and the phase speed and attenuation were measured experimentally between 10 kHz and 90 kHz. The bulk properties of bitumen were determined from measurements of attenuation and phase speed of T(0,1) and a set of contour plots generated by DISPERSE [21].

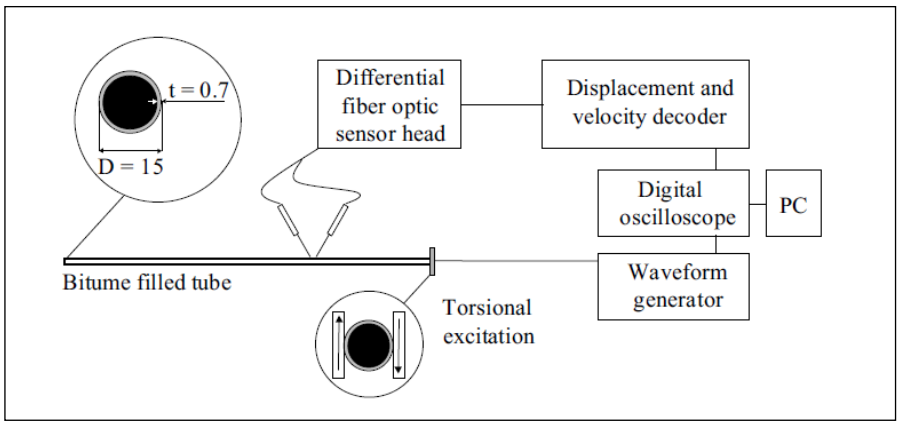

Figure 2.11: Experimental setup [14].

The results of Simonetti [14] shown in Fig. 2.12 reveal that the bulk shear velocity and attenuation for liquid bitumen are frequency dependent. Their validity is investigated by comparing the measured phase speed and attenuation spectra against predictions based on relations derived from the Kramers-Kroning relationships [14, 48].

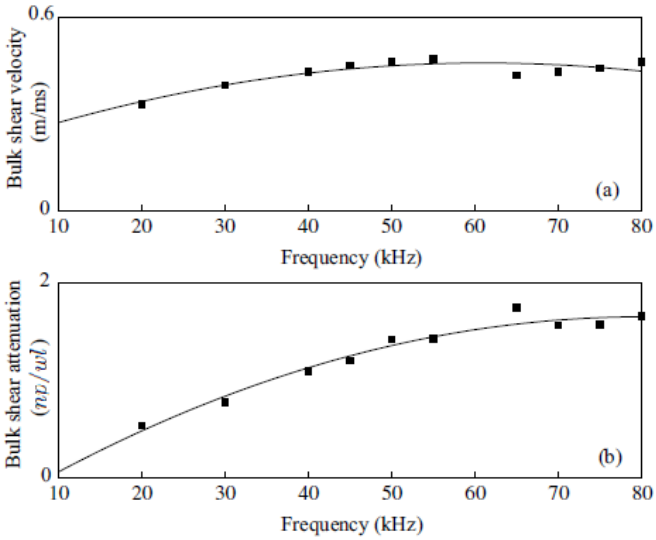

Figure 2.12: Dispersion curves for bitumen TML 24515 45/60: (a) bulk shear velocity against frequency; (b) bulk shear attenuation against frequency. From [14].

However, the method for characterisation of liquid bitumen materials reported by Simonetti in [14, 48] is not applicable to solid materials, and so Simonetti proposes a second method suitable for analysing solid viscoelastic materials and these are described in [14, 49]. This method is based on frequency interferometry, where the sample's acoustic properties are derived from the measured reflection and transmission coefficients of a T(0,1) mode traveling through a thin sample that is firmly clamped between two identical cylindrical bars acting as waveguides. The experimental set up is shown in Figure 2.13 and this was used by Simonetti for the acoustic characterisation of an 18.5 mm long Acetal Copolymer Plastic (POM) cylinder with a diameter of 6mm.

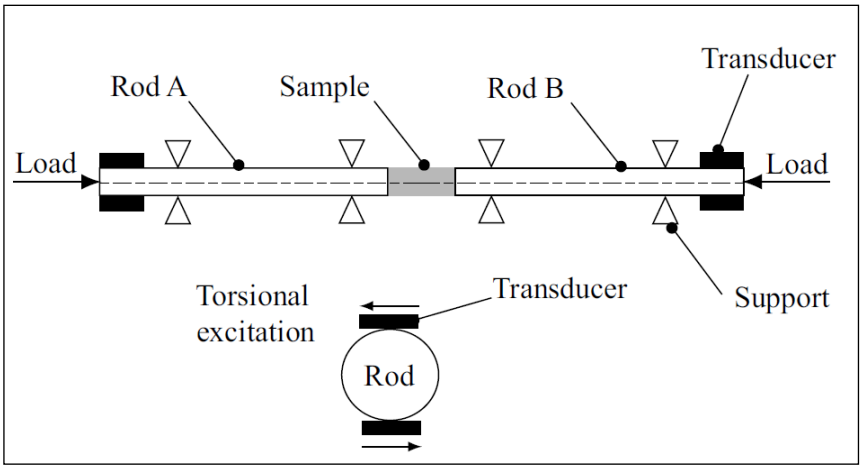

Figure 2.13: Experimental setup, from [14].

Simonetti studied the transmission coefficient spectra and concluded that the bulk shear speed for the material investigated was constant and equal to 870 m/s over the frequency range investigated. The bulk shear attenuation was found to be 0.105 Np/wl. The method was validated using a variation of the method for acoustic characterisation of liquid bitumen material described in [14, 48]. The measured values of bulk shear speed and bulk shear attenuation were 2.3% higher and 5% lower, respectively.

The method for measuring shear acoustic properties in solid materials reported by Simonetti was also used to measure the shear bulk properties of four different bitumen coating materials. These coating materials have been in use and their properties are influenced by aging. The results from these measurements are summarised in Chapter 3.

Several characterisation methods based on conventional pulse-echo and through-transmission technique used in MHz frequency range [73,74] have been used by Luo, [53], Van Velsor [16], and Barshinger [20] to determine the bulk properties of bitumen materials. The main disadvantage of these methods is that they determine the bulk properties in MHz frequency range and the direct application of these properties in the kHz frequency range can be associated with significant errors.

The methods for acoustic characterisation reviewed so far can be categorised as local, this is because they can be used to determine the bulk properties of a sample of coating material with limited dimensions. In reality the bulk acoustic properties of a coating material will

vary along the pipeline and it would be much better if we can determine some average values for the bulk properties of the coating material which are valid for the entire coated pipe of interest. The method presented by Hua and Rose in [15] uses a new, experiment based method, which can determine the bulk shear attenuation constant of bitumen material from guided wave attenuation data measured in a pipe coated with the bitumen material of interest. Figure 2.14 shows a flow chart of the method.

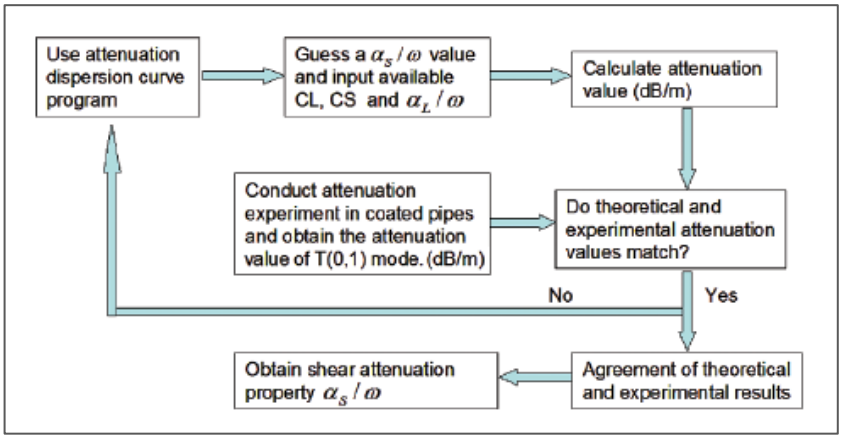

Figure 2.14: Flow chart of the method for shear attenuation determination, from [15].

The attenuation dispersion curve program is based on the SAFE formulation reported in [67] and the shear attenuation constant is obtained after a few iterations by comparing experimentally measured T(0,1) guided wave attenuation against SAFE predictions based on suggested values for the shear attenuation constant. The comparison was conducted at single frequencies by varying only the shear attenuation constant and keeping the other bulk properties constant. The method was used to determine the shear attenuation constant of four different coating materials, two of which were bitumen based. The other acoustic properties of the coating materials were measured by the previously discussed reflectometry and through-transmission based methods in the MHz frequency range. The bulk acoustic properties of the four coating materials measured were used as input parameters for FEM simulations carried out at single frequency of 80 kHz. The FEM predictions were compared against experimental measurements for T(0,1) guided wave attenuation at 80 kHz and the results show differences no larger than 10% between measurement and prediction.

The method presented by Hua and Rose in [15] provides values for the shear attenuation constant which is valid at the frequency at which it was determined. However, in the work presented in this thesis values for the bulk acoustic properties of the coating material are required between 20 kHz and 100 kHz. However, this method is much more advanced compared to the methods for local coating materials characterisation reviewed so far. This is mostly because the method provides values for the shear attenuation constant valid for the whole coating material applied on the pipe and these values also take into account the coupling between the pipe wall and the coating material.

2.7 Summary

Most of the methods for the acoustic characterisation of coating materials available in the literature are based on conventional ultrasonic techniques utilizing ultrasonic bulk waves in the MHz range. Although it has been reported that these methods can be successfully used for coating materials characterization in the MHz range, the problems associated with using the bulk properties determined in the frequency range of interest (below 100 kHz) have not been investigated completely. Most researchers extrapolated acoustic properties measured in the MHz range to lower frequencies by assuming that the attenuation for the coating materials investigated is linear function of frequency, and its acoustic speed is constant with frequency. This approach can be used for the theoretical demonstration of some general dependence between the coating material acoustic characteristics and the guided wave propagation characteristics. If we want a method which can predict the actual guided wave propagation characteristics in coated pipe, we need a method which is capable of characterising the coating material properties in the frequency range of interest. The other possibility is to find a valid method for extrapolating coating material properties measured in MHz frequency range towards the kHz frequency range. The guided wave based methods suggested by Simonetti can characterise the bulk shear properties of liquid and solid bitumen coating materials in kHz range, unfortunately these methods are not suitable for the Bitustik 4000 and Bituthene 4000 semisolid bitumen coating materials selected for this study. The method reported by Hua and Rose in [15] can determine the shear attenuation constant in different materials as long as they are successfully applied on a pipe,

but the other bulk acoustic speed needed as input for the method still needs to be determined by separate measurement. The method also needs T(0,1) guided wave attenuation data at certain frequency as an input parameter.

The bulk acoustic properties of coating materials vary significantly and even the same coating materials could have different bulk acoustic properties depending on temperature variations and ageing. These variations in bulk acoustic properties of coating materials could be determined if a method for on-site coating material characterisation is used.

The shear bulk properties of a given coating material are more difficult to measure experimentally. This is mostly because of the difficulties related to the coupling between the transducer and the specimen and the high rate of shear attenuation. The difficulties associated with the high rate of attenuation could be solved if an ultrasonic through transmission technique is utilised.

Some of the bulk acoustic properties of the coating material of interest could be derived from experimental data showing the dynamic response of a coated pipe. The methods which derive the coating material properties from measured guided wave attenuation reported in the literature are applicable to pipes with a limited length. If we want to use that concept on-site we need to find a method which can do these measurements on-site.

Those researchers who have studied the dynamic behaviour of different viscoelastic coating materials suggest that the bulk acoustic properties of viscoelastic coating materials are frequency dependent and this dependence is unique for each coating material. This frequency dependence is not investigated with respect to its influence on the accuracy of the numerical predictions on guided wave propagation characteristics in a coated pipe. Most researchers achieved good correlation between guided wave attenuation predictions and measurements by using a constant (not frequency dependent) bulk acoustic speed and attenuation.

Chapter 3

Methods for acoustic characterization of Bitustik 4000

Introduction

The results reported in the literature clearly show that a coating material will have a significant effect on guided wave attenuation in pipes. One possibility to understand this effect is model guided wave attenuation using numerical predictions based on independently measured bulk properties for the coating material, and then to compare this against experimental data. The main aim in this chapter is to develop experimental methods capable of measuring the longitudinal and shear bulk properties of the coating material of interest and then later to compare this to theoretical predictions. The bitumen coating material selected for this study is Bitustik 4000 [75]. This material is a semisolid, rubberized bitumen compound pre-formed in a waterproof membrane with a nominal thickness of 1.5mm and a density $\rho = 990\ \mathrm{kg/m^3}$. A schematic diagram showing the cross section of the material studied is shown in Figure 3.1.

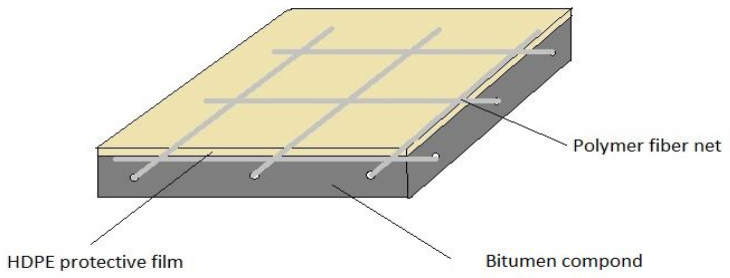

Figure 3.1: Cross section of Bitustik 4000 coating material.

The sticky bitumen compound is moulded around a fibre net made of 0.15mm thick polymer fibres. The main function of the polymer net is to avoid stretching of the material when it is applied to a surface. The top surface of the bitumen layer is protected by 30μm thin layer made of high-density polyethylene (HDPE). When supplied, the bottom sticky

surface of the bitumen layer is protected by wax coated paper sheet which is removed prior installation.

The properties required in order to study guided waves are the bulk acoustic properties and the material density. The density is taken from the manufacturer datasheet [75], although in realty the density of bitumen materials changes with time as it ages. The best way to obtain the density for a bitumen material that has aged is to measure it under specific material conditions. The next two sections present experimental methods for measuring longitudinal and shear bulk acoustic properties in Bitustik 4000 that may in principle be applied to the material under new or aged conditions.

3.1 Bulk longitudinal acoustic properties

The experiment described in this section is designed to measure the longitudinal acoustic properties of bitumen, and in particular Bitustik 4000. The experimental set up is shown in Figure 3.2 and this replicates the immersion reflectometry technique used for the acoustic characterisation of highly viscoelastic plastic materials presented in [76]. Although this technique measures the bulk longitudinal properties of the bitumen material in the MHz frequency range, it was selected because it provides a reliable acoustic contact between the transducer and specimen. According to the manufacturer specification, the investigated material is waterproof which also makes this method applicable here. The specimen shown in Figure 3.3 is made of a single layer of Bitustik 4000 that was stuck to a 3mm thick, 100 mm x 100 mm, flat aluminium base. The aluminium base was used to support the flexible bitumen material, which tends to bend if it is not supported this promotes better acoustic reflection from the bottom surface of the coating material. The bitumen material thickness was measured using a micrometer at nine positions and thickness of the Bitustik 4000 material was determined to vary between 1.18 mm and 1.26 mm, as shown in Figure 3.2. The thin HDPE layer was removed from the top face of the bitumen layer and the assembly was submerged in an immersion tank filled with distilled water, as shown in Figure 3.3. The distilled water in the tank served as an acoustic coupling media between the ultrasonic transducer and the specimen being investigated.

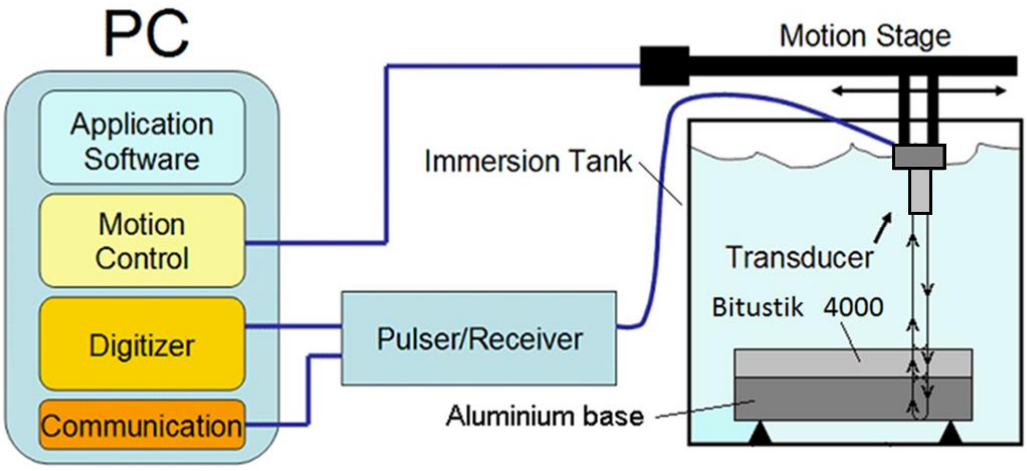

Figure 3.2: Experimental set up. Immersion reflectometry technique.

The specimen was kept in the immersion tank for 30 minutes before measurements were taken in order to equalize its temperature with the surrounding water. The water temperature in the immersion tank was monitored and remained constant at 20°C during the experiment. The acoustic transducer used was a focused, immersion type, ultrasonic transducer with a centre frequency of 8 MHz, and an active element with a diameter of 12.5 mm and a focal length of 75 mm. The ultrasonic transducer was excited and the reflected signal from the specimen was recorded using an ultrasonic pulse/receiver unit, model DUI 1200 equipped with XYZ motion stage, see Table 3.1.

Pulse		Receiver	
Pulse type	Negative spike pulse	Sampling Rate	500 MSPS
Pulse amplitude	100V	Gain	18.5dB
Pulse duration	70ns	Averaging	64
Pulse repetition rate	1000Hz	High/Low pass filter	2.5MHz / 15MHz

Table 3.1: Ultrasonic pulse/receiver settings.

The experiment begins by placing the ultrasonic transducer at position 1, see Figure 3.3, and a short ultrasonic pulse is sent towards the specimen and the reflected signal was

recorded. This was repeated 64 times and the data recorded was averaged in order to reduce the level of random noise.

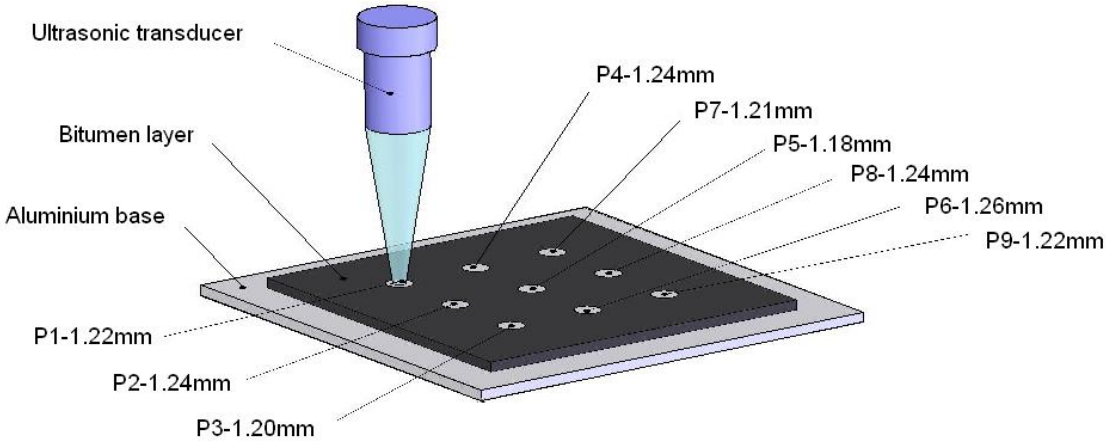

Figure 3.3: Specimen investigated.

The recorded A-scan at position 1 is shown in Figure 3.4. The A-scans for the remaining eight positions were collected in the same way. In Figure 3.4, R1 is the signal reflected from the top surface of the coating material, and T3 is the signal reflected from the coating material/aluminium base boundary. The reflections after T3 that appear in Figure 3.4 are multiple internal reflections between the top and the bottom surface of the aluminium base.

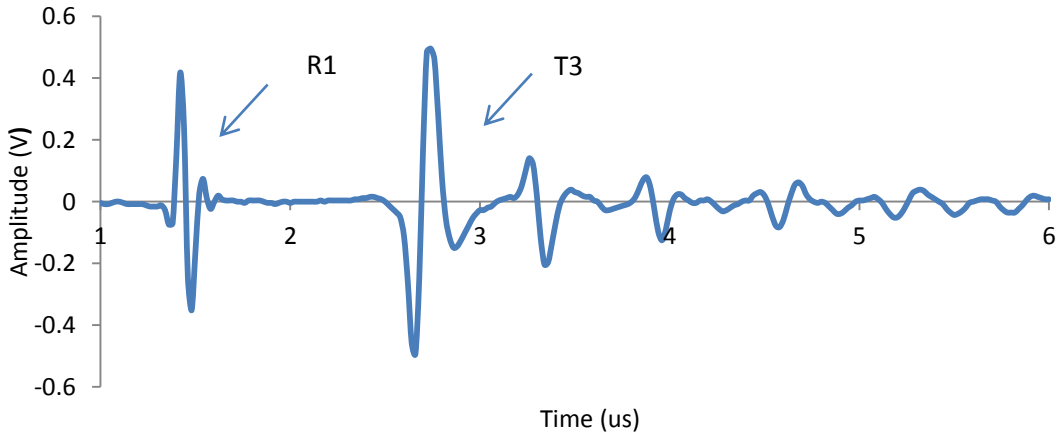

Figure 3.4: A - scan from a single layer of Bitustik 4000, position 1.

Figure 3.5 show a schematic representation of the signals reflected and transmitted at the boundaries. The transducer focal point was kept positioned at the boundary between the viscoelastic material and the aluminium base, as shown in Figure 3.5. This was done in order to reduce the error caused by the acoustic beam divergence. In Figure 3.5, I1 is the signal incident to the coating material, R1 is the signal reflected from the top surface of the coating material and T3 is the signal reflected from the coating material/aluminium base boundary. Some of the signals paths shown in Figure 3.5 are presented at an angle for better visualization, but in reality the paths of all signals are normal to the specimen face.

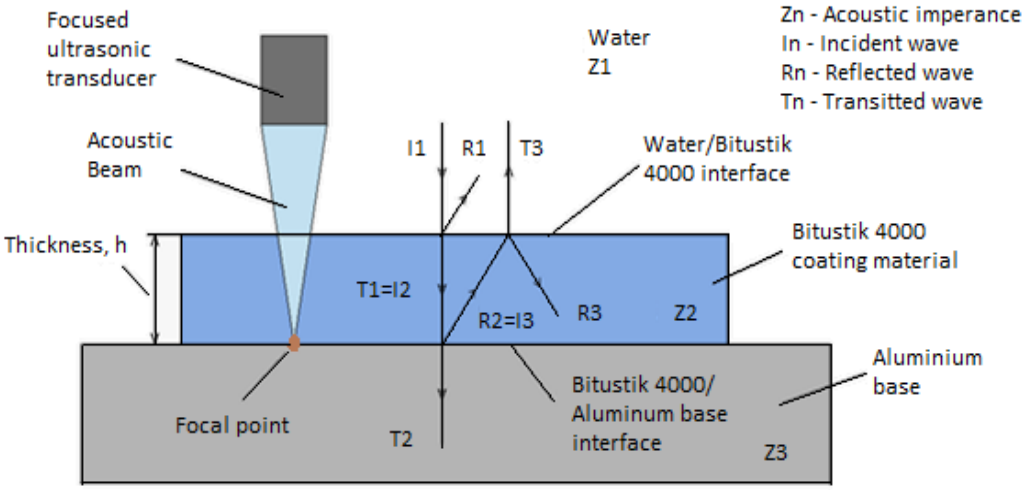

Figure 3.5: Schematic diagram of the signals reflected and transmitted.

The experimental data collected above using A-scans are used in the next section to determine the bulk longitudinal speed and attenuation for Bitustik 4000.

3.2 Bulk longitudinal acoustic speed

The acoustic speed in the bitumen coating material may be determined from the difference in the time of flight, Δt, between the reflection R1 from the top surface and the reflection T3 from the bottom surface of the bitumen layer. The difference Δt therefore corresponds to the time required for the pulse to travel twice the thickness of the specimen. The signals of interest were windowed with a rectangular window and their spectrogram was calculated using the MATLAB "$specgram$" function, which computes the windowed discrete-time

Fourier transform of a signal using a sliding window. The MATLAB code used to calculate the spectrogram of the windowed signals R1 and T3 is shown in the Appendix . Figure 3.6 shows a spectrogram representing the reflections R1 and T3 in the time-frequency domain.

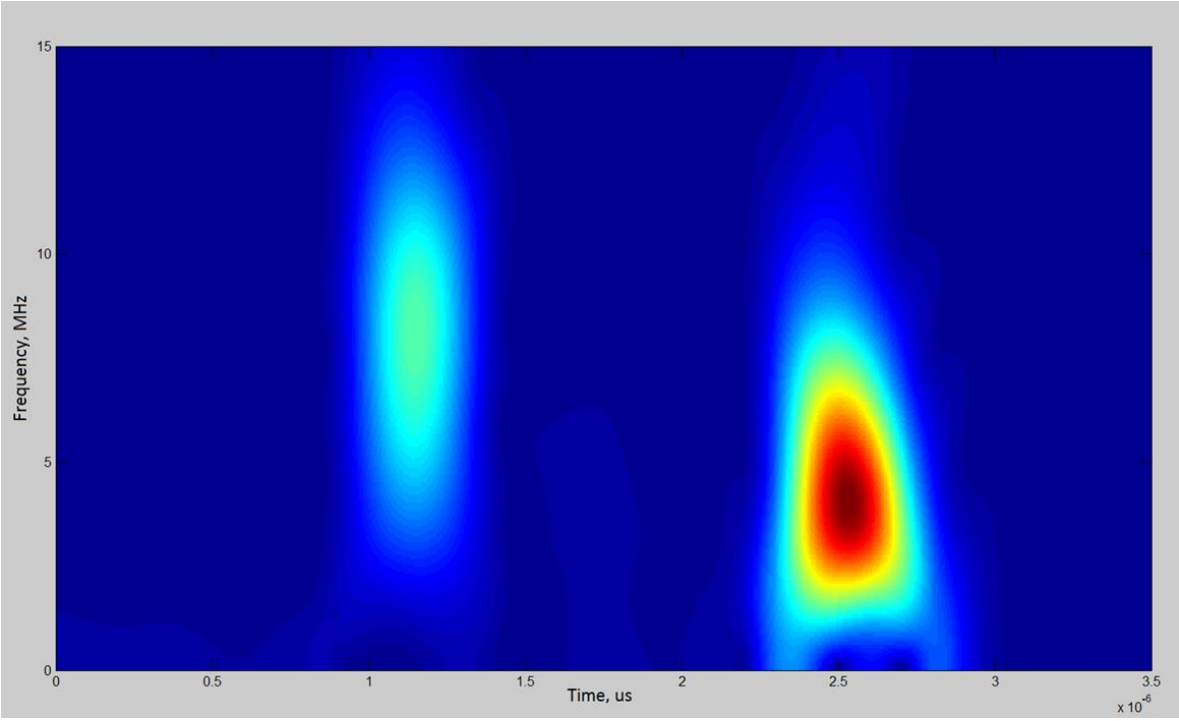

Figure 3.6: Spectrogram of reflections R1 and T3.

The time of flight Δt is determined over a frequency range from 3 MHz to 10.5 MHz with 0.5 MHz steps using the maximum amplitude for each reflection at each frequency. Figure 3.7 shows the power spectra for reflections R1 and T3, and the positions of t1 and t2 at a frequency of 8 MHz.

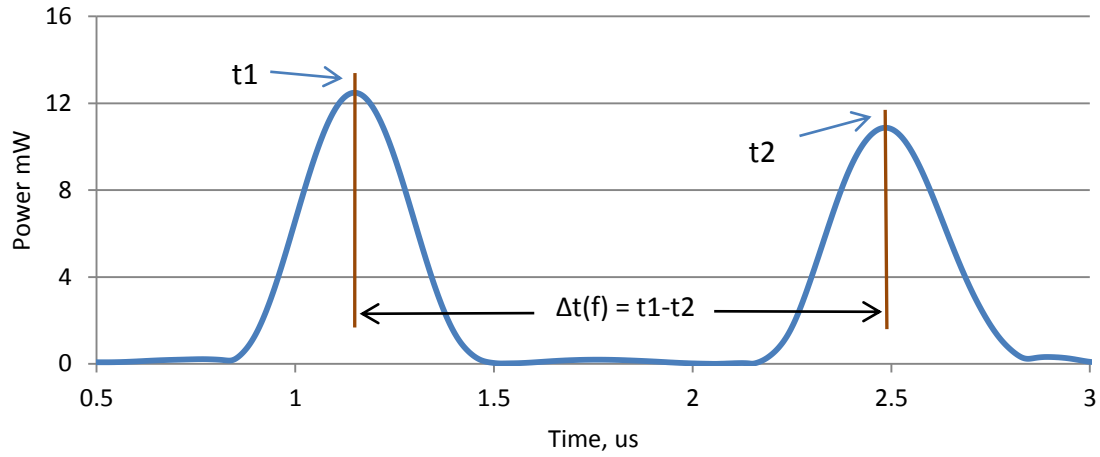

Figure 3.7: Power spectrum of reflections R1 and T3 at 8 MHz.

Based the on the time Δt obtained at each frequency, the thickness of the bitumen layer was calculated and the longitudinal acoustic speed can then be obtained. The averaged longitudinal speed, with a standard deviation obtained after processing nine separate A-scans, is shown in Figure 3.8. The standard deviation of the data was found to vary between 3.3% and 3.6% over the range of frequencies measured. This shows that the method selected provides stable results and that accuracy of the measurements is sufficient to calculate the longitudinal speed. The measurements shown in Fig. 3.8 also demonstrate that the sound speed is frequency dependent and this is because of the way the material reacts to the propagation of a sound wave. This frequency dependence has also been observed by Simonetti in [14]. In this study we are interested in longitudinal speed below 100 kHz and one possibility is to extrapolate the experimental data measured in MHz frequency range to frequencies below 100 kHz. This can be done simply by assuming a constant speed [15, 16, 22], or another possibility is to extrapolate the data below 100kHz by using the relations between the acoustic speed spectra and the attenuation spectra reported in [76-78].

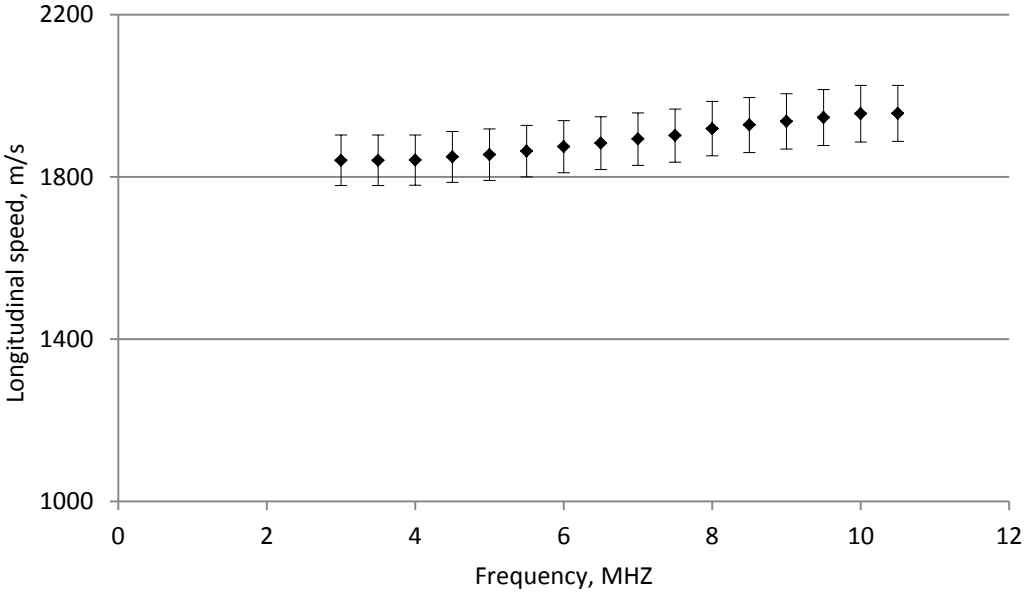

Figure 3.8: Longitudinal acoustic speed in Bitustik 4000.

3.3 Bulk longitudinal attenuation

The frequency dependent longitudinal attenuation in dB/m can be described as

$$A_{(\omega)} = \left[10log_{10}\left(\frac{U_{R1(\omega)}K_{(\omega)}}{U_{T3(\omega)}}\right)\right]/2h, \tag{3.1}$$

where, $A_{(\omega)}$ is the frequency dependent attenuation, $U_{R1(\omega)}$ is the Fast Fourier Transform (FFT) of the reflection R1, $U_{T3(\omega)}$ is the FFT of reflection T3, h is the thickness of the bitumen material, and $K_{(\omega)}$ is a coefficient which takes into account the energy transmitted and reflected at the boundaries of the bitumen layer. Following Figure 3.5, the coefficient $K_{(\omega)}$ can be described with respect to the acoustic impedance of the distilled water Z_1, the bitumen layer Z_2 and the aluminum base Z_3 using the following equations:

$$R_{w,b} = \frac{A_{r_1}}{A_i} = \frac{Z_2 - Z_1}{Z_1 + Z_2}, \tag{3.2}$$

$$T_{w,b} = \frac{A_{t_1}}{A_i} = \frac{2Z_2}{Z_1 + Z_2}, \tag{3.3}$$

$$R_{b,a} = \frac{A_{r_2}}{A_{t_1}} = \frac{Z_3 - Z_2}{Z_2 + Z_3}, \tag{3.4}$$

$$T_{b,w} = \frac{A_{t_3}}{A_{r_2}} = \frac{2Z_1}{Z_2 + Z_1}, \tag{3.5}$$

$$K_{(\omega)} = \left(\frac{T_{w,b}\, R_{b,a}\, T_{b,w}}{R_{w,b}}\right)^2. \tag{3.6}$$

The acoustic impedance of the distilled water Z_1, and the aluminium base Z_3, are taken from the literature [79]. The acoustic impedance of the bitumen layer Z_3 is calculated by using the density $\rho = 990\,\mathrm{kg/m^3}$ provided by the manufacturer datasheet for Bitustik 4000, and the frequency dependent acoustic speed is determined in Section 3.2. Figure 3.9 then shows the frequency dependent coefficient $K_{(\omega)}$ calculated using Eqs. (3.2) to (3.6) with the date measured in the previous section.

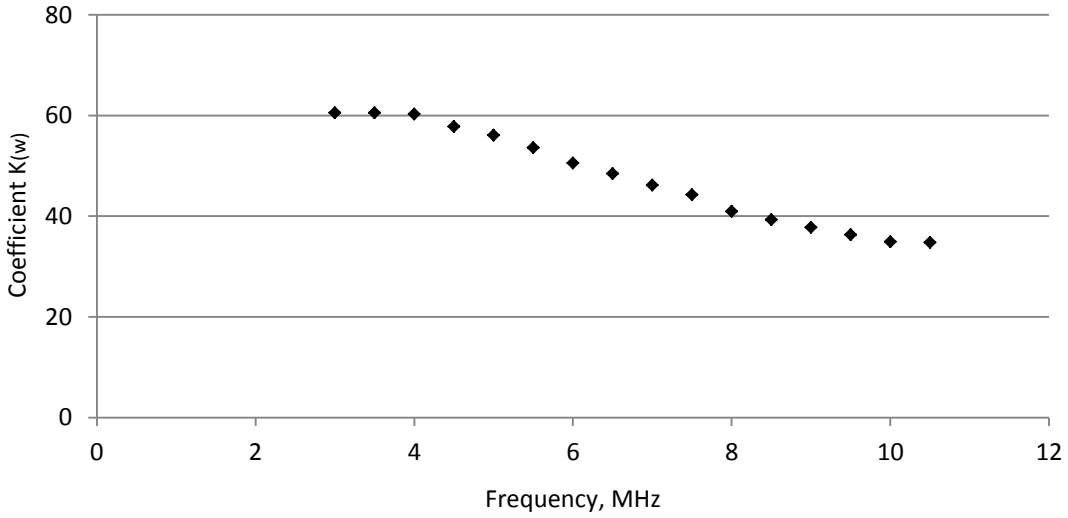

Figure 3.9: Calculated frequency dependence for coefficient $K_{(\omega)}$.

To carry out these calculations, the reflections R1 and T3 were windowed in the time domain with a rectangular window as shown in Figure 3.10, and their FFT was obtained using the MATLAB "fft" function, see the Appendix for the code used.

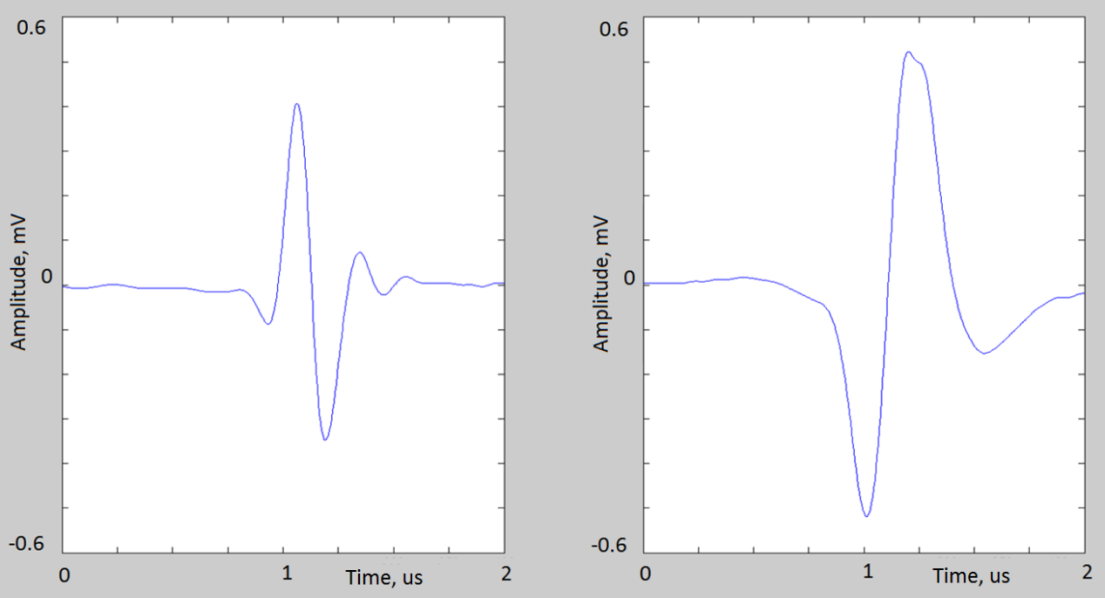

Figure 3:10: Reflections $R1$ and $T3$.

Figure 3.11 shows the FFT of $U_{R1(\omega)}$ and $U_{T3(\omega)}$, and here the frequency shift between the maximum of $U_{R1(\omega)}$ and $U_{T3(\omega)}$ indicates that the attenuation is increasing with frequency. The frequency dependent attenuation $A_{(\omega)}$ is then calculated in frequency range between 3 MHz and 10.5 MHz, with 0.5 MHz frequency steps, using Eq. (3.1). The experimental data below 3 MHz and above 10.5 MHz was omitted because of the poor signal to noise ratio. In Fig. 3.12 the final values for attenuation are shown, which are calculated following an averaging of all nine A-scans.

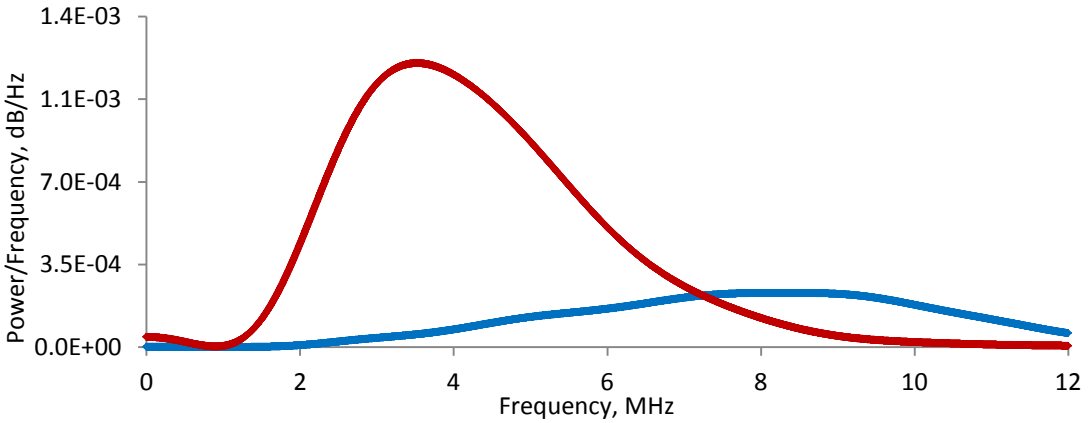

Figure 3.11: Fourier transform of $U_{R1(\omega)}$ (♦) and $U_{T3(\omega)}$ (♦).

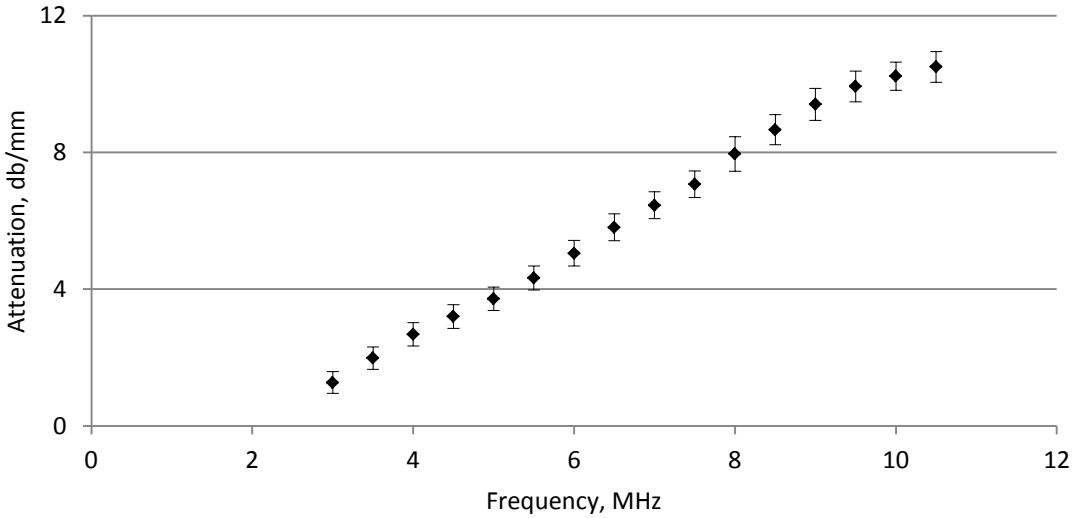

Figure 3.12: Longitudinal attenuation $A_{(w)}$ of Bitustik 4000.

The experimentally measured longitudinal attenuation presented in Fig. 3.12 shows how the attenuation changes with frequency over the range 3 MHz to 10.5 MHz. The data trend corresponds well with the power-law dependence of Eq. (3.11), which is discussed later. Note that the error bars in Fig. 3.12 are obtained by first calculating the standard deviation of $U_{R1(\omega)}, U_{T3(\omega)}, K_{(\omega)}$ for all measured data, and then calculating the standard deviation of the attenuation at each frequency. In this current study we are interested in the attenuation at frequencies below 120 kHz. One possibility is to extrapolate the attenuation data measured in the MHz range into the kHz using linear regression starting from the origin, and then using the slope of this line to determine the attenuation coefficient of the material and this method has been reported by other researchers [15, 16, 20]. Another possibility is to use relations between the longitudinal speed spectra and the longitudinal attenuation spectra [76-78], and this procedure is reviewed in the next section.

It is difficult to validate the experimental results for longitudinal acoustic speed and attenuation obtained in this study by comparing them with data reported in the literature. This is mostly because of the limited data in the literature on acoustic properties for this type of coating material. The acoustic properties may also vary significantly between the different bitumen materials, even if they look similar in appearance. However, the results achieved in the previous section are generally in good agreement with the results reported

in Table 3.2, which summarise the bulk longitudinal acoustic properties of bitumen coatings reported in the literature.

However, a partial validation of the experimental methods described in the previous section, comes from the fact that the acoustic speed spectra and attenuation spectra obtained for the bitumen material investigated are in reasonable agreement with the relations described by Kazys et al. [76]. They also note that the bulk attenuation spectra can be derived from the attenuation spectra and vice versa, and Kazys et al. define the bulk attenuation and bulk velocity spectra using Eqs. (3.7) and (3.8), which are derived from the Kramers-Kroning relations described in [77]:

$$\alpha(\omega) = \frac{\pi\omega^2}{2C_{aL,S}v_p^2(\omega)}\frac{dv_p(\omega)}{d\omega}, \tag{3.7}$$

$$\frac{1}{v_p(\omega_R)} - \frac{1}{v_p(\omega)} = \frac{2}{\pi}\int_{\omega_2}^{\omega_1}\frac{\alpha(\omega')}{\omega'^2}d\omega'. \tag{3.8}$$

Here $v_p(\omega_R)$ is the acoustic velocity at the reference frequency $\omega_R = 2\pi f_R$, ω_1 and ω_2 define the frequency range of investigation, and $\alpha_{L,S}(\omega)$ is the bulk attenuation in nepers per m.

In order to understand how well the measured experimental data corresponds with the relations in [76], the bulk velocity dispersion spectra $v_p(f)$ is calculated from the measured attenuation spectra $\alpha(f)$ using Eqs. (3.9) and (3.10) reported by Kazys et al. [76]:

$$\frac{1}{\Delta v(f)} = (2\pi)^n\frac{\alpha_R}{f_R^n\pi^2(n-1)}(f^{n-1} - f_R^{n-1}) \tag{3.9}$$

$$v_p(f) = \frac{v_p(f_R)}{1-\frac{v_p(f_R)}{\Delta v(f)}} \tag{3.10}$$

Here α_R is the measured attenuation in $\mathrm{dB/cm}$ and $v_p(f_R)$ is the measured bulk velocity in $\mathrm{m/s}$ at reference frequency f_R (in Hz) and n is the power in the power-law dependence. The attenuation spectra $\alpha(f)$ is then given as

$$\alpha(f) = a_0(\frac{f}{f_o})^n \tag{3.11}$$

The value of n may be determined by fitting a power trend line to the experimentally measured attenuation spectra, as shown in Figure 3.13. The value obtained is $n = 1.628$.

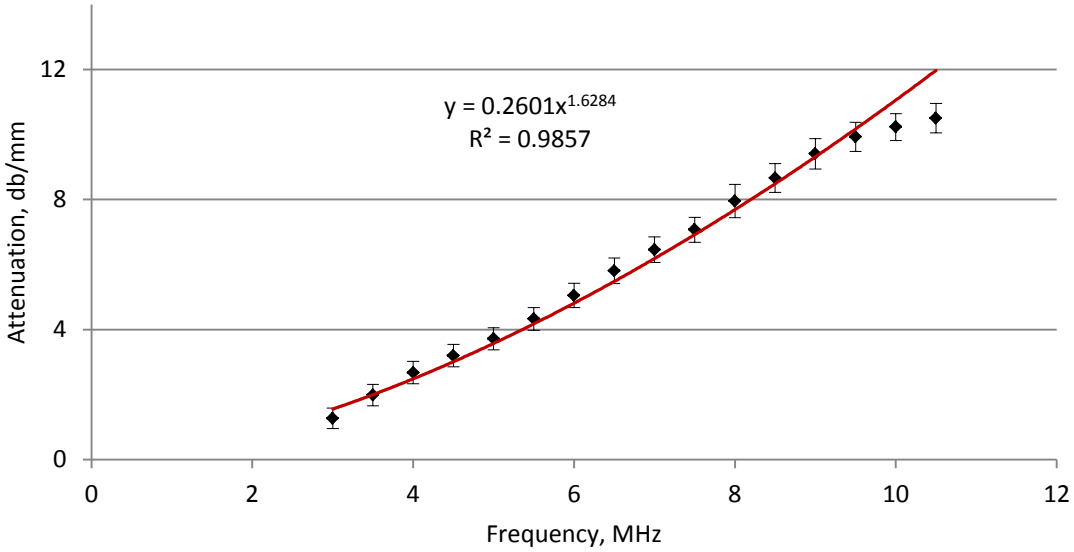

Figure 3.13: Attenuation spectra. Experimental result (♦). Best fit power trend line (—).

The following values are then used to solve Eqs. (3.9) and (3.10): a reference frequency $f_R = 7$ MHz, a reference bulk velocity $v_p(f_R) = 1893.45$ m/s, a reference bulk attenuation $\alpha_R = 64.5$ dB/cm, and $n = 1.628$. The measured longitudinal velocity calculated using these data is shown in Fig. 3.14 and this is seen to correlate well with predictions based on Eqs. (3.9) and (3.10).

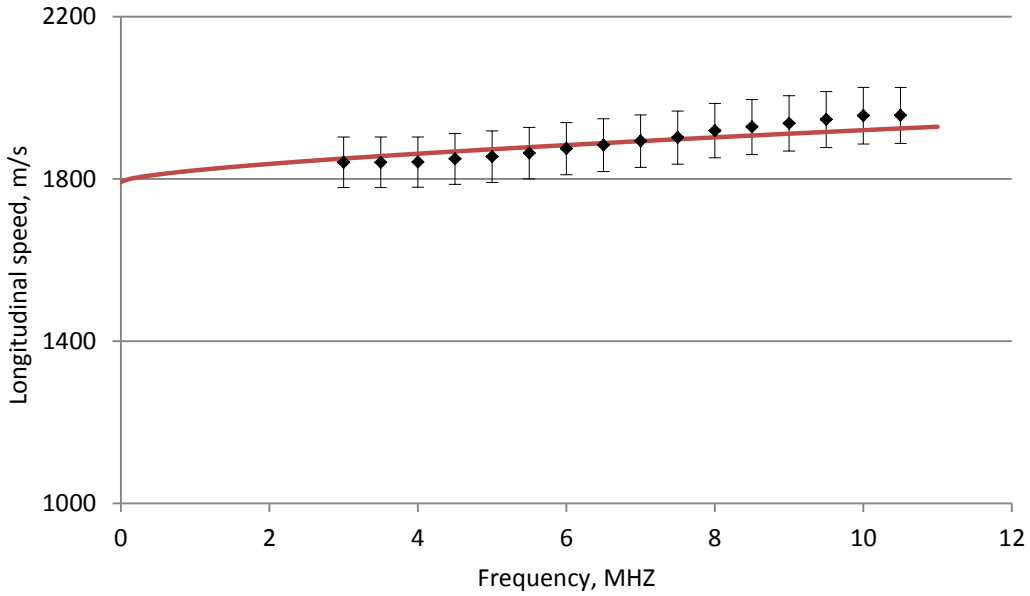

Figure 3.14: Longitudinal speed of Bitustik 4000. Experimental data (♦) Prediction based on (3.9) and (3.10) (—).

The predictions also confirm that the bulk speed in highly attenuative materials is dispersive and it increases with frequency. In reality, all materials exhibit some attenuation which leads to changes in their bulk acoustic speed and dispersion. These phenomena have also been reported elsewhere [80, 81]. The validity of the data presented is further investigated in the next section. Where the values determined by extrapolation of the data towards low frequencies are compared against data reported in the literature.

3.4 Acoustic properties of Bitustik 4000 below 100kHz

The bulk longitudinal properties measured between 3 MHz and 10.5 MHz are not directly applicable in the frequency range of interest. One possibility is to extrapolate the experimental measurements below 100 kHz using the relations obtained in Section 3.4. Figure 3.15 shows the longitudinal acoustic speed between 20 kHz and 100 kHz calculated using Eqs. (3.9) and (3.10), and this demonstrates relatively low levels of dispersion.

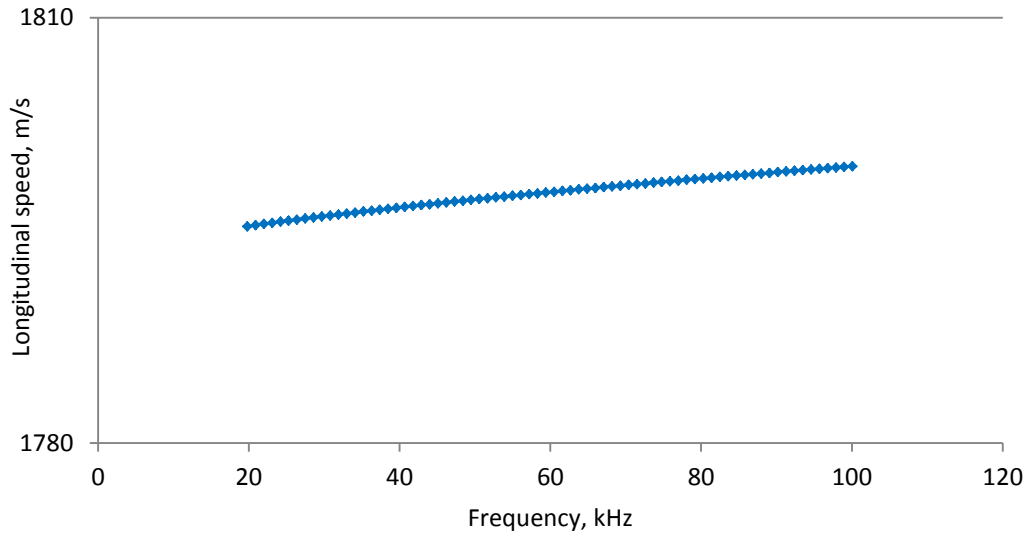

Figure 3.15: Longitudinal acoustic speed based on Eqs. (3.9) and (3.10).

The actual dispersion determined from the data presented in Figure 3.15 is less than ±0.2% for a mean value of 1798 m/s. This means that the longitudinal speed can be approximated as constant over the frequency range, with little reduction in accuracy and so a value equal to $\tilde{a}_c = 1798\ \mathrm{m/s}$ is specified here.

The longitudinal attenuation was also measured between 3MHz and 10.5MHz. The attenuation data is extrapolated to below 100 kHz using an exponential line fitted through the experimental data shown in Figure 3.13. The extrapolated attenuation data is shown in blue in Fig. 3.18. It is seen in Fig. 3.18 that at lower frequencies the experimental data follows an approximately linear relationship with frequency. In the literature it is normally assumed that the longitudinal attenuation is approximately constant over the limited frequency range shown in Fig. 3.18 and so this assumption is also adopted here, especially as it is seen to fit with the extrapolated experimental data reasonably well. A linear relationship with frequency is shown in Fig. 3.18 where the gradient is determined using a line that starts from the origin to avoid negative values. The gradient of the linear regression curve in Fig. 18 yields a longitudinal attenuation of $\alpha_L = 0.94 \times 10^{-6}\ \mathrm{s/m}$.

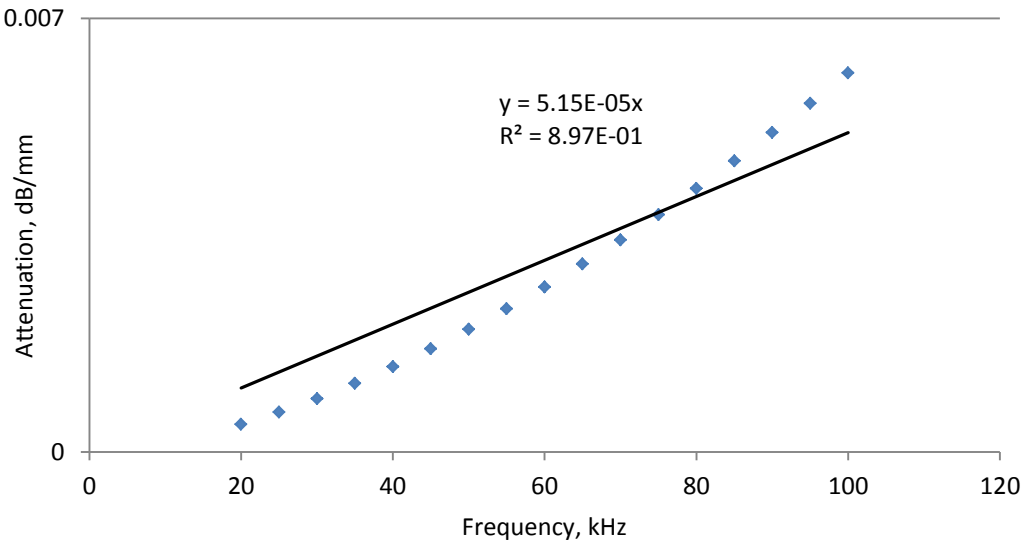

Figure 3.16: Longitudinal attenuation. Extrapolated data (♦) Lin. best fit line (—).

The validity of the bulk longitudinal properties measured here are investigated by comparison with data on bitumen bulk longitudinal properties reported in the literature. This is shown in Table 3.2 and Fig. 3.17, which summarise data reported by other researchers whose studies were also reviewed in Chapter 2. The last row of Table 3.2 also shows the bulk longitudinal acoustic properties of Bitustik 4000 determined in this section.

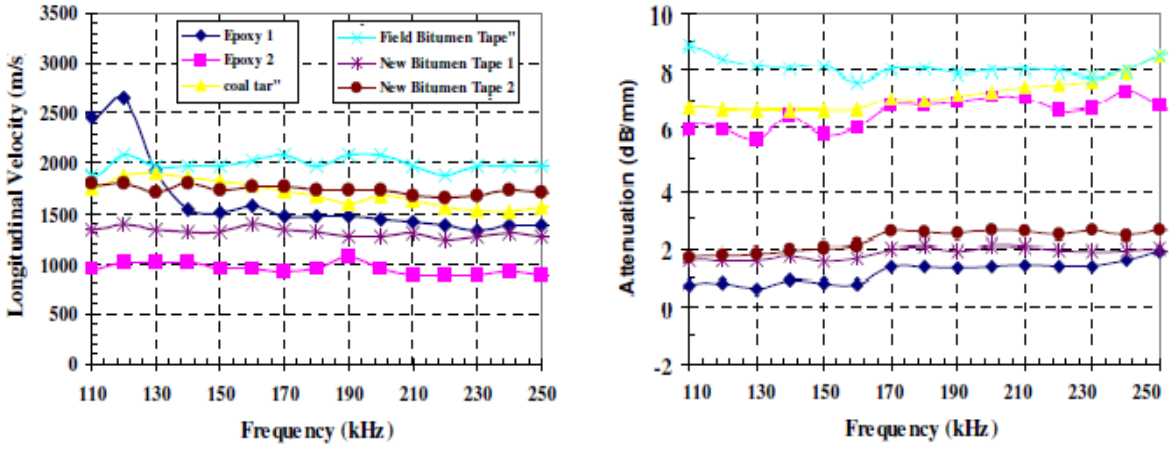

Figure 3.17: Bulk longitudinal acoustic properties of coating materials reported in [53].

		$\tilde{a}_c$	α_L	Frequency	Density	Thickness	Source
No	Material	m/s	s/m	MHz	kg/m^3	mm	-
1	Bitumastic B50	1900	52e-6	3-8	1200	0.27	[16]
2	Bitumen Tape BT	1900	47e-6	1-13	1200	0.74	[16]
3	Bitumastic B300M	1500	62e-6	3-8	600	0.20	[16]
4	Bitumastic B50	1860	23e-6	1-5	1500	0.15	[20]
5	Bitumen Tape BT	1900	47e-6	1-13	1200	0.74	[15]
6	Bitumastic B50	1900	52e-6	3-8	1200	0.27	[15]
7	Field tape	2000	862e-6	0.11-0.25	1100	1.50	[53]
8	New tape 1	1350	220e-6	0.11-0.25	1308	1.00	[53]
9	New tape 2	1800	293e-6	0.11-0.25	1107	1.00	[53]
10	Bitustik 4000	1798	0.94e-6	2-11	990	1.25	Ch. 3

Table 3.2: Bulk longitudinal acoustic properties of bitumen coating materials.

The bulk longitudinal acoustic speed $\tilde{a}_c = 1855\ \mathrm{m/s}$ of $\mathrm{Bitustik\ 4000}$ corresponds well with data on bitumen reported by other researchers. However, the measured bulk longitudinal attenuation constant of $\alpha_L = 0.94 \times 10^{-6}\ \mathrm{s/m}$ is much lower in comparison with the majority of values reported in Table 3.2. Partial validation of the attenuation values measured in the MHz frequency range comes from the fact that they correspond well with the attenuation values ($2 - 4\ \mathrm{dB/mm}$ at $4\ \mathrm{MHz}$) reported in [82] for highly viscoelastic rubber materials, which are quite frequently used as additives in bitumen materials [83]. This raises questions about the assumption that the attenuation of the bitumen material investigated is continuously increasing with frequency and that there are no local minima or maxima in the attenuation spectra. In reality, it might appear that below 100 kHz the attenuation spectra does not follow the power-law dependence of Eq. (3.11).

The next step is to determine the bulk shear acoustic properties of the bitumen material of interest. The literature review presented in Chapter 2 showed that the measurement of the bulk shear properties of highly viscoelastic materials like bitumen is quite difficult and the shear properties also have a strong influence on guided wave attenuation in coated pipes.

The following section deals with measurement of the bulk shear acoustic properties of $\mathrm{Bitustik\ 4000}$. The section presents a new hybrid method which is based on conventional

through-transmission technique, but also utilises the fundamental shear guided wave mode T(0,1).

3.5 Bulk shear acoustic properties

Measuring bulk shear acoustic properties is difficult because of the very high levels of attenuation found in these materials. It is possible to use conventional ultrasonic techniques such as the pulse-echo and through-transmission techniques described in [84, 85] but these become difficult to apply to highly attenuative materials. In these techniques the acoustic speed and attenuation is determined by measurement of the time of flight as well as the drop in amplitude of a bulk wave traveling through a viscoelastic specimen [15, 16, 20]. However, these methods have only been applied in the MHz frequency range and they are not applicable in the frequency range of interest here, which is between 20 kHz and 100 kHz. Another disadvantage of the bulk wave based methods is that they are always accompanied with difficulties related to acoustic beam spreading and acoustic coupling between the transducers and the specimen [14].

The guided wave based frequency interferometry method proposed by Simonetti [14, 49] solves most of the difficulties related to the methods based on bulk waves. This method relies on the resonant behaviour of a cylindrical solid specimen clamped between two identical rods. A good overview of this technique can also be found in [86-88]. The method involves measuring the transmission and reflection coefficients through the specimen using two rods working as delay lines which drive an acoustic wave pulse through the sample. The frequencies where the transmission maxima and reflection minima occur correspond to the through thickness resonance of the viscoelastic specimen. This method is applicable to solid materials which do not tend to flow under the clamping load. The accurate determination of speed relies on through thickness resonance occurring in the frequency range of interest. The viscoelastic material Bitustik 4000, which needs to be characterised in this study, is in semi-solid state and it tends to flow under relatively low external clamping loads. The preliminary calculations based on the material's thickness (~1.2 mm) and expected shear acoustic speed (400-700 m/s, using data from the literature) shows that the first through thickness resonance will occur outside of the frequency range of interest

here. This makes the method proposed by Simonetti not applicable for measurement of the shear acoustic properties for the current study.

The aim of the current study is to determine the shear bulk speed and attenuation in the viscoelastic material of interest at 20°C and below 120 kHz. In general bulk waves and guided waves propagation characteristics are not the same for a given material/waveguide. In general, the bulk longitudinal and shear acoustic speeds are not equal to the phase speed of guided shear and longitudinal modes. However, there are some exceptions like the propagation characteristics of the shear bulk wave and the fundamental shear mode T(0,1) in cylindrical structures, where the acoustic speed and the attenuation of the shear bulk waves are equal to the phase speed and attenuation of the shear fundamental mode T(0,1). This relation is described by Simonetti [14]. In order to use this relation to find viscoelastic properties for the current study, the material under investigation is be formed into a short tube, as shown in Figure 3.18. The material studied here is in a semi-solid state and this allows it to be shaped in a tube with a relatively small diameter (10-20 mm). The cross section, A, of the tube with a known length, L, could be excited by a few cycles of a tone burst signal in a way which preferentially generates the T(0,1) mode in the tube. The amplitude and the time of flight of the acoustic signal transmitted through the tube at cross section B is then measured and recorded. In order to reduce the errors and simplify the derivation of the phase speed and attenuation, the experiment is repeated with a tube of length $L + x$.

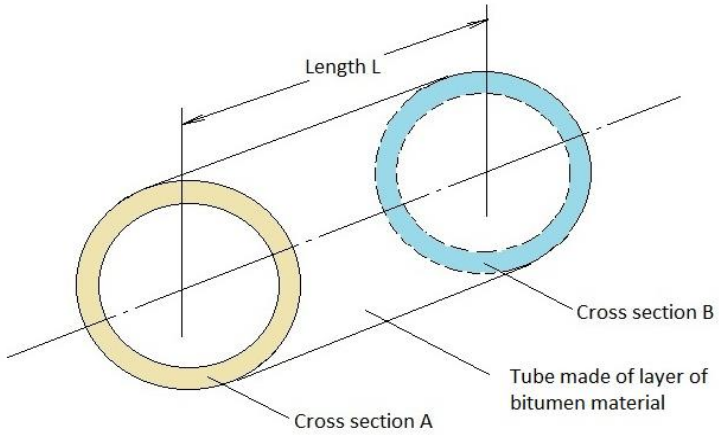

Figure 3.18: Tube made of thin layer of bitumen material.

The use of two separate measurements means that the phase speed and attenuation can be calculated in the same way as the conventional bulk wave based ultrasonic through-transmission technique. The shear phase speed $\tilde{c}_c$ [m/s] and shear attenuation A_s [dB/mm] is then calculated using the following equations:

$$\tilde{c}_c = \frac{t_{l+x} - t_l}{x} \tag{3.12}$$

$$A_s = \frac{20 * \log(A_{l+x}/A_l)}{x} \tag{3.13}$$

where t_{l+x} and t_l is the time required for the signal to travel through each specimen, and A_{l+x} and A_l is the amplitude of the signals transmitted through the specimen and measured at cross section B. Undertaking the measurements described is however not an easy task because a specialised experimental set up is needed. One possibility to do this is to use the method described in the next section.

3.6 Method for measuring bulk shear acoustic properties

The experimental setup shown in Figure 3.19 consists of two identical 1500 mm long aluminium tubes with external diameter of 16 mm and wall thickness of 1.5 mm. The alignment of the tubes is maintained using four supports made of low density polymer. The supports were manufactured and arranged in a way which allowed the tubes to align and slide axially in order to have the possibility to adjust the gap between them. A pair of Teletest® shear mode piezoelectric transducers generating in plane displacements were mounted at the end of each tube. The transducers are aligned with the tubes in a such way that the in plane displacements generated are directed along the circumference of the tubes, which excites the T(0,1) mode. More information about the transducers and their operation can be found in [33]. A second pair of shear mode transducers is also mounted 1000 mm from the end of each tube. The second pair of transducers monitors the amplitude of the incident pulse as well as the pulse reflected from the end of the tube. The position and orientation of the transducers is shown in Figure 3.19.

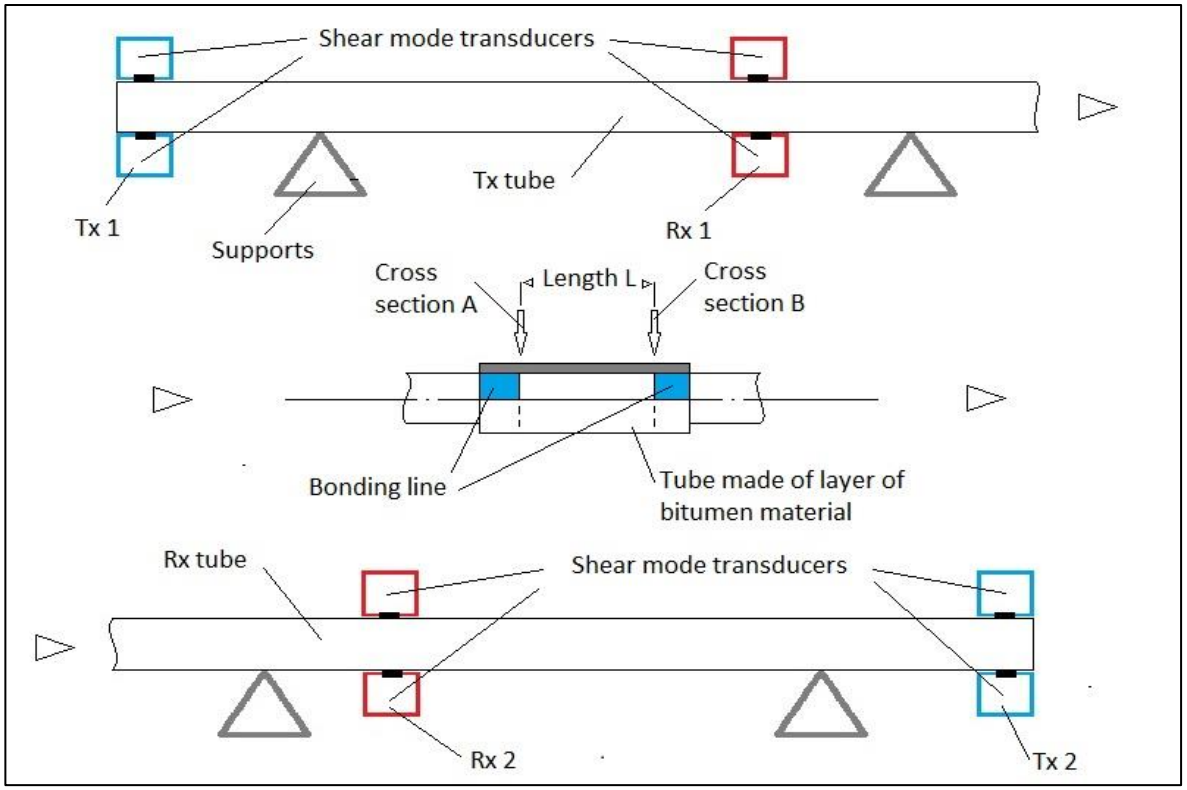

Figure 3.19: Experimental setup.

All transducers were permanently attached to the tubes by using Araldite 2011 [89]. The acoustic response of each tube was evaluated by exciting T(0,1) using 10 cycles of a Hanning modulated tone burst signal applied to the first pair of transducers, and monitoring/recording the propagation of the signal along the pipe. Initial tests showed that the T(0,1) mode could be successfully generated in the tubes between 20 kHz and 100 kHz, with a typical signal to noise ratio of between 32 dB and 36 dB. After the initial tests the distance between the tubes was set equal to 5mm and the tubes were firmly clamped by a purpose made U shaped clamp shown in Figure 3.20. A rectangular piece of Bitustik 4000 material was cut and wrapped around the ends of the tubes forming a 15mm long bitumen tube. The seam of that tube was formed by pressing the ends of the viscoelastic material to one another. The adhesive bond to the tubes in the area of the seam was ensured by the excellent adhesive qualities of the viscoelastic material investigated. However, special care was taken when the seam was formed so it does not affect the geometry of the tube.

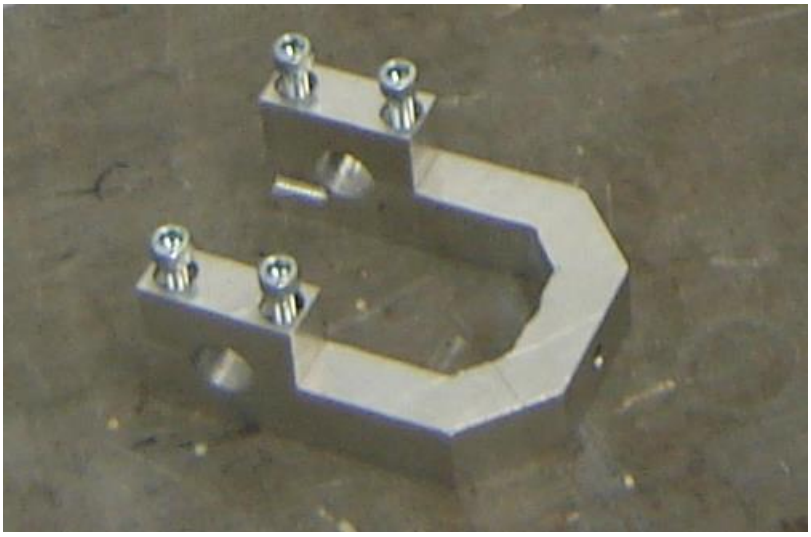

Figure 3.20: U shaped clamp.

The width of the bonding line between the bitumen material and the end of each tube was kept at 5 mm. When the measurements with 5 mm separation between the tubes were finished, the 15 mm long bitumen tube was removed and the tubes ends were cleaned with organic solvent. The distance between the tubes was set to equal 10 mm and a single layer of 20 mm long rectangular bitumen material was wrapped around the ends. The wrapped bitumen material then forms a 20 mm long bitumen tube. The width of the bonding line at the ends of the aluminium tubes was again kept equal to 5 mm.

In order to simplify the following explanations, the left positioned tube will be referred as the Tx tube, the right positioned tube will be referred as Rx tube, the boundary between the Tx tube and the bitumen tube will be referred as Tx/Bitu, and the boundary between the viscoelastic tube and the Rx tube will be referred as the Bitu/Rx boundary. The pair of shear transducers mounted on the tubes will be referred to using the labels shown in Figure 3.19.

The Tx1 transducers are excited in T(0,1) mode using a ten cycle of Hanning window. The amplitude of the incident signal I and the reflected signal R from the Tx/Bitu boundary at the end of the Tx tube was monitored by the Rx1 transducers. This measurement ensures that the same amount of energy is transmitted towards the bitumen tube through the Tx/Bitu boundary. The signals recorded when the length of the bitumen tube was 15 mm

and 20 mm are shown in Fig. 3.21 (a) and (b), respectively. The spike between 0 ms and 200 ms is the result of the pulse/receiver signal generation.

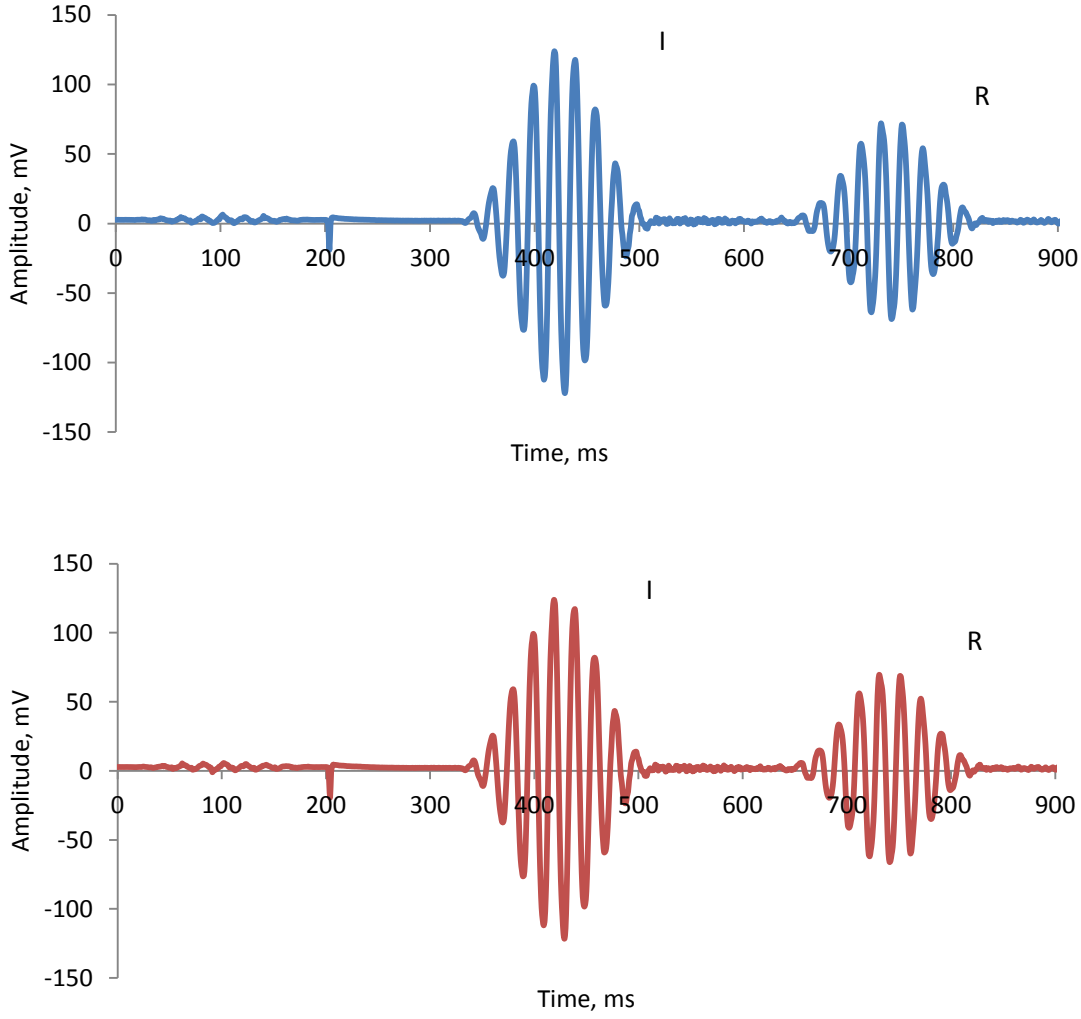

Figure 3.21(a) Rx1 signals at 50 kHz, 15 mm bitumen tube length; (b) Rx1 signals at 50 kHz, 20 mm bitumen tube length.

The signal T transmitted through the Tx/Bitu boundary, the bitumen tube Bitu/Rx boundary, and transmitted towards the Rx tube was monitored using the Rx2 transducers mounted on the Rx tube. The signals T_{15} and T_{20} are recorded at 50 kHz when the length of the bitumen tube was 15mm and 20mm, respectively, and these are shown in Fig, 3.22 (a) and (b).

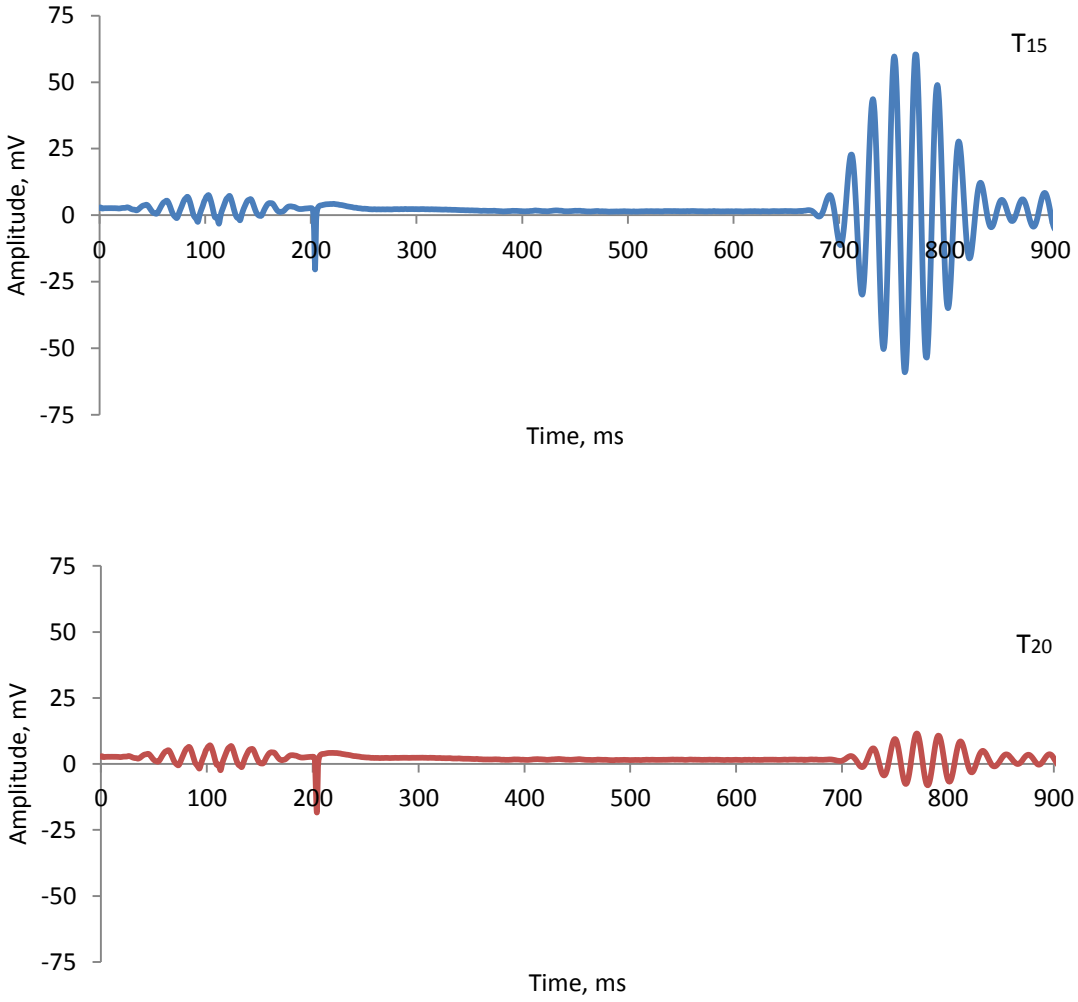

Figure 3.22 (a) Rx2 signals at 50 kHz, 15 mm bitumen tube length; (b) Rx2 signals at 50 kHz, 20 mm bitumen tube length.

The coupling at the Bitu/Rx boundary was monitored by exciting the Rx tube only, with the Tx2 transducers in T(0,1) mode, and monitoring the amplitude of the signal incident to and reflected from the Bitu/Rx boundary and the end of the Rx tube. This measurement was done in order to ensure that the coupling at Bitu/Rx boundary was kept the same during each experiment. The signals recorded when the length of the bitumen tube was 15 mm and 20 mm are shown in Fig. 3.23 (a) and (b), respectively.

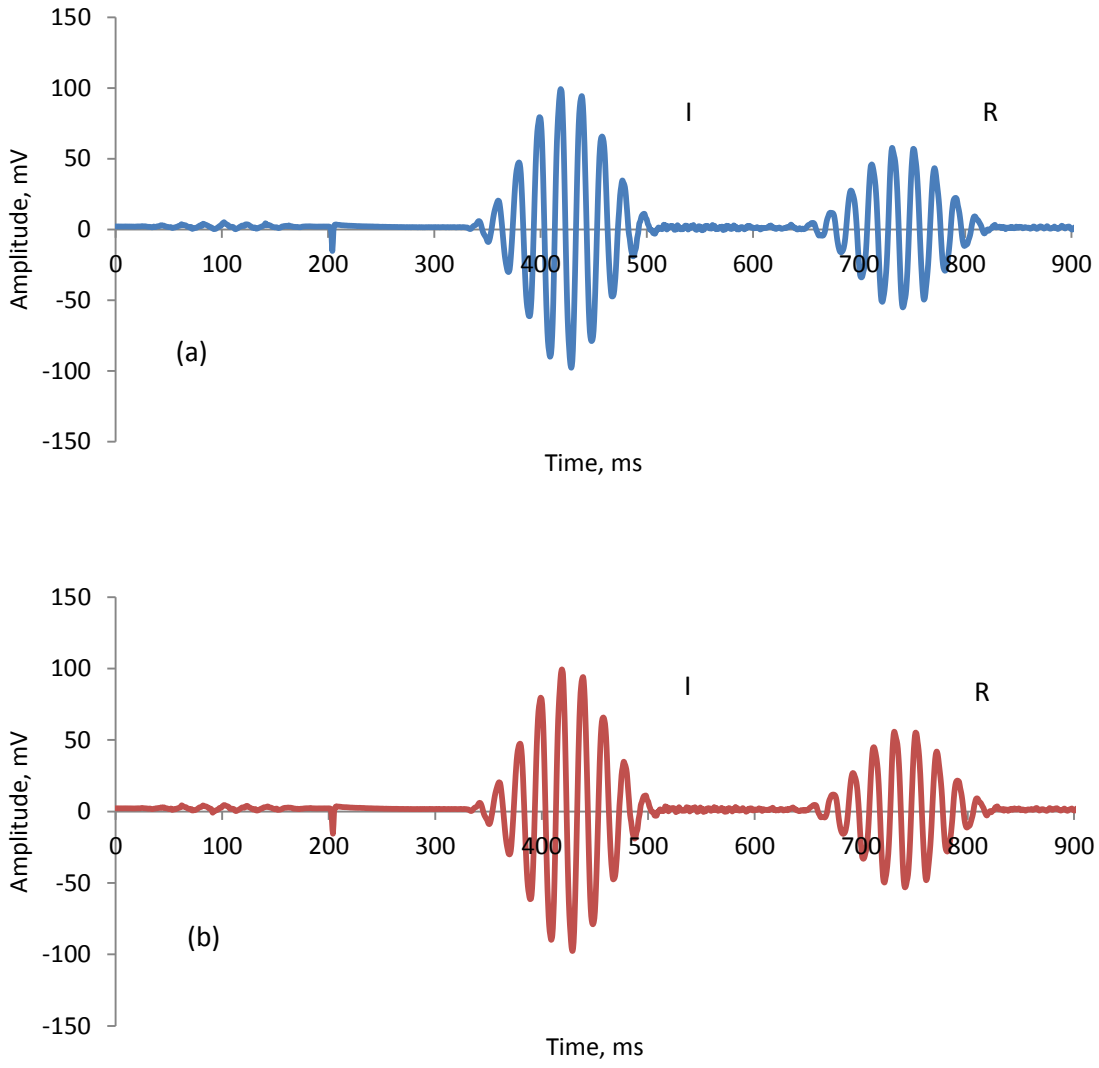

Figure 3.23 (a) Rx2 signals at 50 kHz when the end of the Rx tube was excited, 15 mm bitumen tube length (b) Rx2 signals at 50 kHz when the end of the Rx tube was excited, 20 mm bitumen tube length.

During the data collection the ambient temperature was monitored with a thermocouple attached to the bitumen tube, and this was measured to be 20°C. The frequency content of the Hanning modulated excitation pulse was varied between 20 kHz and 100 kHz in 5 kHz steps. At each frequency step the data was collected 64 times and averaged in order to reduce the level of random noise. The experiment was repeated three times with 15 mm, 20 mm and 25 mm bitumen tube lengths. However, it was found that the signal to nose ratio for the 25 mm measurements was not acceptable and so this set of data was discarded.

3.7 Data processing and results

The stability of the coupling at the Tx/Bitu and Bitu/Rx boundaries is investigated first by calculating the transmission coefficient at the boundaries using the six data sets. The transmission coefficient is calculated using Eq. (3.14) and this will generate the part of the energy transmitted towards the bitumen tube when it was independently excited in the T(0,1) mode. This gives

$$T(f_n^c) = 1 - \frac{A_n^R(fft)}{A_{n(fft)}^I}; \quad 1 < n < 17, \tag{3.14}$$

where $T(f_n^c)$ is the transmission coefficient at centre frequency f_n^c, and $A_n^I(fft)$ and $A_n^R(fft)$ are the Fourier transforms of the incident and reflected signals with a centre frequency f_n^c. Each signal was windowed with a rectangular window selected to be 20% wider than the original length of the signal in the time domain. The Fourier transform of the signals was calculated by using the MATLAB "fft" function. This was repeated for all sixteen data sets collected between 20 kHz and 100 kHz in 5 kHz steps. The incident and reflected signals for a 50 kHz centre frequency that have been used to calculate the transmission coefficients at the Tx/Bitu and Bitu/Rx boundaries are shown in Fig. 3.21 (a) and (b), and Fig. 3.23 (a) and (b), respectively. Figure 3.24 (a) and (b) also show the reflection coefficients calculated for the Tx/Bitu and Bitu/Rx boundaries, respectively.

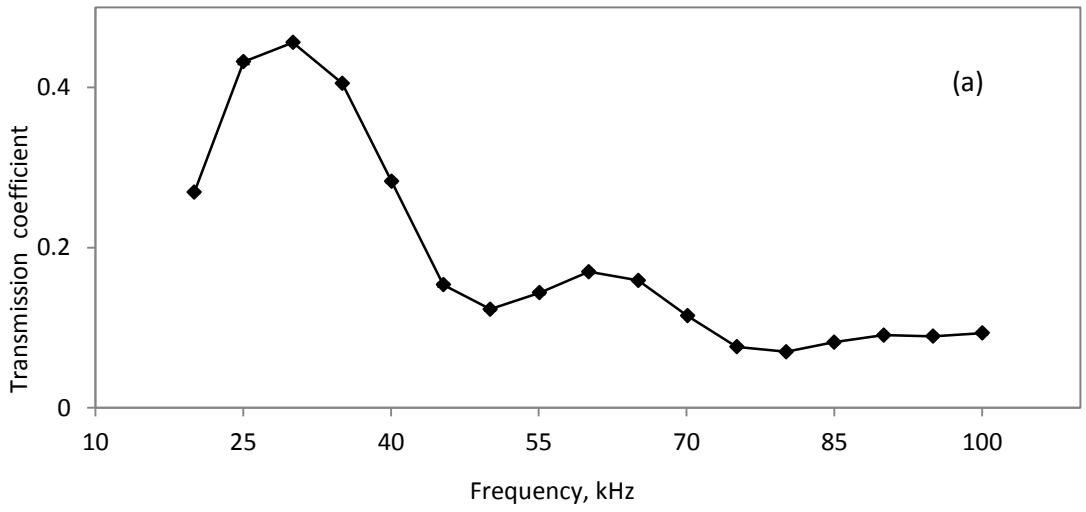

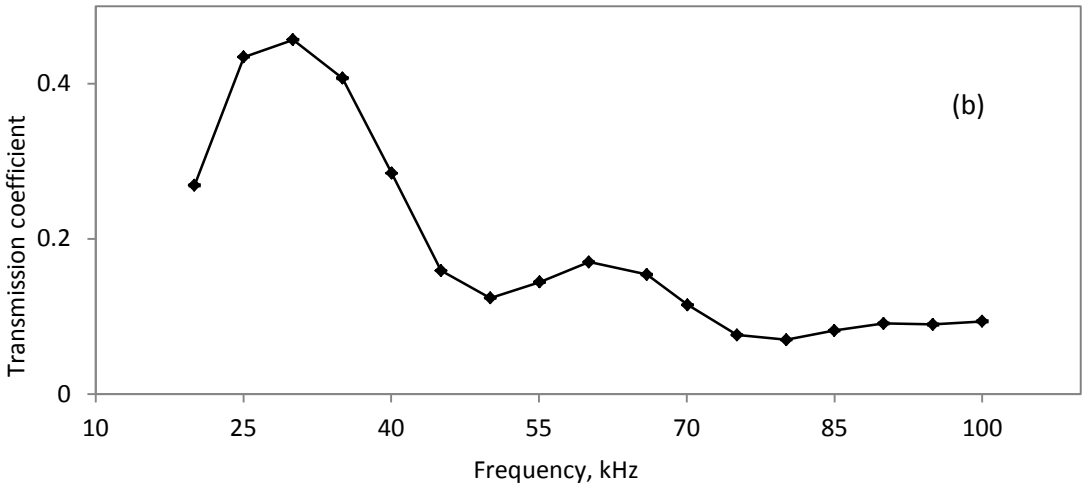

Figure 3.24 (a) Transmission coefficient at the Tx/Bitu boundary; (b) Transmission coefficient at the Bitu/Rx boundary.

The measurement of transmission coefficient at the Tx/Bitu and Bitu/Rx boundaries shows a standard deviation of less than 1.7% for all six data sets.

The bulk shear speed and attenuation in Bitustik 4000 was determined by processing the experimental data in the time-frequency domain using the MATLAB code shown in Appendix. The signals transmitted through the bitumen tube when the gap between the tubes was 5 mm and 10 mm were windowed with a rectangular window that is 20% wider than the original length of the signals, and this is shown in Fig. 3.25.

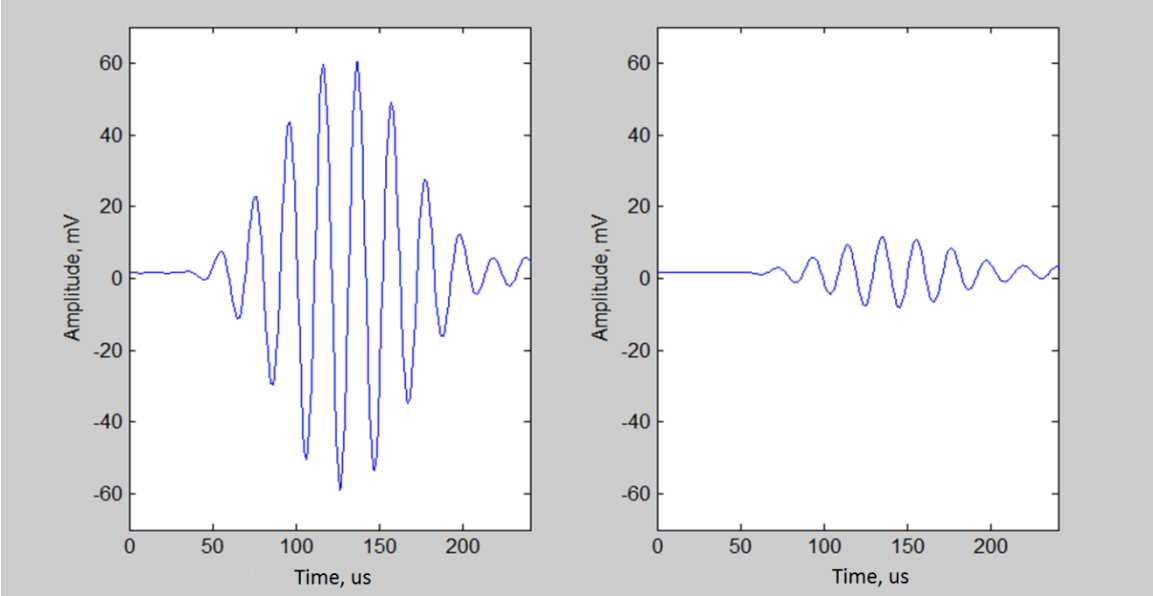

Figure 3.25: Transmitted signals at 50 kHz.

The spectrogram of the signals is shown in Fig. 3.26 and this was calculated using the MATLAB "*specgram*" function, see the Appendix.

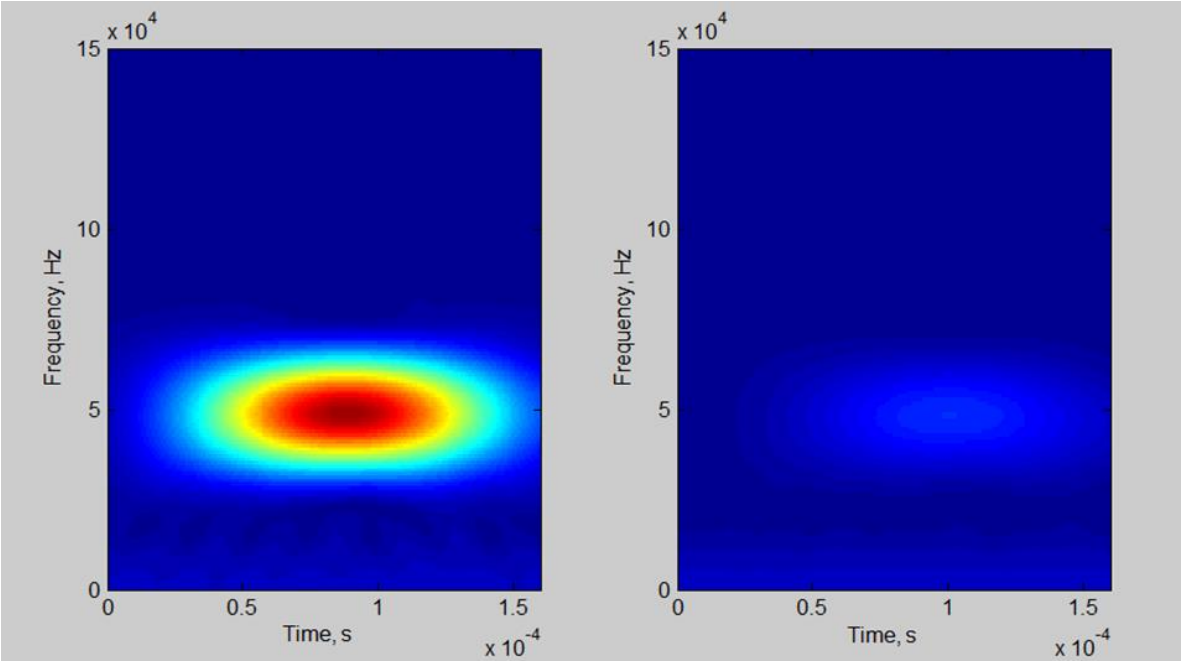

Figure 3.26: Spectrogram of the transmitted signals at 50 kHz.

For a reference frequency f_n^r, the time of flight and amplitude corresponding to the maximum amplitude of the signal are denoted t_n^5, A_n^5, respectively for the 5 mm gap, and t_n^{10} , A_n^{10} and f_n^r for the 10 mm gap. These values are calculated for each data set consisting of 17 A-scans covering a frequency range between 20 kHz and 100 kHz using 5 kHz steps. The frequency dependent amplitudes A_n^5 and A_n^{10} are then used to calculate nine frequency dependent attenuation spectra $A_s(f)$ using Eq. (3.15):

$$A_s(f_n^r) = \frac{20\log(A_n^5/A_n^{10})}{\Delta x}; \quad 1 < n < 17, \tag{3.15}$$

where Δx is the difference in the gap between the two measurements. Figure 3.27 shows the averaged frequency dependent shear attenuation, with values for the standard deviation determined from the nine attenuation measurements.

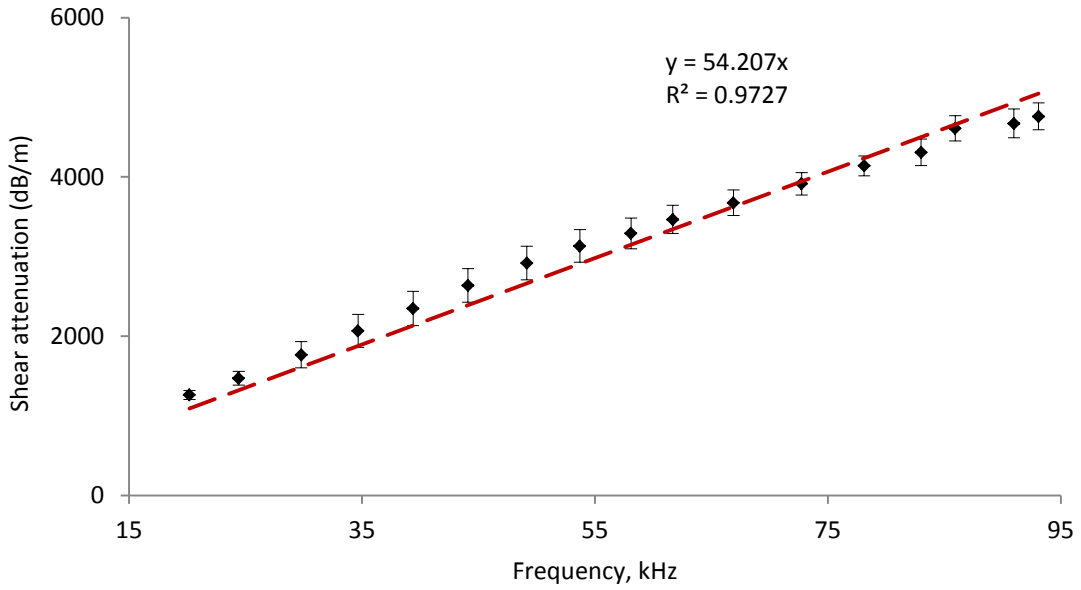

Figure 3.27: Shear attenuation. Experimental data (♦), Linear best fit line (—).

The shear attenuation constant, α_c, is determined by fitting a straight line through the data in Fig. 3.27 and using the gradient of this line to calculate the shear attenuation constant. This gives a value of $\alpha_c = 0.994 \times 10^{-3}$ s/m.

The shear speed is determined in the frequency domain using Eq. 3.16, and the frequency dependent time of flight t_n^5 and t_n^{10} is determined from the data sets collected when the tubes were separated 5mm and 10mm, respectively.

$$\tilde{c}_c(f_n^r) = \frac{t_n^{10} - t_n^5}{\Delta x}; \qquad 1 < n < 17\ . \tag{3.16}$$

Here, Δx is the difference in the gap between the tubes for the two measurements. Nine frequency dependent shear speed spectra were calculated and the averaged of this date is shown in Fig. 3.28.

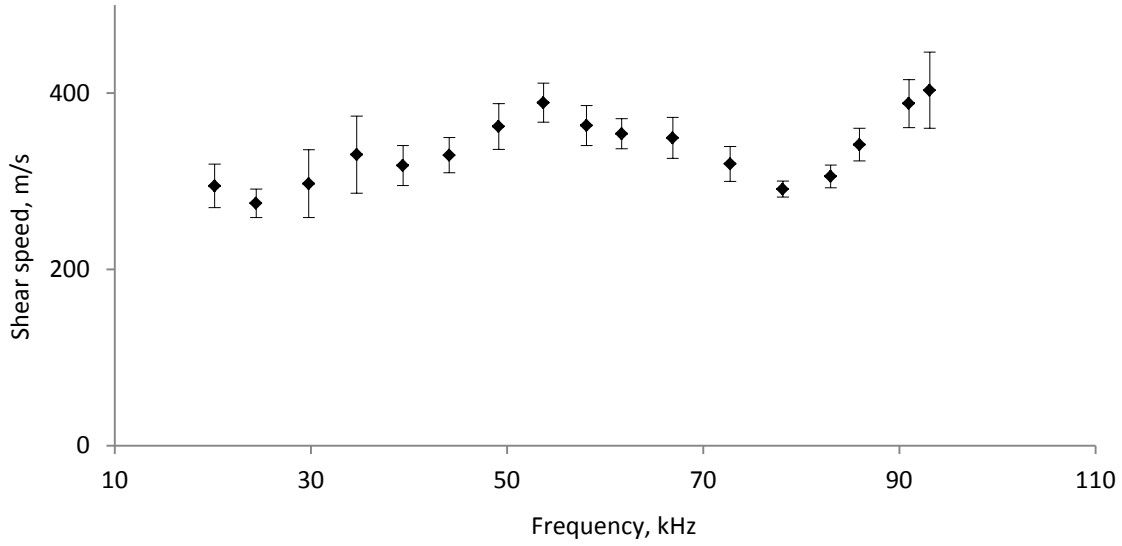

Figure 3.28: Shear speed in Bitustik 4000.

The measured values for shear speed shown in Fig. 3.28 vary with frequency. However, it should be remembered here that very high levels of shear attenuation are often found in a viscoelastic material and this makes it difficult to measure the shear properties accurately. This is because of the significant drops in the level of a signal over a relatively short distance in the material. In the literature $\tilde{c}_c$ is normally accepted to be constant [15, 16, 20] and so for the theoretical predictions that follow a constant value for $\tilde{c}_c$ is also chosen here. Following this approach the data in Fig. 3,28 was averaged to give a value of $\tilde{c}_c = 336\ \mathrm{m/s}$.

It is difficult to validate the bulk shear properties of Bitustik 4000 coating determined in this section. This is because this type of coating material has not been studied by other researchers and so values for its bulk shear properties are not available. One possibility is to compare this data with other data reported in literature for similar materials, and Table 3.3 summarises measured values for bulk shear acoustic properties of bitumen. Table 3.3 shows that the measured shear acoustic speed of $\tilde{c}_c = 336\,\mathrm{m/s}$ for Bitustik 4000 is approximately half that of the shear speed measured for other bitumen materials. However, the bitumen materials in Table 3.3 with a bulk shear speed of $\tilde{c}_c > 624\,\mathrm{m/s}$ are for materials in a solid state. The only value which is close to the measured bulk shear acoustic speed of $C_{Sc} = 338\,\mathrm{m/s}$ for Bitustik 4000 is the value of $\tilde{c}_c = 430\,\mathrm{m/s}$ measured for the liquid bitumen material TML 24515. This could validate the data for the semi-solid Bitustick 4000 as this also deforms plastically under very low external pressure.

		$\tilde{c}_c$	α_c	Frequency	Density	Thickness	Source
No	Bitumen material	m/s	s/m	-	kg/m3	mm	-
1	Bitumastic B50	750	520 x e-6	3-8 MHz	1200	0.27	[16]
2	Bitumen tape BT	860	470 x e-6	1-13 MHz	1200	0.74	[16]
3	Bitumastic B300M	680	620 x e-6	3-8 MHZ	600	0.20	[16]
4	Bitumastic B50	750	240 x e-6	1-5 MHZ	1500	0.15	[20]
5	Bitumen tape BT	850	597 x e-6	80 kHz	1200	0.74	[15]
6	Bitumastic B50	860	142 x e-6	80 kHz	1200	0.27	[15]
7	Field tape	1550	183 x e-6	0.5-0.9 MHz	1100	1.50	[53]
8	New tape 1	1250	422 x e-6	0.5-0.9 MHz	1308	1.00	[53]
9	New tape 2	1600	312 x e-6	0.5-0.9 MHz	1107	1.00	[53]
10	TML 24515 liquid	430	510 x e-6	10-80 kHz	970	-	[14]
11	Bitumen Dallington	770	123 x e-6	20-120 kHz	1750	4.90	[14]
12	Bitumen Kuwait	1012	385 x e-6	20-120 kHz	1640	4.90	[14]
13	Bitumen Oncor	1065	678 x e-6	20-120 kHz	1442	4.90	[14]
14	Bitumen Louisiana	642	788 x e-6	20-120 kHz	1544	4.90	[14]
15	Bitustik 4000	338	994 x e-6	20-100 kHz	990	1.25	Ch. 3

Table 3.3: Bulk shear acoustic properties of bitumen based coating materials.

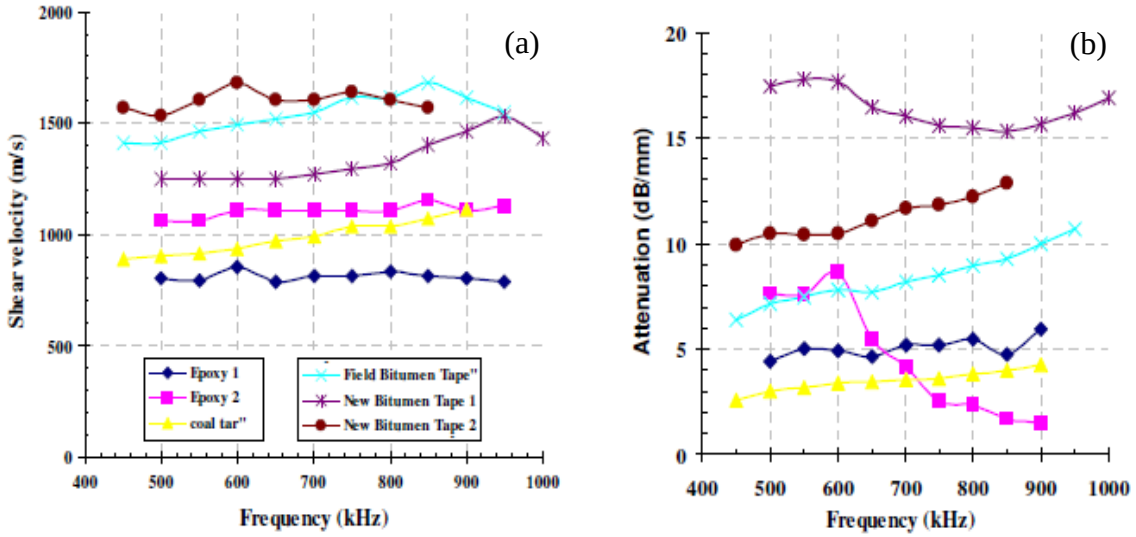

Figure 3.29: Bulk shear acoustic properties of coating materials from [53]: (a) Shear velocity; (b) Attenuation.

The measured data for the bulk shear speed in Fig. 3.28 for Bitustick 4000 is seen to compare well with data taken from the literature shown in Figure 3.29 (a). Note that there is also some variation in the data for shear speed in Fig. 3.29 (a) and this is further evidence of the difficulty of measuring this value accurately over an extended frequency range. The data shown from the literature for attenuation in Fig. 3.29 (b) also correspond well to the general trend for the attenuation seen in Fig. 3.27 for Bitustick 4000, at least for those materials that may be considered to be similar in construction.

The validity of the bulk shear properties of Bitustik 4000 coating determined in this section, and the assumptions about the constant acoustic speed and linearly increasing attenuation will be further investigated in Chapter 6, where numerical predictions of guided wave attenuation based on the bulk shear properties determined in this section will be compared against measurements on a coated pipe.

3.8 Summary

A novel technique for acoustic characterisation of shear properties in a semisolid bitumen based coating material has been presented. It was demonstrated that the bulk shear speed

and attenuation of a semisolid viscoelastic material could be measured by forming it into a tube and exciting it using T(0,1). A specialised experimental set up was designed in order to measure the shear stress propagation and attenuation rate with distance. The bulk shear speed was determined by measuring the time required for the shear stress to propagate through two specimens/tubes with different lengths. The bulk shear attenuation was determined by measuring the difference in the drop in amplitude drop for two specimens of different length.

The technique presented is attractive for semi-solid coating materials which easily deform under relatively low external pressure, but have enough elasticity to maintain their shape when formed into a cylindrical tube. However, the need for the material to be formed into a cylindrical tube does not make it so suitable for use on liquid and solid coating materials.

Chapter 4

Attenuation measurements in coated pipes

Introduction

One of the main aims in this work is to find a set of numerical methods which can accurately predict guided wave attenuation in pipes coated with a layer of viscoelastic material. The bulk acoustic speed and attenuation in the bitumen coating material Bitustik 4000, which were measured in the previous section, can be used as input parameters to generate numerical predictions on guided wave attenuation. To do this we require a method with enough accuracy to be used to determine the LRUT inspection range in coated pipes. One possibility to determine how accurate the numerical predictions on guided waves attenuation are is to compare them against experimental attenuation data measured in pipes coated with a coating material such as Bitustik 4000.

The attenuation rate of guided waves used for the LRUT of coated pipelines is one of the main parameters which determines the distance that may be covered from a single tool position. One of the main objectives in this work is to find an experimental method or methods which can be used for studying the attenuation of L(0,2) and T(0,1) in real conditions, where the operator has access to a section of a continuous pipeline coated with a viscoelastic material. In general it is accepted that the rate of attenuation in coated pipes is constant with distance [14, 15, 16, 20]. This means that amplitude of the pulse of given guided wave mode exponentially decreases with distance, as shown in Fig. 4.1. The guided wave attenuation is typically measured in dB/m. In a pipe without a coating material the attenuation rate is usually relatively low, around 0.2-0.3 dB/m, and the LRUT test range can reach tens of meters in each direction [9]. The presence of a viscoelastic coating significantly increases the rate of attenuation, as shown in Fig. 4.1, and an LRUT test range is then reduced to much smaller distances, as reported in [9, 13-17].

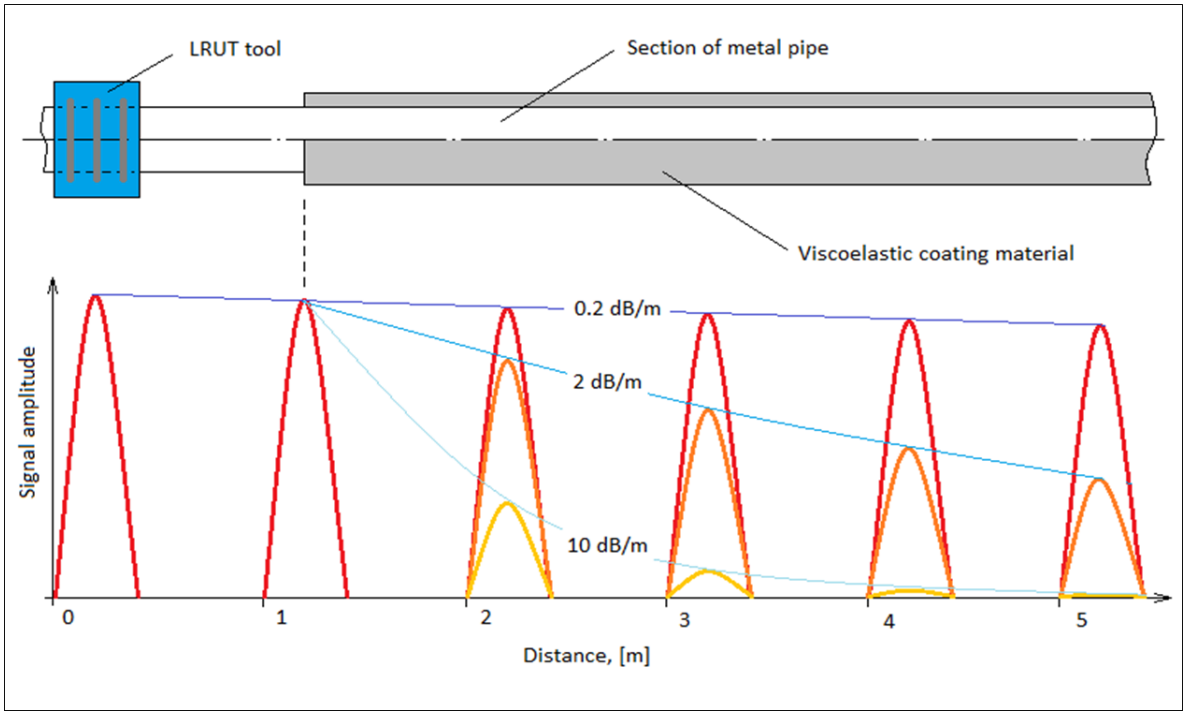

Figure 4.1: Schematic diagram of a typical LRUT in coated pipeline.

4.1 Previous work

The measurement of attenuation in a coated pipe is a problem which has occupied researchers for many years. Luo is one of the first who suggested a method applicable to measuring guided wave attenuation in coated pipes [53]. This method uses an experimental set up similar to the one shown in Fig. 4.1. However, instead of a coated section which is part of a continuous pipeline, Luo used a coated pipe with limited dimensions. The desired guided wave mode was generated by a conventional LRUT tool and mounted on the end of the pipe. The attenuation at specific frequencies was determined by measuring the rate of attenuation of multiple signals reflected from the far end of the coated pipe. The method suggested by Luo was successfully used by other researchers too [15, 16, 20].

A similar method to the one suggested by Luo was used by Kwun [71], but instead of an LRUT tool using piezoelectric transducers the desired guided wave modes were generated by belt type magnetostrictive transducers mounted on the end of the coated pipe [72]. The methods relying on measuring the amplitude drop of multiple signals reflected from the far end of the coated pipe available in the literature have also been successfully used for

studying guided wave attenuation. However, they are only applicable for studying guided wave attenuation in coated pipes with limited lengths, where the signal can be completely reflected from the end of the pipe.

The method for studying guided wave attenuation in cylindrical tube filled with viscoelastic coating material suggested by Simonetti [14, 48] relies on the successful measurement of the drop in amplitude along the tube. This is determined by measuring the amplitude of a particular mode at several points along the pipe using a scanning laser vibrometer [90]. The method suggested by Simonetti does not require reflection from the end of the pipe, which makes it suitable for studying guided wave attenuation in continuous waveguides. However, it is difficult to use a laser scanning vibrometer for on-site measurements.

4.2 Measurement Methodology

One possibility to determine the rate of attenuation of given guided wave mode propagating in coated pipe is by measuring its amplitude at a number of positions along the pipeline, as shown in Fig. 4.2. The desired guided wave mode is generated by a conventional LRUT tool mounted on the plane section of the pipe (position 0) and this then travels through the coated section. The amplitude of the guided wave mode propagating along the coated section of the pipe is then measured at several positions (for example, positions 1-5 in Fig. 4.2) using ultrasonic transducers. One possibility to do these measurements is to use conventional contact type ultrasonic transducers. The major problem of using contact type ultrasonic transducers for attenuation measurements is ensuring equal acoustic coupling between the different measurement locations. This is because the output electrical signal of these transducers strongly depends on the acoustical coupling between specimen and transducer.

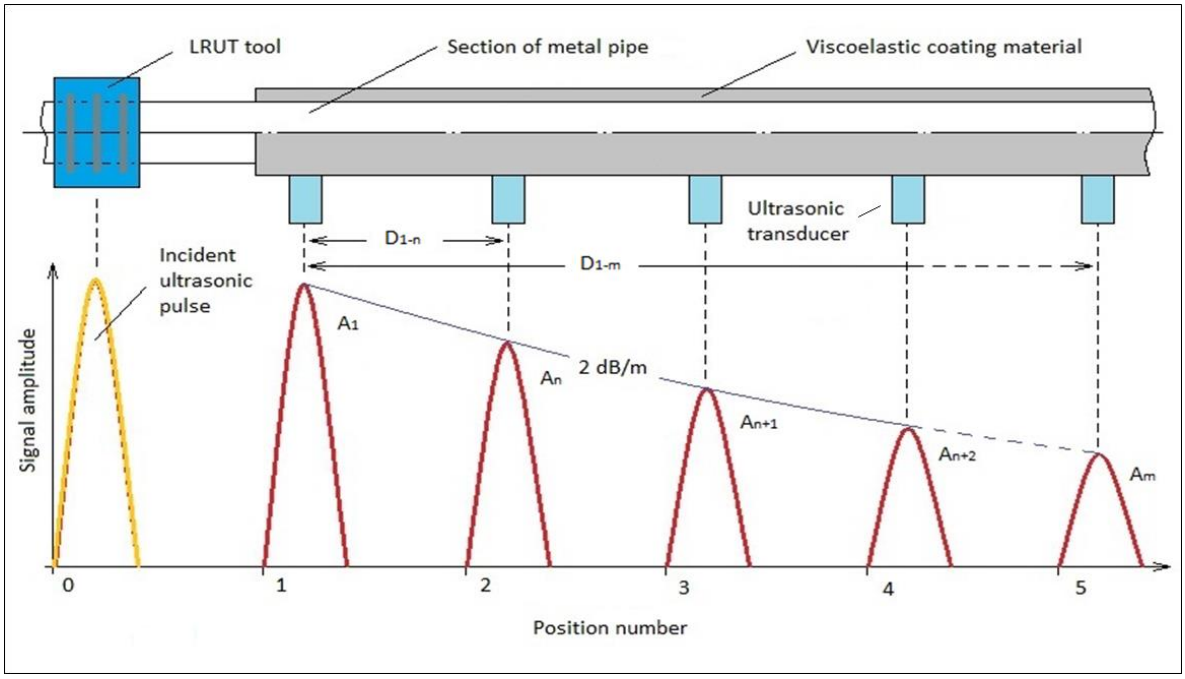

Figure 4.2: Schematic diagram of method for on-site measurement of guided wave attenuation.

An alternative approach is use Electro Magnetic Acoustic Transducer (EMAT). The main advantage of these transducers is that they do not require mechanical coupling with the pipe because they sense the acoustic signal remotely. The acoustic coupling between the EMAT and the specimen is ensured by electromagnetic coupling, not by the direct mechanical/acoustic contact [91, 92], and so they may be used for the remote sensing of dynamic stress in ferromagnetic waveguides and non-metal materials at distances of up to 20mm and more [91]. This makes the use of an EMAT attractive for the measurements required in this study and so the EMAT's operation and construction used in this study is covered in the next section.

The EMAT will measure the modal amplitudes $A_{1,}A_n \ldots . A_m$ at several positions along the coated section of the pipe, and the attenuation at a specific centre frequency Att_f is calculated using the following equations:

$$\mathrm{Att}_n\left[\frac{dB}{m}\right] = \frac{20\log_{10}\frac{A_1}{A_n}}{D_{1-n}} \quad , \quad (2 < n < N) \tag{4.1}$$

$$\mathrm{Att}_f \left[\frac{dB}{m}\right] = \frac{\sum_n \mathrm{Att}_n}{N} \ , \tag{4.2}$$

where Att_n is the attenuation between the reference amplitude A_1 and the amplitude of sensor n, A_n. In addition, D_{1-n} corresponds with the distance between the position where the reference amplitude A_1 and the amplitude A_n are measured, and Att_f is the average attenuation at a centre frequency, f, calculated from the total number of measurements N.

4.3 EMAT design and build

In general an EMAT relies on the direct/inverse Lorenz force effect and Joule (magnetostrictive) effect to generate/sense acoustic waves. More details about these effects may be found in [92-94] and the following description relevant to the measurement undertaken here covers the operation of an EMAT in sensing mode based on the reverse Joule (magnetostrictive) effect.

The electromagnetic coupling between an EMAT sensor and a vibrating medium occurs as a result of the secondary dynamic magnetic field generated when a ferromagnetic material is subjected to a constant magnetic field and dynamical loading (mechanical wave propagating into it). In this case, the secondary dynamic magnetic field has an intensity proportional to the dynamic loading amplitude generated [95]. Following Fig. 4.3, the primary constant magnetic field M_1 is generated by an electromagnet supplied with direct current I_1, or permanent magnets. The secondary dynamic field M_2 is generated under the influence of the dynamic stress $d\sigma/dt$, which is caused by the mechanical wave propagating under the transducer and is picked up and transformed into an electrical signal U_2 by a second coil mounted on a ferromagnetic core, as shown in Fig. 4.3.

The other major advantage of using an EMAT is that they can sense the amplitude of the dynamic stress $d\sigma/dt$ propagating along the waveguide at some distance L, even without having any mechanical connection with the waveguide.

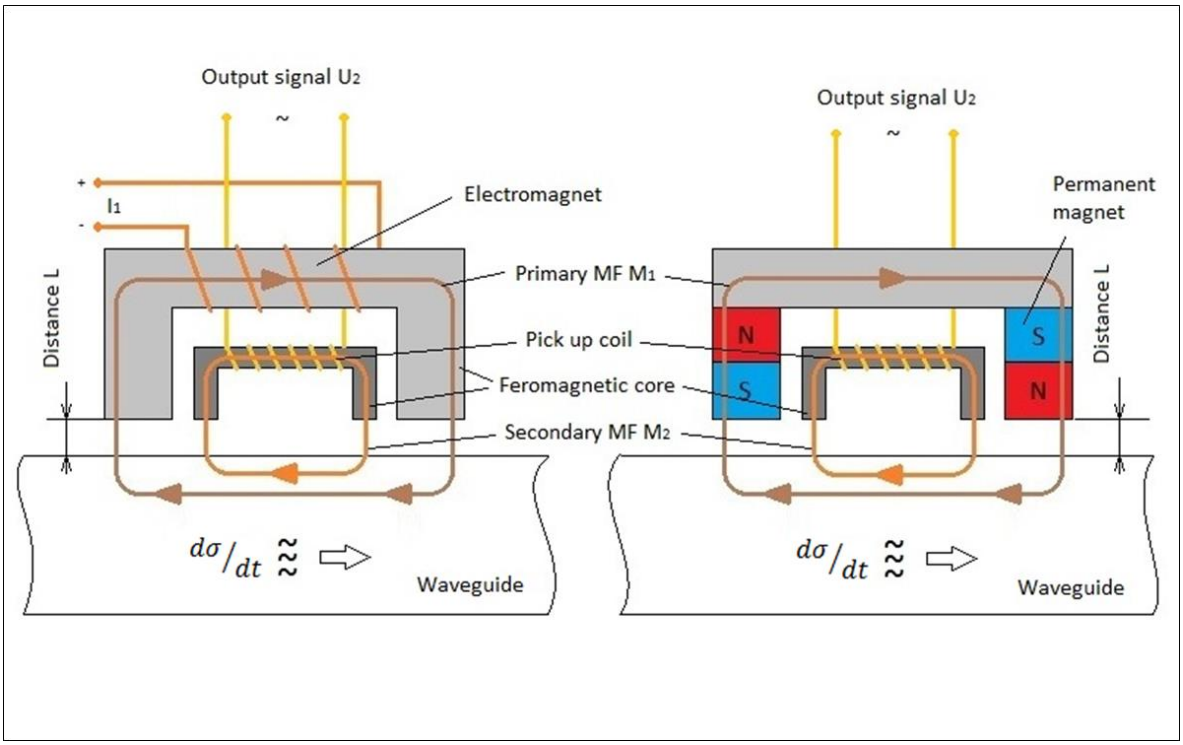

Figure 4.3: Schematic diagram of Electro Magnetic Acoustic Transducer, EMAT.

The EMAT construction and principle of operation is suitable for sensing longitudinal guided wave modes propagating in the direction of travel indicated by the arrow in Figure 4.3. This orientation is suitable for detecting longitudinal modes because the direction of the primary magnetic field M_1 should be parallel to the direction of propagation of the longitudinal wave mode. The described magnetostrictive EMAT can also be used for sensing torsional guided wave modes if the direction of the primary constant magnetic field M_1 is perpendicular to the traveling direction of the torsional guided wave mode. The output amplitude of these types EMATs strongly depends on the magnitude of the primary constant magnetic field M_1, which could be determined by changing its magnitude until achieving maximum output amplitude U_2. More details regarding a magnetostrictive EMAT and how the magnetic fields need to be aligned in order to generate/sense longitudinal and torsional modes may be found in [96].

An EMAT capable of measuring the amplitude of L(0,2) was designed according to the guidelines in [96]. This design is shown in Fig. 4.4 and contains three separate coils

assembled on a cylindrical carrier made of PVC. The internal diameter of the cylindrical PVC base was manufactured to be two millimetres larger than the external diameter of the coated section of the pipe. This allows sliding and positioning of the EMAT assembly along the coated section of the pipe.

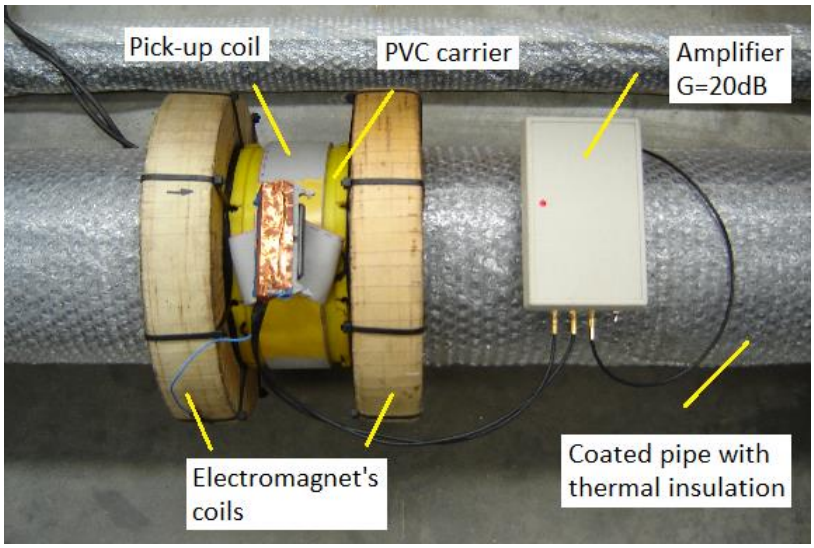

Figure 4.4: EMAT for measuring of L(0,2) modal amplitude in coated pipe.

The pick-up coil is made of two turns of 50 pin 0.3 mm thick ribbon cable. The separate wires of the ribbon cable are connected in such way that a coil consisting of 100 turns was formed. The pick-up coil is wound in the middle of the cylindrical plastic base and the primary constant magnetic field is generated by an electromagnet consisting of two coils connected in series. The coils, each consisting of 1000 turns and made of 1.1mm thick insulated copper wire, are positioned at the ends of the plastic carrier, as shown in Fig. 4.4. The EMAT assembly is then positioned on the coated section of the pipe at location 1 in Figure 4.2, and the electromagnet`s coils were supplied with direct current from a regulated power supply. The EMAT induces a primary magnetic field in the structure, which interacts with a propagating elastic wave to generate a secondary magnetic field, which is then picked up by the receiving coil of the EMAT. The strength of the primary field is changed by varying the amplitude of the current from the regulated power supply. When the amplitude of the input current is increased the magnitude of the output steadily increases until it reaches a maximum value, at which point the magnetic field becomes saturated and

cannot increase further. This point of maximum output was chosen for all tests in order to maximise the signal to noise ratio. Ten cycles of a Hanning modulated L(0,2) mode were then generated and these then propagate towards the coated section of the pipe. The amplitude of the signal detected by the pick-up coil is monitored with a Tektronix TDS2012 digital oscilloscope and recorded using a Teletest Mark 4 tone burst pulse/receiver unit. In this way it was determined that the optimum magnitude of the current through the electromagnet's coils is 5 A.

Figure 4.5 shows the signal recorded at centre frequency of 60 kHz. The sharp peak at the beginning of the time trace is caused by cross talk inside of the equipment. The signal appearing at 500 us is the L(0,2) guided wave mode. The second signal with much lower amplitude appearing after 900 us is L(0,1) guided wave mode, which is also excited by the LRUT tool but with much lower amplitude.

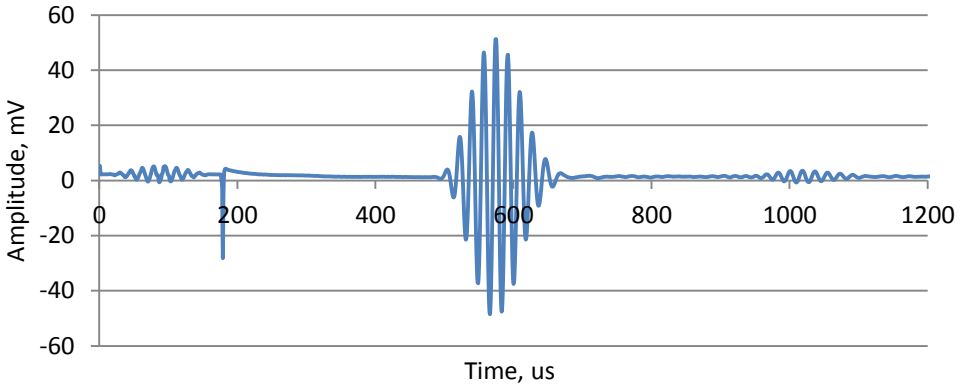

Figure 4.5: L(0,2) signal recorded with EMAT transducer at 60 kHz.

The EMAT designed to measure the amplitude of T(0,1) is shown in Figure 4.6. It was designed according to the guidance in [96] so the primary constant magnetic field is orientated along the circumference of the pipe and is generated using two $25 \times 25 \times 10$ mm neodymium magnets, grade N45. The pick-up coil consists of 100 turns of 0.15 mm thick insulated copper wire wounded around a U shaped ferromagnetic core. The pick-up coil with the ferromagnetic core was oriented along the axis of the pipe so it can detect the secondary magnetic field generated. The signal generated by the pick-up coil was monitored using a digital oscilloscope Tektronix TDS2012.

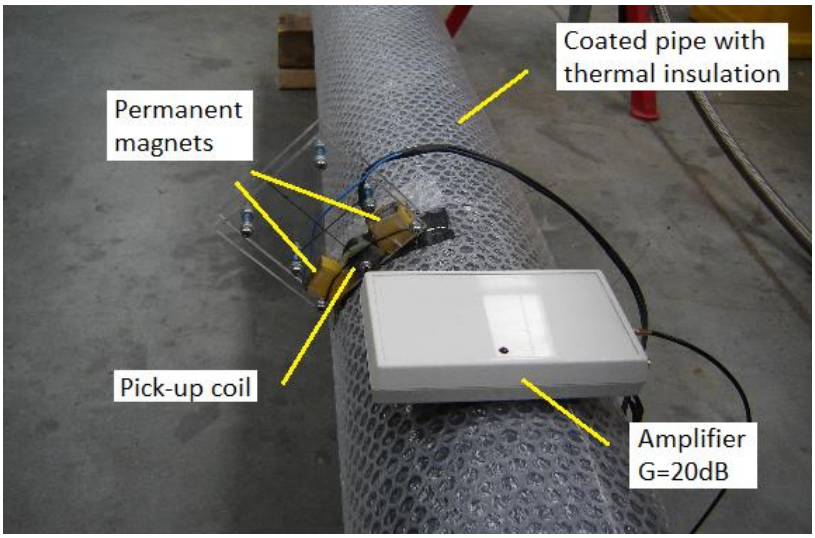

Figure 4.6: EMAT for measuring of T(0,1) modal amplitude in coated pipe.

The EMAT is positioned at location 1 in Figure 4.2 and ten cycles of a Hanning modulated T(0,1) mode were generated. The ferromagnetic core with the pick-up coil is kept fixed and the distance between the permanent magnets was changed until the amplitude of the ultrasonic signal measured by the oscilloscope reaches a maximum. Once the optimum alignment between the components is achieved, they are fixed by clamping the two plastic 5 mm thick plates. The stable positioning of the EMAT on the other surface of the coated ferromagnetic pipe is ensured by the attracting force generated by the two permanent magnets. The signal recorded at a centre frequency of 60 kHz is shown in Fig. 4.7.

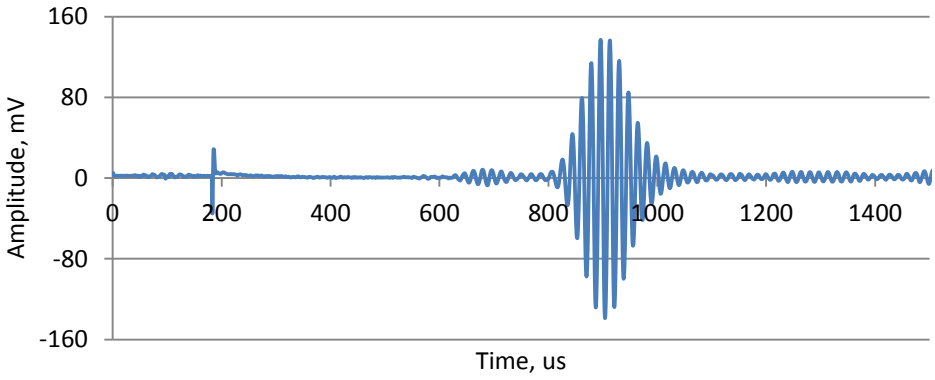

Figure 4.7: T(0,1) signal recorded with EMAT transducer at 60 kHz.

The signal appearing at 800 us is the T(0,1) mode and the rest of the signals appearing on the time traces are flexural components generated as result of uneven sensitivity between the transducers used to generate T(0,1). One downside of using an EMAT for remote sensing of dynamic stress is that their output amplitude rapidly degrades as the lift-off distance between the EMAT and the ferromagnetic waveguide increases. This is likely to induce errors in the measurements and so it is important that a constant distance is maintained between the EMAT and the ferromagnetic waveguide.

4.4 Experimental setup

The experimental set up used for this study is shown in Figure 4.8. It consists of a 6 m long 6 inch Schedule 40 pipe (OD = 168 mm, wall thickness 7.1 mm). Bitustik 4000 coating material is applied at 3.8 m from the far end of the pipe, and the thickness of the coating material is 1.25 mm. The external surface of the pipe was cleaned by applying fine glass beads at a high pressure before then applying the coating material. This cleaning process is a standard procedure recommended by the manufacturer of the coating material. The pipe is supported by two wooden blocks in order to reduce the acoustic coupling between the pipe and its supports. The L(0,2) and T(0,1) modes were generated independently by using conventional LRUT equipment, which is a Teletest Mark 4 tone burst pulse/receiver unit with a cylindrical array of transducers pneumatically clamped to the pipe. The Teletest equipment is positioned at the near end of the pipe, see Fig. 4.8. The amplitude measurements for L(0,2) and T(0,1) are taken separately for each mode at positions from 1 to 6 using the EMAT described in Section 4.3.

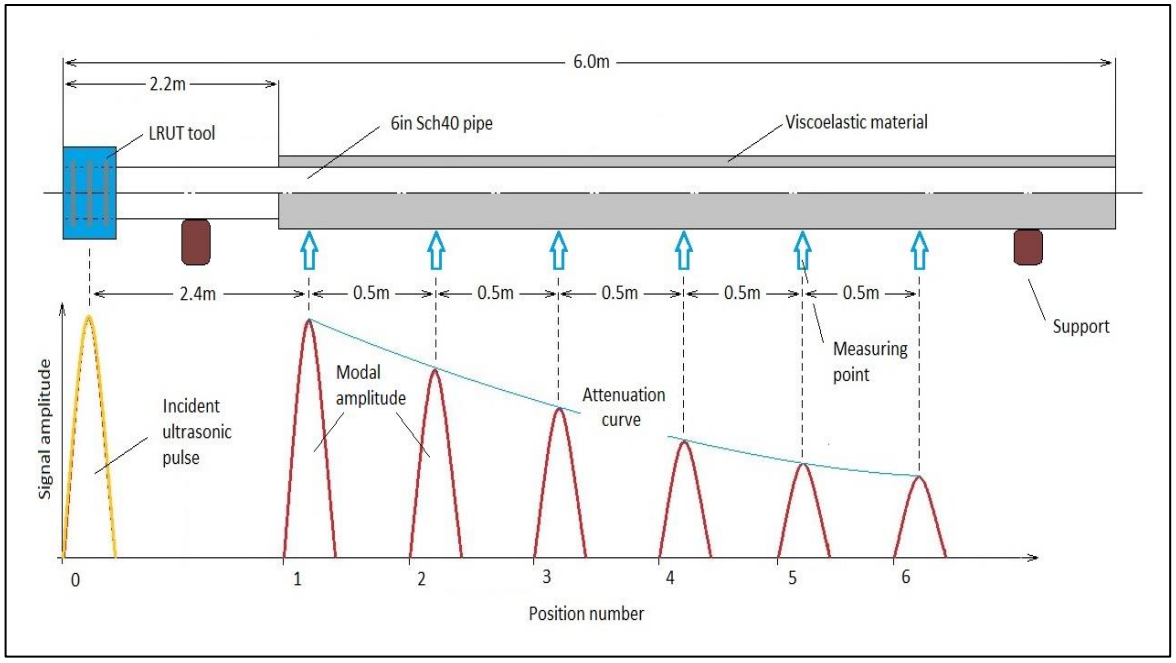

Figure 4.8: Experimental setup.

4.5 Temperature effect

The bulk acoustic properties of viscoelastic coating materials generally depend on temperature [14, 26, 71]. This means that the guided wave attenuation will also be temperature dependent and so the main aim in this section is to measure guided wave attenuation at specific temperatures in a pipe coated with Bitustik 4000.

The effect of temperature on guided wave attenuation is studied here for L(0,2) and T(0,1) modes at 0 ºC, 10 ºC, 20 ºC, 30 ºC and 40 ºC. The temperature along the coated section of the pipe was monitored by six T type thermocouples. The thermocouples were spot welded through the coating directly to the metal pipe at positions 1 to 6, see Figure 4.8, and then connected to a switchable thermocouple display unit, which is shown in Figure 4.9.

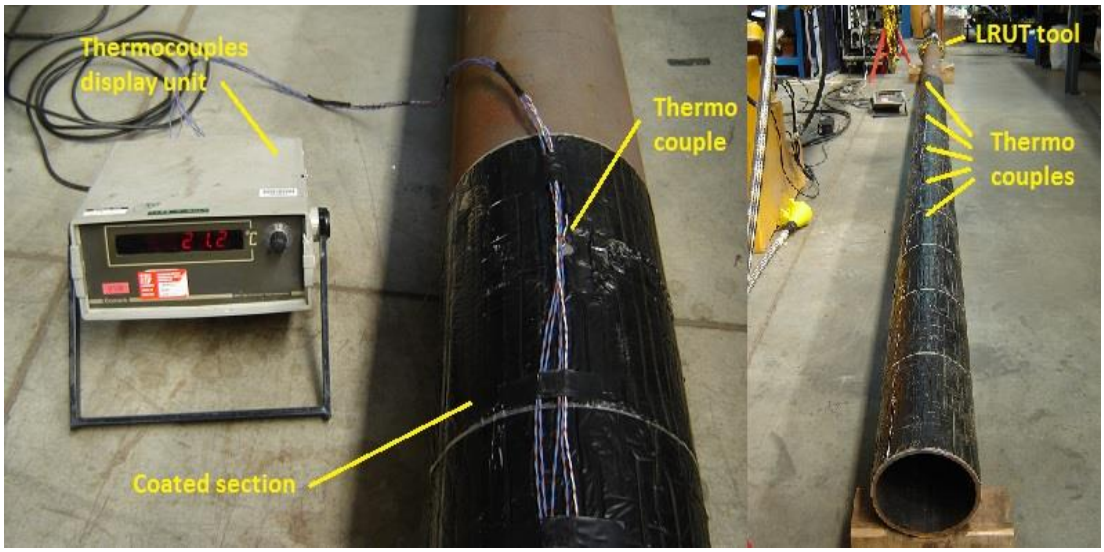

Figure 4.9: Experimental setup with mounted thermocouples and display unit.

The pipe was cooled down by passing cold air through it and monitoring the temperature along the coated section of the pipe. The air circulating through the pipe was cooled down by sending it through purpose designed heat exchanger filled with dry ice. The required temperature was maintained by monitoring the temperature along the coated section of the pipe and manually changing the amount of cold air sent through the pipe. The outer surface of the pipe was covered with thick low density polymer insulating material in order to reduce the effect of the ambient environment. The experimental setup with the cooling system attached is shown in Figure 4.10.

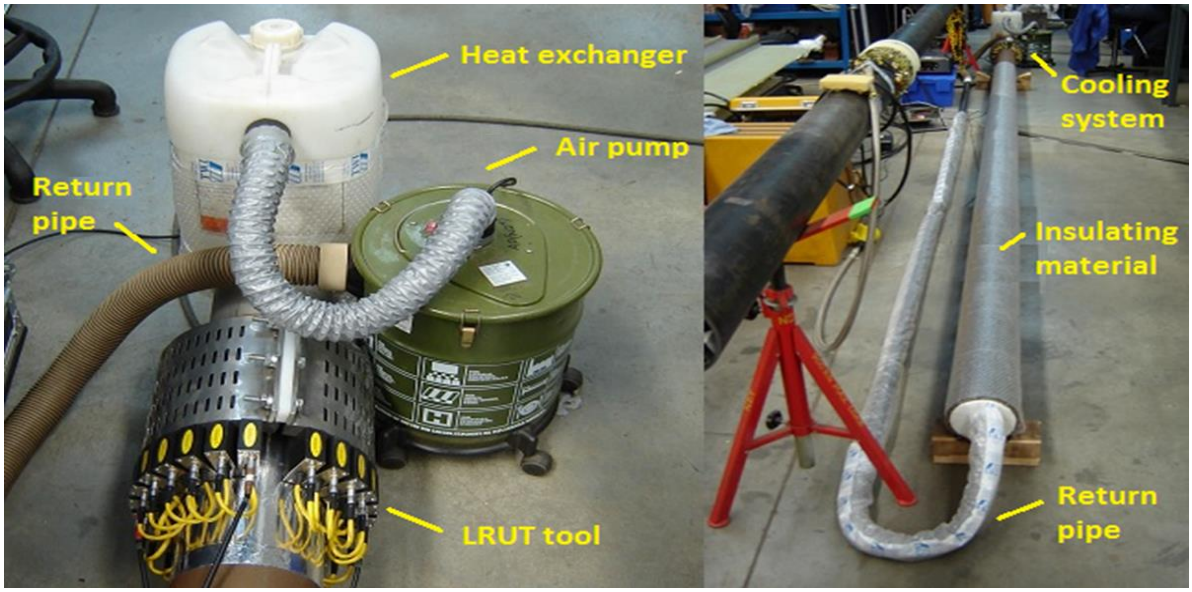

Figure 4.10: Experimental setup with cooling system attached.

The temperature of 30 ºC and 40 ºC was achieved by passing hot air through the pipe and monitoring the temperature along the coated section. The hot air was produced by an electronically controlled hot air gun. The required temperature was maintained by monitoring the temperature along the coated section of the pipe and changing the temperature of the hot air sent through the pipe. The same low density polymer was used for insulating material in order to reduce the effect of the ambient environment. The experimental setup used to warm up the pipe is shown in Figure 4.11.

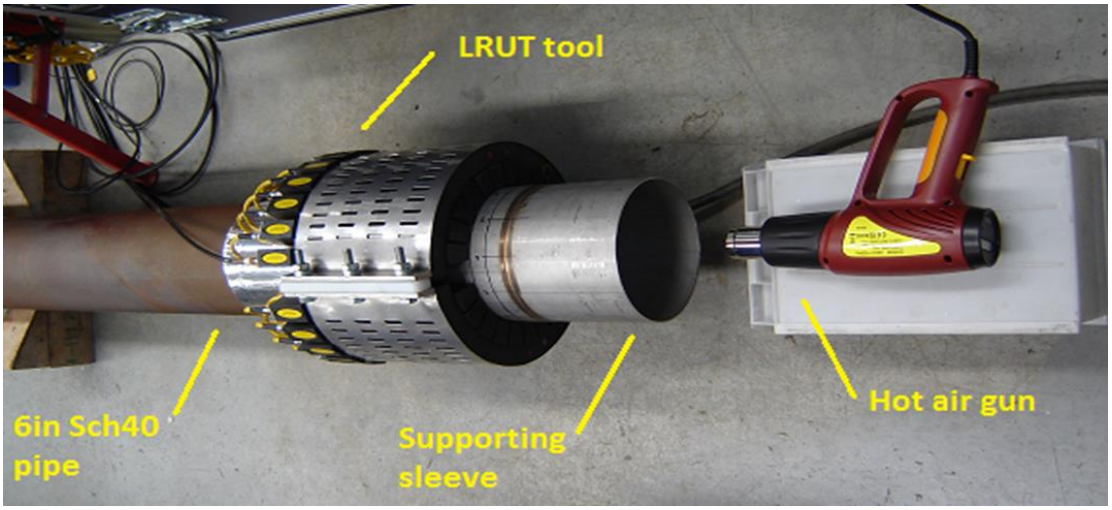

Figure 4.11: Experimental setup used to warm up the pipe.

Initial measurements showed that it was possible to maintain an approximately constant temperature distribution along the coated section of the pipe, although the ability to do this is affected by the level of the ambient temperature relative to the desired temperature. The temperatures obtained are shown in Table 4.1 and Fig. 4.12.

Required temp., °C	0		10		20		30		40	
Achieved temp., °C	T_{ave}	T_{max}	T_{ave}	T_{max}	T_{ave}	T_{max}	T_{ave}	T_{max}	T_{ave}	T_{max}
Position 1	0.03	2.64	10.08	1.71	19.98	1.13	30.05	1.79	40.00	3.12
Position 2	0.00	2.26	9.78	1.65	20.00	1.10	30.15	1.79	40.10	3.00
Position 3	0.03	1.95	9.95	0.82	20.03	0.78	29.88	1.02	39.75	1.91
Position 4	0.20	1.59	10.03	1.07	20.03	0.73	30.23	0.93	40.23	1.59
Position 5	0.05	1.24	9.98	0.44	20.05	0.42	29.80	0.41	40.25	0.65
Position 6	0.33	0.74	10.10	0.08	20.08	0.21	30.20	0.22	40.00	0.48

Table 4.1: Temperature variation along the coated section of the pipe: T_{ave} is the average temperature at each location, and T_{max} is the maximum difference between the temperature required and the value measured.

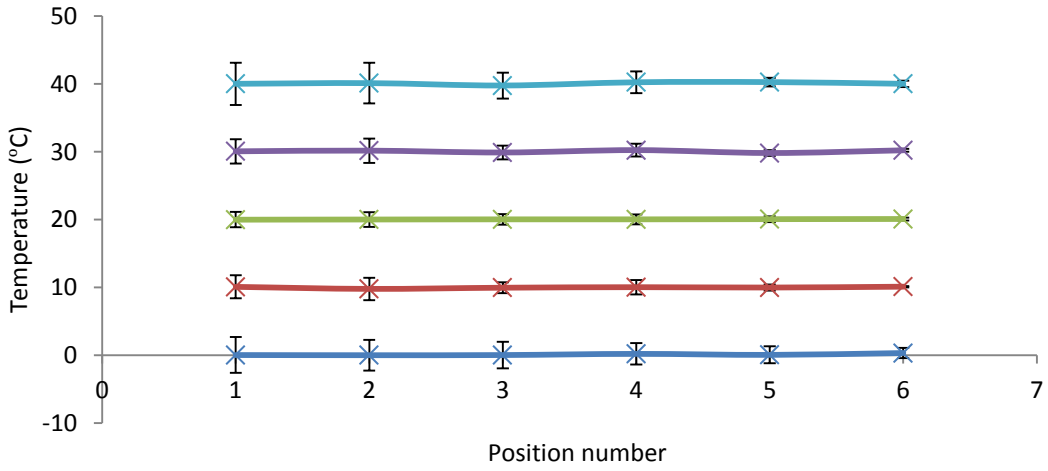

Figure 4.12: Temperature variation along the coated section of the pipe.

It is seen in Fig. 4.12 and Table 4.1 that the average temperature along the coated section of the pipe was maintained relatively well with the heating/cooling system described, however the temperature variation was relatively high at the coated end of the pipe where the

heating/cooling system was attached. The values achieved are, however, considered to be sufficiently stable to allow the measurement of the coating properties.

4.6 Data processing

The attenuation measurements for L(0,2) and T(0,1) were conducted at temperatures of 0 ºC, 10 ºC, 20 ºC, 30 ºC and 40 ºC. The experimental data was collected by first setting the LRUT tool to generate L(0,2) using ten cycles of a Hanning modulated sinusoidal signal. The centre frequency of excitation was varied between 20 kHz and 100 kHz in 5 kHz steps. At each frequency the amplitude of L(0,2) was measured at six points (positions 1 to 6, Figure 4.8) using the purpose designed EMAT transducer described in Section 4.3

Experimental data was collected 128 times and averaged in order to reduce the level of random noise. This means that 17 sets of data were collected at each temperature and then used to calculated the attenuation of L(0,2) at each centre frequency. The attenuation measurements for T(0,1) were conducted in the same way as for L(0,2), but this time with the LRUT tool set to generate T(0,1).

Once the data for L(0,2) and T(0,1) was collected it was processed in the frequency domain using a purpose written MATLAB code. Each signal was windowed using a rectangular window with a width in the time domain chosen to be 20% wider than the original Hanning modulated pulse used to excite each mode. The results for L(0,2) at central frequency of 60 kHz is shown in Figure 4.13.

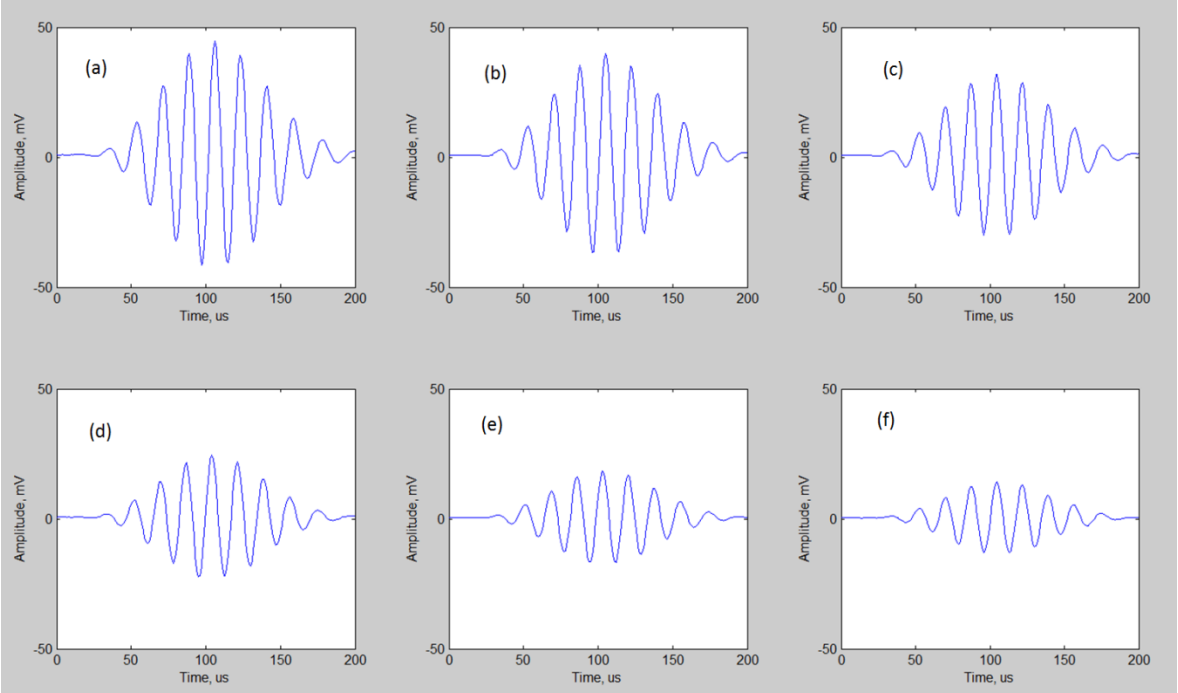

Figure 4.13: L(0,2) signals recorded along the coated section of the pipe. (a) position 1; (b) position 2; (c) position 3; (d) position 4; (e) position 5; (f) position 6.

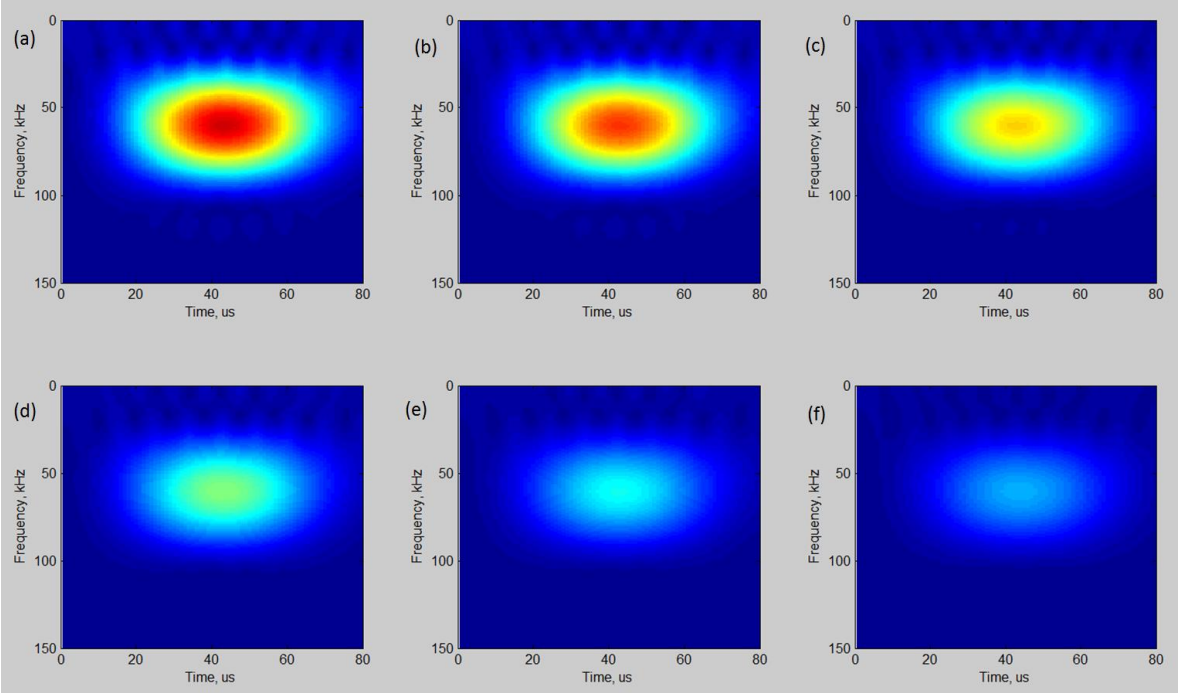

Figure 4.14: Time-frequency representation of the signals. (a) position 1; (b) position 2; (c) position 3; (d) position 4; (e) position 5; (f) position 6.

The amplitude of the different frequency components of the signals were determined by using the MATLAB "*specgram*" function, which computes the windowed discrete-time Fourier transform of a signal using a sliding window. The result is a matrix representing the signals in the time-frequency domain, and this is shown in Figure 4.14. The row of each matrix corresponds with a centre frequency and the maximum amplitude of the signal for each row was determined. These values correspond with the modal amplitudes $A_{1,}A_n$ ….A_{n+4} and this then permits the attenuation to be calculated using Eqs. (4.1) and (4.2). The experimental data for each guided wave mode, centre frequency and temperature was processed in the same way and the results are presented in the next section.

4.7 Results and discussion

Figures 4.15 shows the measured attenuation of L(0,2) against centre frequency at temperature of 0 ºC, 10 ºC, 20 ºC, 30 ºC and 40 ºC.

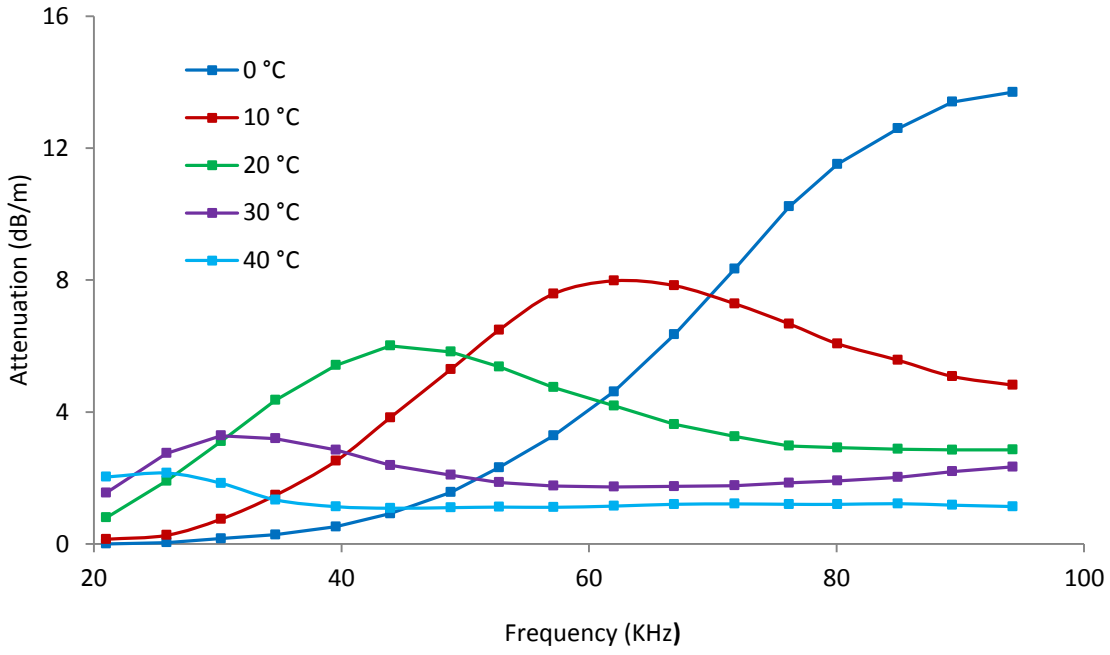

Figure 4.15: Attenuation of L(0,2) at temperatures of 0ºC, 10ºC, 20ºC, 30ºC and 40ºC.

In Fig. 4.15 the attenuation is seen to increase to a maximum and then drops as the frequency increases. This behaviour is caused by the attenuation mechanisms within the

viscoelastic material, which respond differently to variations in the wavelength incident sound wave, as well as guided wave mode. This produces the familiar behaviour in where attenuation increases to a maximum and then decreases [15, 47, 55, 56]. The position of the peak is influenced by the shear velocity of the material and this in turn depends on the temperature of the material and this is why the peak moves. The attenuation of L(0,2) in Fig. 4.15 shows that the attenuation also depends on temperature. Therefore it appears to be desirable to use a lower frequency for testing at lower temperatures, and at higher temperatures it appears to be sensible to move beyond the peak in attenuation and to use higher frequencies. This will help to maximise the inspection distance for a pipe and it is seen that at higher temperatures the attenuation is sufficiently low to penetrate distances of over 10 m. Figure 4.16 shows the attenuation spectra of T(0,1) at temperatures of 0 ºC, 10 ºC, 20 ºC, 30 ºC and 40 ºC.

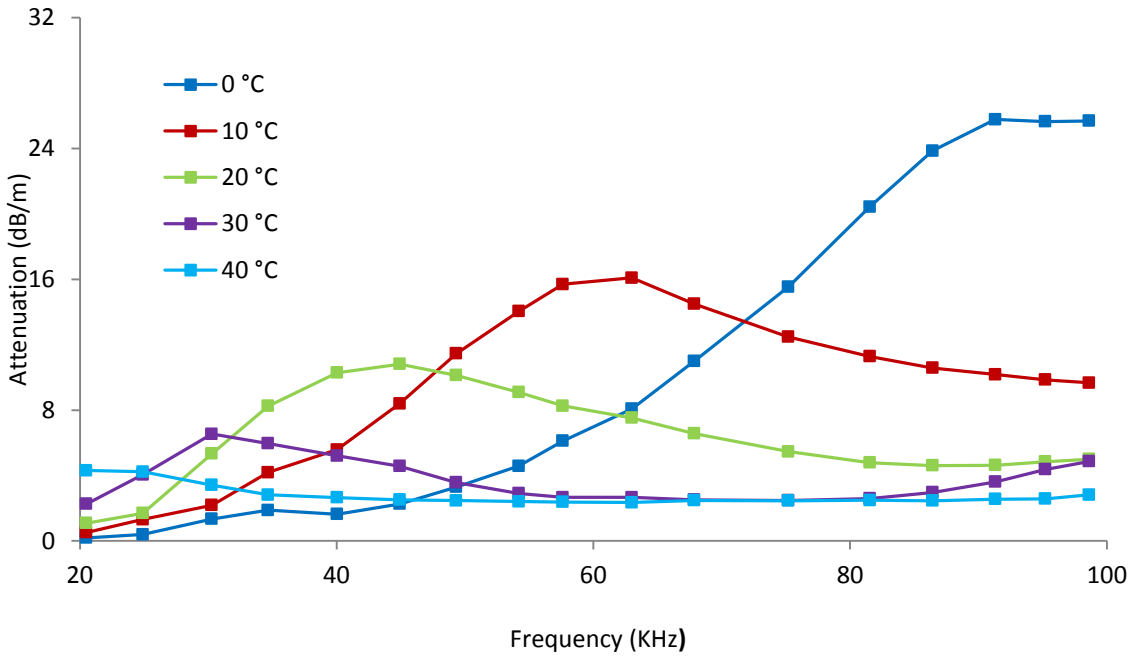

Figure 4.16: Attenuation of T(0,1) at temperatures of 0ºC, 10ºC, 20ºC, 30ºC and 40ºC.

Figure 4.16 shows that the attenuation of T(0,1) follows a very similar pattern to that seen for L(0,2). The main difference is that the attenuation of T(0,1) is about 90% higher than the attenuation of L(0,2). At lower temperatures it is seen that low frequencies deliver lower values of attenuation, however the lowest frequency for testing with T(0,1) is limited

by the spatial resolution of T(0,1). In this study a frequency of 20 kHz for T(0,1) corresponds to the same spatial resolution as a frequency of 33 kHz for L(0,2). The similarity in the shape of the attenuation plots for T(0,1) and L(0,2) was also observed by Rose [13-16, 67].

The attenuation of T(0,1) at 20 ºC is above 4 dB/m over the frequency range above 27 kHz. This means that it is likely to be difficult to locate defects using T(0,1), even between 80 kHz and 90 kHz where the attenuation is around 4.6 dB/m. The only possibility appears to be to use frequencies below 27 kHz, which is in the low end of the optimum frequency range for most piezoelectric LRUT tools. At a temperature of 30 ºC the frequency range where the attenuation is below 4 dB/m is between 48 kHz and 90 kHz and so is much wider then for 20 ºC. The test range based on the minimum and maximum attenuation over this frequency range is 6.8 m and 4.2 m, respectively. Therefore, based on the values quoted for T(0,1) at 20 ºC and 30 ºC we can achieve a better inspection range at 20kHz when the temperature is 20ºC, and at 60kHz when the temperature is 30ºC. In reality it is much better to conduct LRUT at frequencies in the mid frequency range around 60 kHz to deliver good spatial resolution and an improved signal to noise ratio. This demonstrates that problems are likely to occur when studying pipes coated with Bitustik 4000 at room temperatures.

The last attenuation measurement for T(0,1) in Figure 4.16 was conducted at 40 ºC. The temperature change from 30 ºC to 40 ºC moves the first attenuation peak towards lower frequencies and reduces the attenuation, as was observed for L(0,2). In this case the attenuation is below 4 dB/m over most of the frequency range investigated and this improves the situation for LRUT.

4.8 Summary

A technique for the remote (non-contact) measurement of modal amplitudes for T(0,1) and L(0,2) modes in a pipe coated with a viscoelastic material has been presented here. The technique is based on using two types of electromagnetic acoustic transducers (EMATs) that are sensitive to dynamic stress created by the propagation of torsional T(0,1), and longitudinal L(0,2), guided wave modes. This technique is attractive because it allows the

signal to be traced along the coated section of the pipe and does not depend on fixing transducers to the pipe.

The technique has been successfully used to measure the attenuation of T(0,1) and L(0,2) for a 6 inch Schedule 40 pipe coated with 1.25 mm thick Bitustic 4000 coating material. The attenuation measurements of T(0,1) and L(0,2) were conducted at temperatures of 0 ºC, 10 ºC, 20 ºC, 30 ºC and 40 ºC and they demonstrate the dependence between guided wave attenuation in a coated pipe and temperature. The results show that temperature has a strong influence on pipe attenuation and this is likely to play a major role in the success of LRUT inspection regimes. In some cases, even modest variations in the temperature could have significant effect on the LRUT inspection range. The experimental data on guided wave attenuation temperature dependence presented also suggest that if we want to develop an accurate method which to predict guided wave attenuation in a coated pipe, the method should also take into account the effects of temperature.

The change in guided wave attenuation with temperature is most likely caused by the temperature dependent bulk acoustic properties of the bitumen coating material. One possibility to take into account the temperature change is to develop a method which can determine the bulk acoustic properties of the coating material on site, or to find what the temperature dependence is, and then to use this to modify the bulk acoustic properties of the coating material.

The experimental data obtained at specific temperatures shows that the attenuation of T(0,1) is about 90% higher compared than L(0,2), although the trend in the data appears to be similar. The higher attenuation of T(0,1) could be explained by the shear displacement, which carries the energy of that mode for T(0,1). The data reported in the literature, and the experimentally determined shear and longitudinal attenuation in previous chapters, suggest that when the material is deformed in shear mode it will dissipate more energy. This is likely to be the cause of the higher levels of attenuation observed for T(0,1).

Chapter 5

Method for acoustic characterization of coating materials

5.1 Introduction

The accurate prediction of guided wave attenuation in a coated pipe depends on how accurately the bulk properties for the coating material are characterised. The experimental methods for the acoustic characterisation of coating materials reviewed previously show how difficult is to find a method which can accurately determine the bulk acoustic properties in situ. Some on-site trials on the characterisation of coating materials reported in the literature also suggest that the bonding between the coating material and the pipe wall is not always perfect. This means that even if we have a set of methods which can determine independently the material bulk properties, there is no certainty that numerical predictions based on these properties will be accurate.

The following sections describe a new method for deriving the material properties of a coating from guided wave measurements based on reflection coefficients. A reflection coefficient spectra is determined by measuring the amplitude of a guided wave sent towards and then reflected back from a discontinuity with a known geometry located in a pipe coated with the coating material of interest. The method has been reported in two journal articles [69, 70], where the theoretical framework of the method and the method itself is described in detail. The theoretical work was developed by the author's supervisor Dr. Kirby and all predictions generated in this chapter were generated by the author using software written by Dr. Kirby. The main focus of this work and contribution of the author in the Thesis are the experimental measurements and the practical application of this method.

The logical question is why do we need another method to determine the bulk acoustic properties of the coating material of interest? The methods reported in the literature and Chapter 3 are suitable mostly for laboratory use. Those methods which could be used on-

site are not suitable for measuring the bulk shear attenuation constant of highly viscoelastic semisolid materials like bitumen. The methods in the literature provide values for the bulk acoustic properties of the coating material itself, but these values do not take into account the coupling between the pipe wall and coating material. The method reported by Hua and Rose in [15] is capable of determining the shear attenuation constant in highly viscoelastic materials like bitumen, and it takes into account the coupling between the pipe wall and the coating material. However, the disadvantage of this method is that it needs a number of parameters, such as the bulk longitudinal properties and bulk shear speed of the coating material, which need to be measured by separate methods. The main advantages of the method described in this chapter, when compared to other methods for coating materials are:

- The method can determine the bulk shear and longitudinal acoustic properties from experimental data collected on-site with conventional LRUT equipment.
- The method does not require *a priori* knowledge of the bulk longitudinal and shear acoustic properties of the coating material. The only parameter required before undertaking the tests is the density of the coating material, which can be easily measured on-site with a mobile handheld densitometer.
- The SAFE method utilised in this approach finds the solution for the torsional and longitudinal modes separately. This makes the method more computationally efficient compared to the methods using the generic SAFE formulation which calculates all guided wave modes simultaneously.
- The bulk acoustic properties of the coating material provided by the method are determined in the frequency range typical for LRUT and take into account the coupling between the coating material and pipe wall.
- There is no need to remove the coating material from the pipeline before undertaking the tests, and there is no need to form it into a specimen with a specific shape.
- The method is applicable for the on-site acoustic characterization of liquid, semisolid and solid coating materials.
- Once the experimental data is collected the bulk acoustic properties of the coating material can be derived in the matter of several minutes.

The downside of this method is that it relies on reflection coefficient data from an axisymmetric discontinuity with a known geometry, such as a weld or flange. This is not always convenient because the tool cannot always be positioned close enough to a discontinuity with known geometry.

The first part of the method for deriving the bulk shear properties $\tilde{c}_c$ and α_c uses an iterative trial and error technique shown in Figure 5.1. After a few iterations the method finds the shear bulk properties of the coating material, which give the best correlation between predicted and measured data for the refection coefficient of T(0,1) .

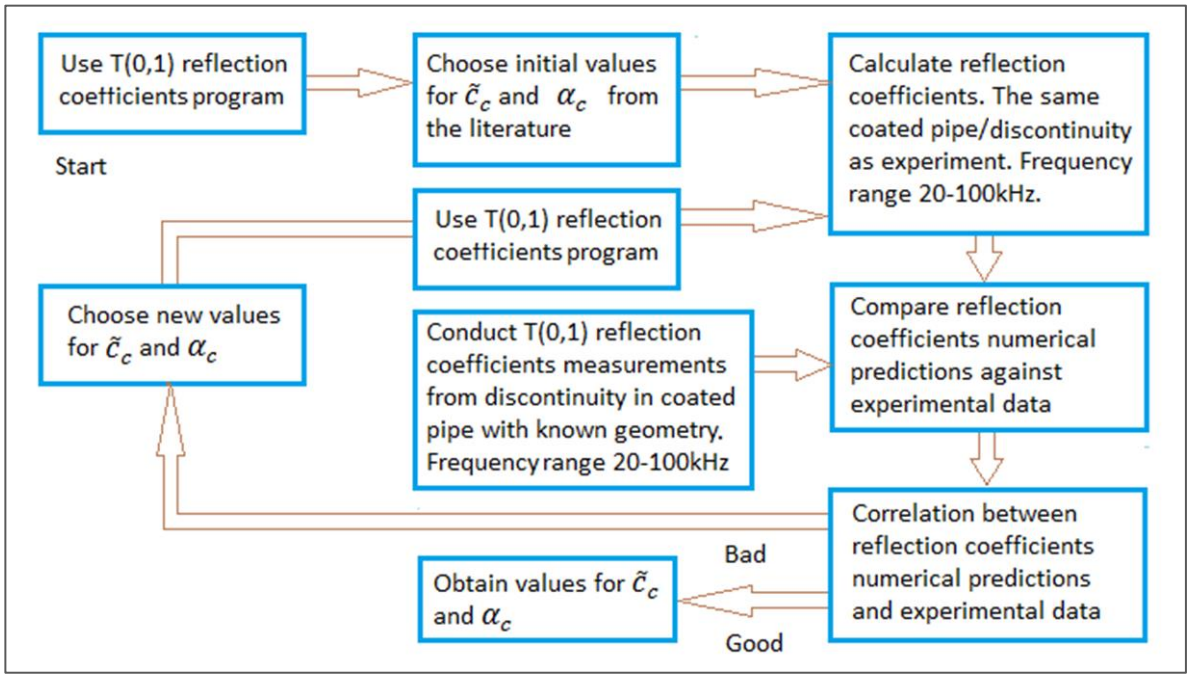

Figure 5.1: Iterative method for acoustic characterization of coating material. First part.

The initial values for the bulk shear speed and attenuation constant are those values reported in the literature for a coating material of a type similar to those studied here. The first part of the method provides values on the bulk shear acoustic properties of the coating material $\tilde{c}_c$ and α_c. Most researchers have reported that the shear properties of the coating material are those playing a major role in guided wave attenuation and reflection coefficients, respectively. Before we use these values as input parameters we need to check their validity using the second part of the method, which deals with the longitudinal

properties of the coating material. The second part of the method is shown in Fig, 5.2 and this checks the correlation between numerical predictions and experimental data for reflection coefficients for L(0,2) using the same coated pipe discontinuity as used for T(0,1).

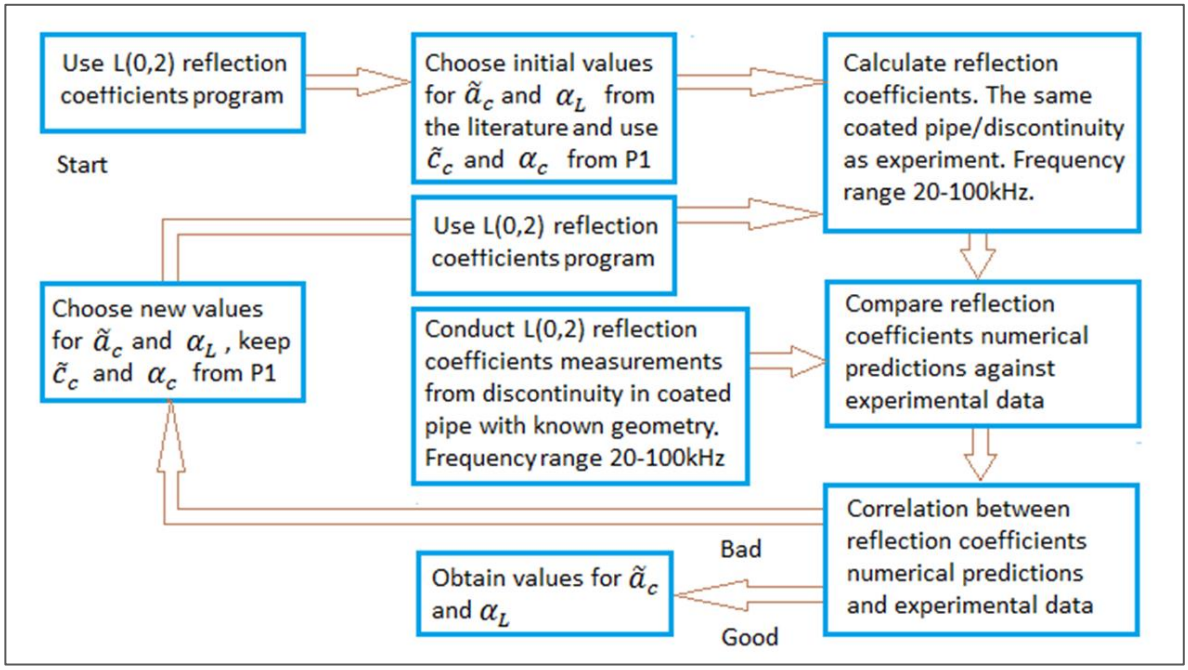

Figure 5.2: Iterative method for acoustic characterization of coating material. Second part.

The second part of the method also uses an iterative trial and error technique but the main difference is that it determines the bulk longitudinal properties $\tilde{\alpha}_c$ and α_L of the coating material by using the bulk shear properties $\tilde{c}_c$ and α_c of the coating material determined in the first part of the method. The second part of the method finds values for the bulk longitudinal properties that give good correlation between measurements and numerical predictions for the L(0,2) reflection coefficients.

It is possible to get good correlation between measured and predicted values for the L(0,2) reflection coefficients in the second part of the method using different values of the bulk longitudinal properties of the coating material $\tilde{\alpha}_c$ and α_L. The reason for this is that the guided wave reflection coefficients and attenuation below 100 kHz is usually strongly

influenced by the bulk shear properties of the coating material and the bulk longitudinal properties of the coating do not play such a significant role.

It is important to note that the bulk shear properties determined in the first part of the method need to be checked in the second part of the method. If good agreement between measurement and prediction cannot be achieved in the second part of the method then it means that that the predicted values using the T(0,1) data is not correct.

This approach requires the prediction of both the T(0,1) and L(0,2) reflection coefficients for axisymmetric discontinuities located in the coated pipe over the frequency range of interest. This is achieved in two steps. The first part uses the semi analytic finite element (SAFE) method to calculate the guided wave attenuation and phase speed in the coated section of the pipe, and the second part calculates how much energy is reflected back by the axisymmetric discontinuity located in the coated section of the pipe.

The SAFE method used to determine phase speed and attenuation in the coated and uncoated pipe is reported by Kirby et al. [69, 70]. The SAFE method uses separation of variables to separate the axial component of displacement from the components in the radial and circumferential direction. This can be done for structures such as pipes where the axial geometry is uniform. The SAFE method substitutes a time harmonic analytic expansion for the axial displacement, u_z, into the governing Navier's equation and then uses the finite element method to solve the eigenvalue problem that follows for the radial and circumferential directions. This provides the eigenmodes for a pipe and is easily applied to coated or uncoated pipes. The use of the finite element method to solve the eigenproblem also avoids difficulties associated with root finding, which can be a problem when using an analytic approach such as Disperse [21]. The SAFE method provides solutions for the mode shape, phase speed, attenuation and group velocity and these are of great practical interest for non-destructive testing. Kirby et al. also showed that the SAFE method may be used to solve only for torsional modes [69], or longitudinal modes [70], in order to solve the problem quickly. Finding the solutions for the torsional and longitudinal modes for uncoated and coated pipe separately simplifies the problem significantly by reducing the system of equations in comparison with a solution that includes all modes,

such as flexural modes. This approach also partially solves the problems associated with mode differentiation reported in [67]. An example of the predictions obtained using the SAFE method is shown in Figs. 5.3 and 5.4, where predictions for guided wave attenuation and phase speed are shown. The predictions are generated for the torsional T(0,1) and longitudinal L(0,2) modes propagating in a pipe with an outside diameter of 168 mm, a wall thickness of 7.1 mm, and a 3 mm thick bitumen coating. The acoustic properties reported by Barshinger and Rose in [20] are used as input parameters for the numerical predictions shown in Figs. 5.3 and 5.4. Note that these predictions, and all future theoretical computations, are obtained by the author using software written by Dr Kirby.

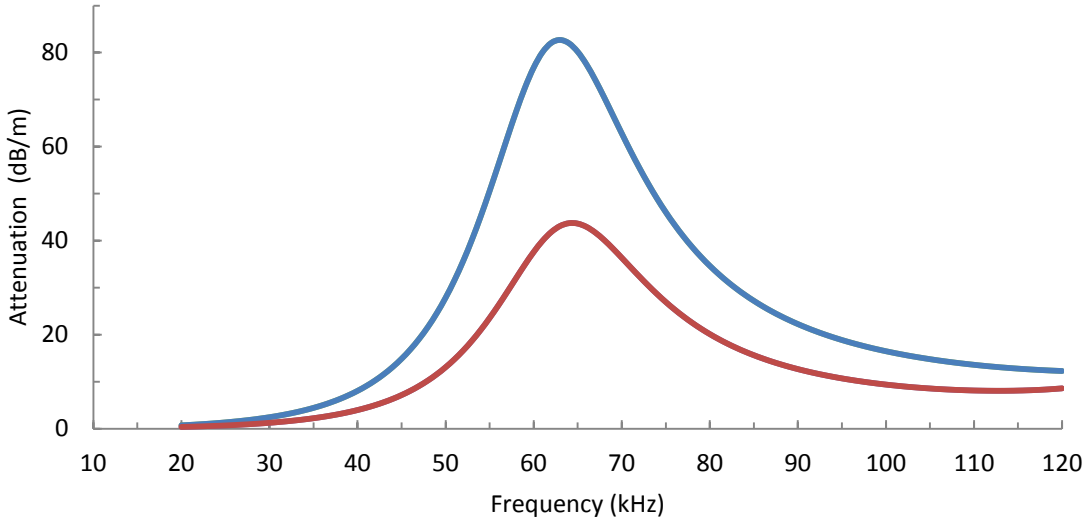

Figure 5.3: Predicted attenuation for a 6in Sch40 pipe coated with bitumen: ——, T(0,1); ——, L(0,2).

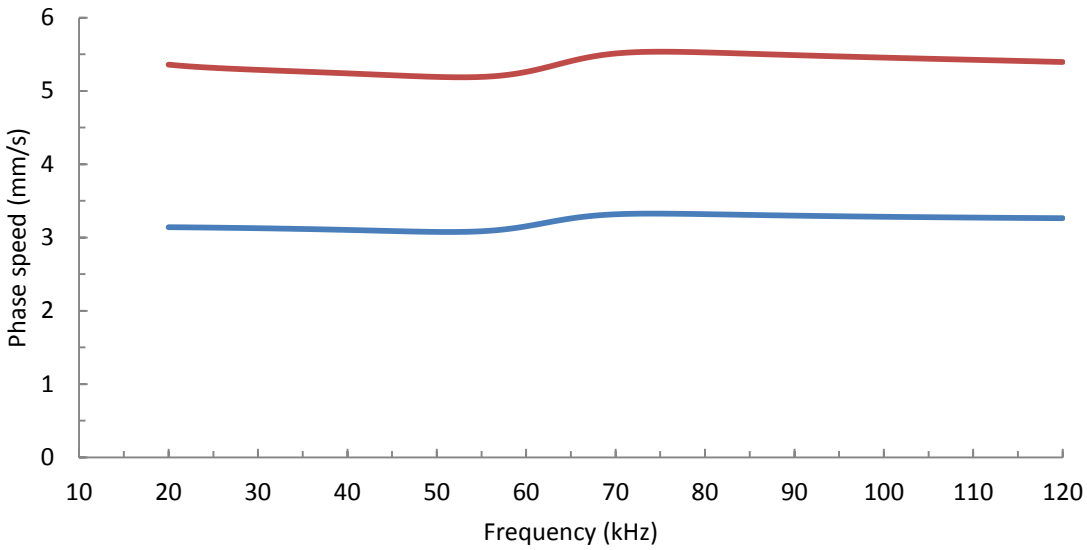

Figure 5.4: Predicted phase speed for a 6in Sch40 pipe coated with bitumen: ——, T(0,1); ——, L(0,2).

The presence of a viscoelastic coating material is seen to attenuate the sound wave in Fig. 5.3 and significant levels of attenuation are seen for both modes. In Fig. 5.4 the phase speed is shown to be relatively constant and this is to be expected over the frequency range shown, although the phase speed can change when a coating is added and this effect becomes more significant as the thickness of the coating is increased. The sudden rise in the phase speed in the mid frequency range is caused by the large material thickness, which means that the wavelength of sound becomes a multiple of the coating thickness in the mod frequency range and this causes a rise in the phase speed.

In Fig. 5.3, it may be suggested that the optimum frequency range is where the attenuation of the guided mode of interest is a minimum because this will ensure a longer propagation distance. In reality it is more important to determine the optimum frequency for testing coated pipes with respect to the energy reflected from defects with a given geometry. One possibility to do this is to utilise the results from the SAFE method to study the reflection coefficient for a defect in coated and uncoated pipes, as reported by Kirby et al. [69, 70]. This method uses the eigenmodes found from the SAFE method to construct the sound field on either side of a defect. If the defect is uniform, then the SAFE method is also used

to find the eigenmodes for the defect, and the scattered sound field is then calculated following application of continuity of displacement and tractions in the axial direction on either side of the defect [69, 70]. If the defect is non-uniform then it is modelled using the finite element method and this solution is joined to the eigensolution on either side of the defect following application of the same continuity conditions. This is the hybrid method described by Kirby et al. [69, 70] and the software written by Dr. Kirby to implement this and other methods is used by the author to generate the predictions that follow. The theoretical methods described by Kirby et al. [69, 70] can be used for studying guided wave reflection coefficients from axisymmetric uniform defects of length L_n and radius a_2, and the hybrid numerical method is used for axisymmetric tapered defects of length L_n, radius a_2 and taper angle γ.

The successful determination of the bulk acoustic properties of the coating material by the method shown in Figs. 5.1 and 5.2 depends on accurate numerical predictions generated by the numerical methods utilised. Once we have the bulk acoustic properties of the coating material determined, it is of great practical interest to have a set of methods which can then accurately predict guided wave attenuation, as well as reflection coefficients from discontinuities in coated pipes.

Part of the work described in the next section deals with the experimental validation of the numerical predictions generated using the methods reported by Kirby et al. [69, 70]. This is achieved by comparing numerical predictions against experimentally measured reflection coefficients for uncoated and coated pipes. The experimental data are obtained using the methodology described in Section 5.2. The bitumen coating material investigated in this chapter is 1.5 mm thick Bituthene 4000 coating material. This coating material is different to the Bitustik 4000 used in Chapters 3 and 4. This is because the Bitustik 4000 coating material was not available on the market when the experimental work presented in this section was conducted and it was substituted with Bituthene 4000.

5.2 Experimental work

The numerical predictions give useful information on the characteristics of guided wave modes and their interaction with defects with different geometries from a theoretical point of view. In reality we need numerical methods which can accurately do these predictions for real pipes. In order to understand how accurate the predictions are, they are compared against data obtained experimentally. A set of experiments are undertaken in order to measure the reflection coefficients of T(0,1) and L(0,2) using axisymmetric defects located in uncoated and coated pipes. The reflection coefficients measured are also used to calculate the attenuation in the coated section of the pipe. The experimental set up is shown in Fig. 5.5 and consists of a 6 m long 3 inch Schedule 40 mild steel pipe, so that $a_1 = 39\text{mm}$ and $b_1 = 44.65\text{mm}$.

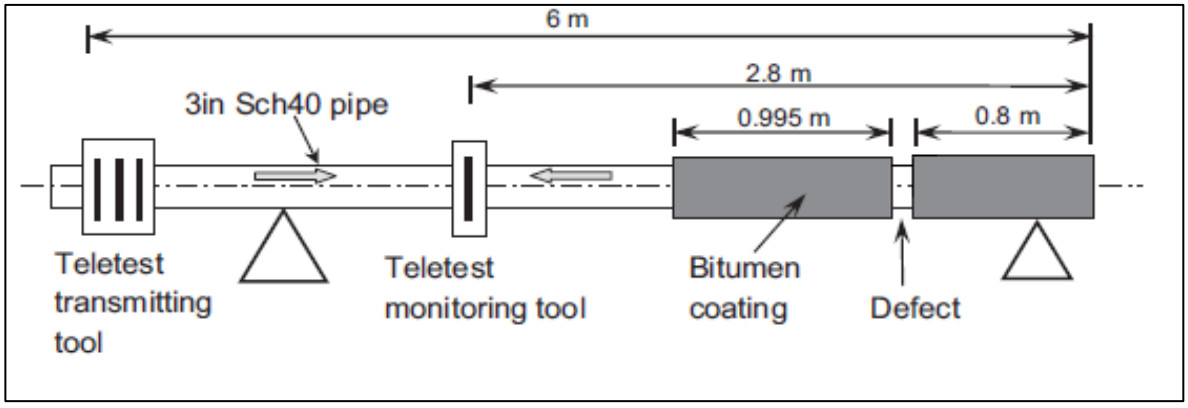

Figure 5.5: Experimental set up.

The defect shown in Fig. 5.5 is machined 0.8 m from the far end of the pipe. The depth of the defect represents 50% of the pipe wall thickness. The geometry of the uniform and non-uniform defect is shown in Figs 5.6 and 5.7, respectively. The experiments were performed with and without a coating material applied.

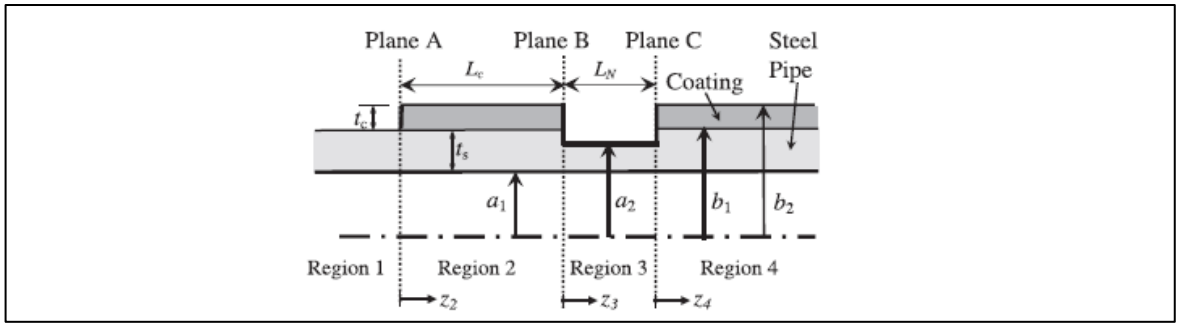

Figure 5.6: Geometry of axisymmetric uniform defect.

The desired guided wave mode is first excited using a commercial Teletest system [35]. For the shear guided wave mode the device was set to generate the T(0,1) mode only, and for longitudinal modes it was set to generate the L(0,2) mode only. The Teletest system is also designed to suppress the generation of unwanted modes.

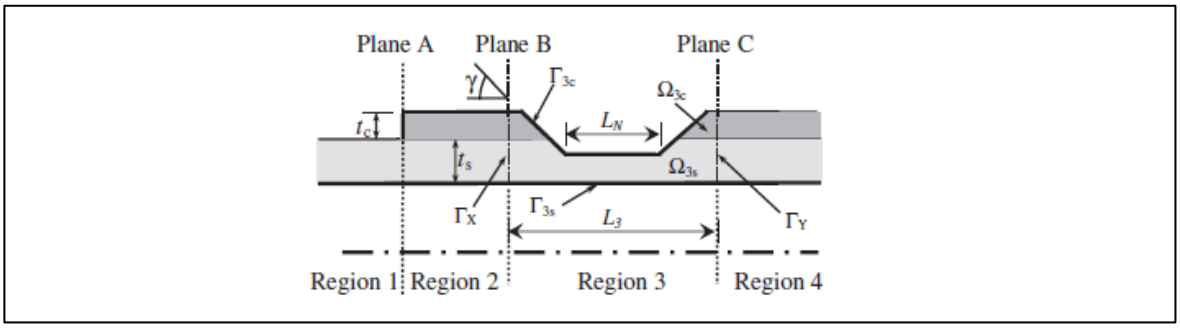

Figure 5.7: Geometry of axisymmetric tapered defect.

A purpose designed monitoring ring made of four Teletest transducers was used to monitor the amplitude of the incident and reflected signals coming back from the defect. The four transducers were equally spaced at 90^o around the circumference of the pipe and clamped by a spring loading mechanism. The position of the transmitting tool and the monitoring ring are shown in Figure 5.8.

Figure 5.8: Experimental setup and monitoring ring.

The desired guided wave mode was excited using 10 cycles of a Hanning modulated tone burst signal. The centre frequency of excitation was varied between 20 kHz and 120 kHz in 5 kHz increments. The acoustic signal reflected back from the defect is detected using the monitoring ring and recorded by the Teletest pulse/receiver unit. The data were collected 64 times and averaged at each frequency step in order to reduce the level of random noise. The averaged data of T(0,1) collected at centre frequency of 40 kHz is shown as an A-scan in Figure 5.9.

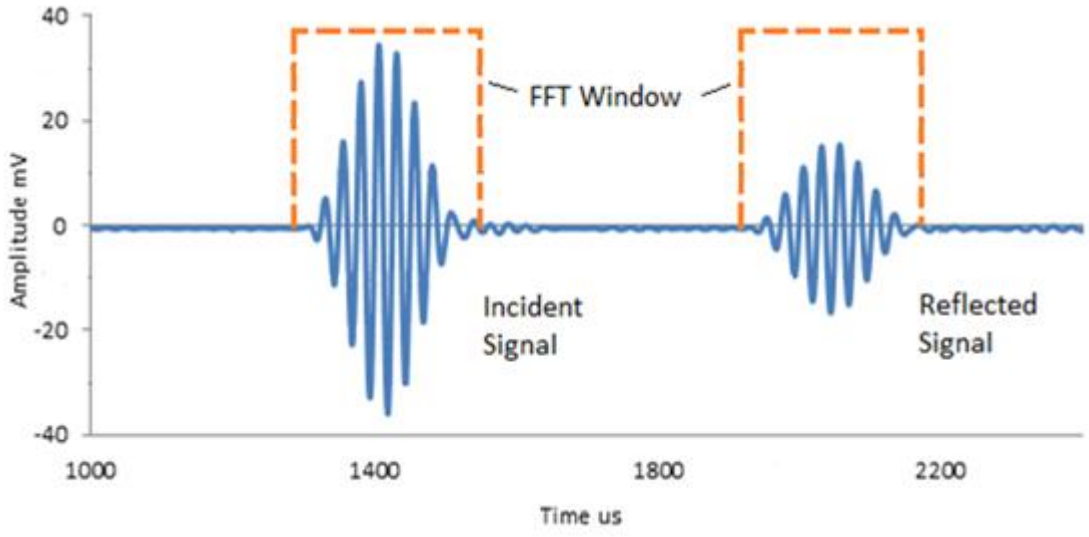

Figure 5.9: A-scan of T(0,1) at 40 kHz.

The first signal is the incident wave and the second signal is the wave reflected by the defect. The frequency amplitude spectra (FAS) of the incident and reflected signals were calculated by applying a rectangular window on each pulse, as shown in Figure 5.9. The width of the window in the time domain was chosen to be 20% wider than the length of the original Hanning modulated signal. A frequency bandwidth of 125Hz was used when transferring from the time into the frequency domain. Equation (5.1) is then used to calculate in the reflection coefficient in the frequency domain using the amplitudes of the incident and reflected signals I and R:

$$\Lambda_n = \frac{R_{FAS}}{I_{FAS}}, \tag{5.1}$$

The bitumen coating material used to coat the area of the pipe before and after the defect is 1.5 mm thick Bituthene 4000 coating material. It has a flexible waterproof membrane combining a high performance cross laminated HDPE carrier film, with a unique super sticky self-adhesive rubber bitumen compound. More information about the material can be found in [98].

Following [20], the complex shear and longitudinal velocity of the bulk wave within the (viscoelastic) coating is written as:

$$c_c = \frac{1}{\left[\frac{1}{\tilde{c}_c} + i\frac{\alpha_c}{\omega}\right]}, \tag{5.2}$$

and the bulk longitudinal acoustic velocity as

$$a_c = \frac{1}{\left[\frac{1}{\tilde{a}_c} + i\frac{\alpha_L}{\omega}\right]}. \tag{5.3}$$

Here, c_c and a_c are the complex acoustic shear and longitudinal velocities of the bulk wave within the (viscoelastic) coating, $\tilde{c}_c$ and $\tilde{a}_c$ are the phase velocities for the bulk shear and longitudinal wave within the coating, and α_c and α_L are the shear and longitudinal attenuation constants.

Barshinger and Rose [20] suggest values of $\tilde{c}_c = 750$ m/s and $\alpha_c = 0.24 \times 10^{-3}$ s/m for the shear properties, $\tilde{a}_c = 1860$ m/s and $\alpha_L = = 0.023 \times 10^{-3}$ s/m for the longitudinal properties and a density $\rho_c = 1200$ kg/m^3 for their bitumen coating.

It is easier first to validate the numerical models by comparing numerical predictions against experimental measurements for an uncoated pipe. This is because the numerical predictions for an uncoated pipe are well established in the literature and they also require less input variables, and the acoustic properties for steel are well established [79]. The uncoated pipe case is therefore examined first for axisymmetric uniform and non-uniform defects. The acoustic properties for steel used in these numerical predictions are $c_s = 3260$ m/s , $a_s = 5960$ m/s and $\rho_s = 8030$ kg/m^3.

5.3 Uncoated pipe

Torsional mode

In Figs. 5.10 and 5.11 numerical predictions are shown for a uniform defect in an uncoated steel pipe. These predictions were obtained by running the code developed by Dr. Kirby [69], who used the mode matching method to generate these predictions. The geometry used for the uniform defects is $L_n = 15$ mm in Fig. 5.10 and $L_n = 30$ mm in Fig. 5.11, with $a_1 = 39$ mm, $a_2 = 41.85$ mm and $b_1 = 44.65$ mm (a 50% wall thickness reduction) for both defects, see also Fig. 5.6. The predictions are compared against measurement and it is evident in Fig. 5.10 that the numerical predictions correlate well with measured data up to about 95 kHz. The divergence between prediction and measurement at frequencies above 95 kHz could be attributed to a deteriorating signal to noise ratio, and the data shown in Fig. 5.10 also show that the energy reflected back from the defect drops at higher frequencies. In reality, the typical LRUT frequency range is between 30 kHz and 80 kHz, which is limited mostly by the efficiency of the transducers in the LRUT tool hardware, and this hardware is optimised for this frequency range.

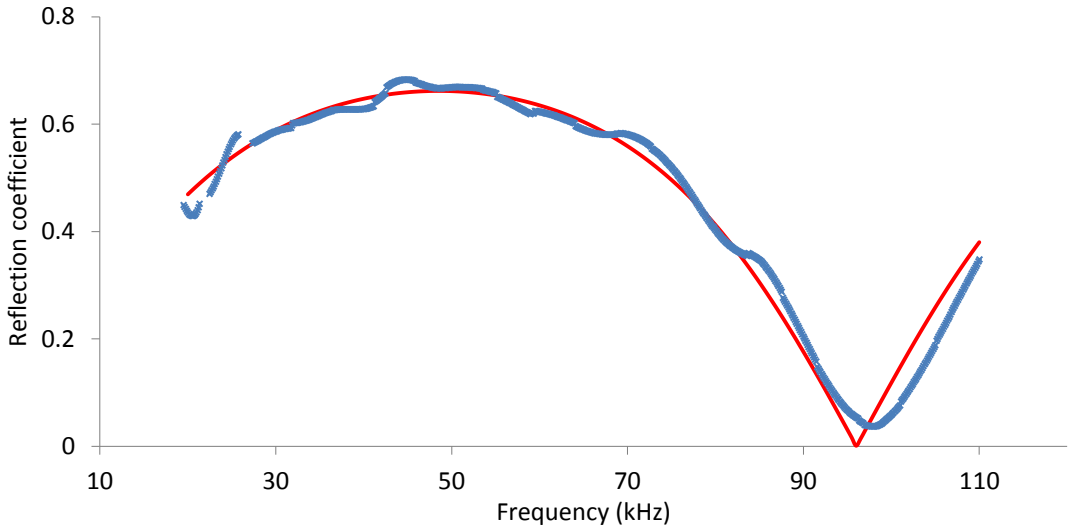

Figure 5.10: Reflection coefficient for a uniform defect of length $L_n = 15$ mm using T(0,1): ×, experiment; ——, prediction.

A comparison between measurement and prediction for a uniform defect with $L_n = 30$mm is shown in Fig. 5.11.

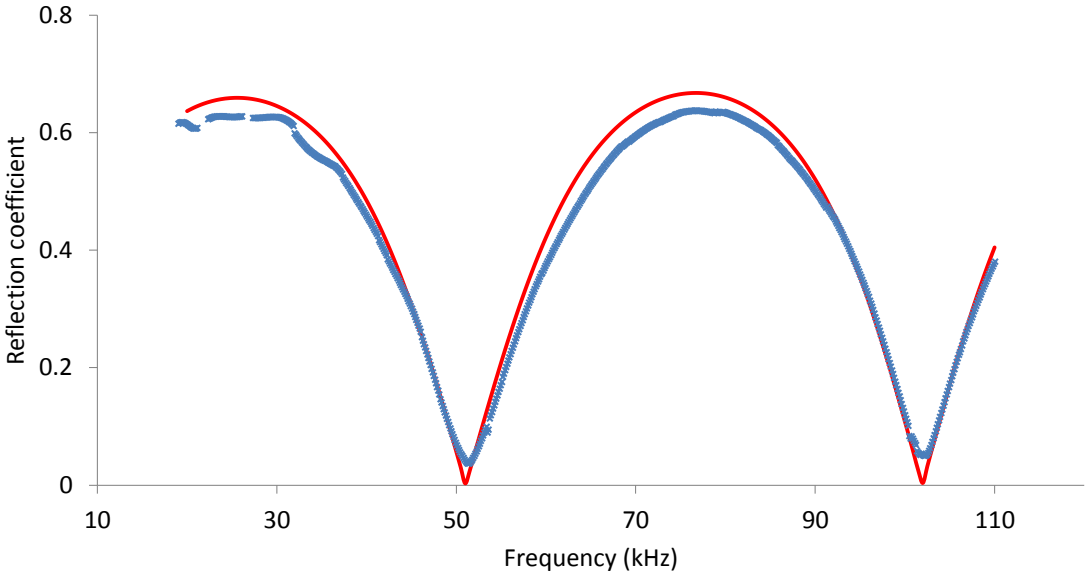

Figure 5.11: Reflection coefficient for a uniform defect of length $L_n = 30$ mm using T(0,1): ×, experiment; ——, prediction.

Prediction is again seen to correlate well with measurement in Fig. 5.11, although a mismatch between measurement and prediction is more obvious than for the smaller defect, but only in the region surrounding the maxima and minima, and here the differences are likely to be caused by attenuation in the steel, which is not accounted for by the theoretical model.

In Figs. 5.10 and 5.11 the reflection coefficient reaches a maximum and then drops to a minimum. This periodic behaviour is caused by the interaction between the incident acoustic wave and the defect. The incident wave hits the defect and a portion of the energy in the wave scatters from the far end of the defect. This energy is either transmitted downstream of the defect or it scatters backwards towards the sound source, and then interacts with the front of the defect. In the same way, some energy is scattered backwards and some transmitted towards the source. The ratio of the energy trapped by the defect and that transmitted downstream of the source depends on the wavelength of the incident sound wave relative to the length of the defect. This then gives a periodic behaviour where for some wavelengths all of the energy is transmitted and at other wavelengths all of the energy is reflected. This behaviour has also been observed by others in the literature [45], see also Kirby et al. [69]. The periodic behaviour seen in Figs. 5.10 and 5.11 is important from a practical point of view because it shows that the optimum frequency range changes with the length of the defect.

The predictions for a uniform defect in Figs. 5.10 and 5.11 show that mode matching method is capable of providing accurate predictions for this type of defect, with a level of agreement between prediction and experiment comparable to that seen in other studies. This is now extended to the validation of a model for non-uniform defects, and this approach uses the hybrid numerical method reported by Kirby et al. in [69, 70]. In Figs. 5.12 and 5.13 predictions are compared against measurement for a tapered defect with $L_n = 15\text{mm}$ and $L_n = 30\text{mm}$, respectively. In addition, $a_1 = 39$ mm, $a_2 = 41.85$ mm, $b_1 = 44.65$ mm (a 50% wall thickness reduction), and the taper angle $\gamma = 60^o$, see also Fig. 5.7.

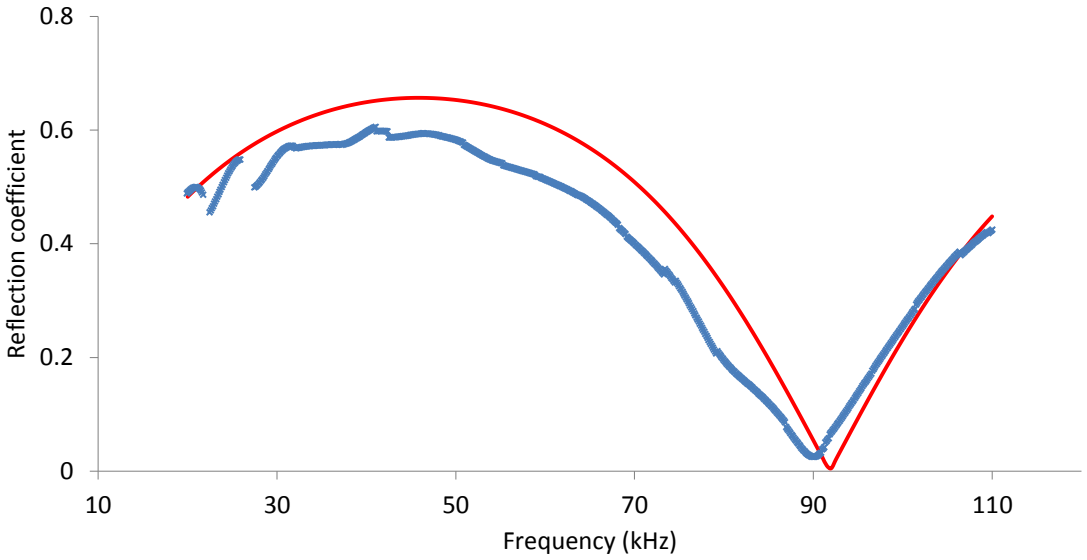

Figure 5.12: Reflection coefficient for a non-uniform defect of length $L_n = 15$ mm with $\gamma = 60°$ and using T(0,1): ×, experiment; ——, prediction.

The agreement between measurement and prediction shown in Fig. 5.12 is generally good for the tapered defect. The mismatch below 90 kHz may be attributed to the previously discussed losses in the system, which are not accounted for in the theoretical model. Compared with the data for a uniform defect with $L_n = 15$ mm, shown in Figure 5.10, the presence of a taper with $\gamma = 60^o$ does not seem to affect the maximum RC value, although the position of the RC minimum is shifted a few kHz lower. The correlation between measurement and prediction shown in Fig. 5.12 is generally good, although below 90 kHz the agreement is not as good as that seen for the uniform defects in Figs. 5.10 and 5.11. This deviation could be attributed to experimental errors, which may be associated with increased coherent noise at lower frequencies in this particular set of data.

In Fig. 5.13 the reflection coefficient for a tapered defect with a longer length of $L_n = 30$ mm is shown, and this shows an increase in periodic behaviour, which is caused by increasing the length of the defect. This means that there are more frequencies where the wavelength of sound is a multiple of the length of the defect so that energy is transmitted through the defect.

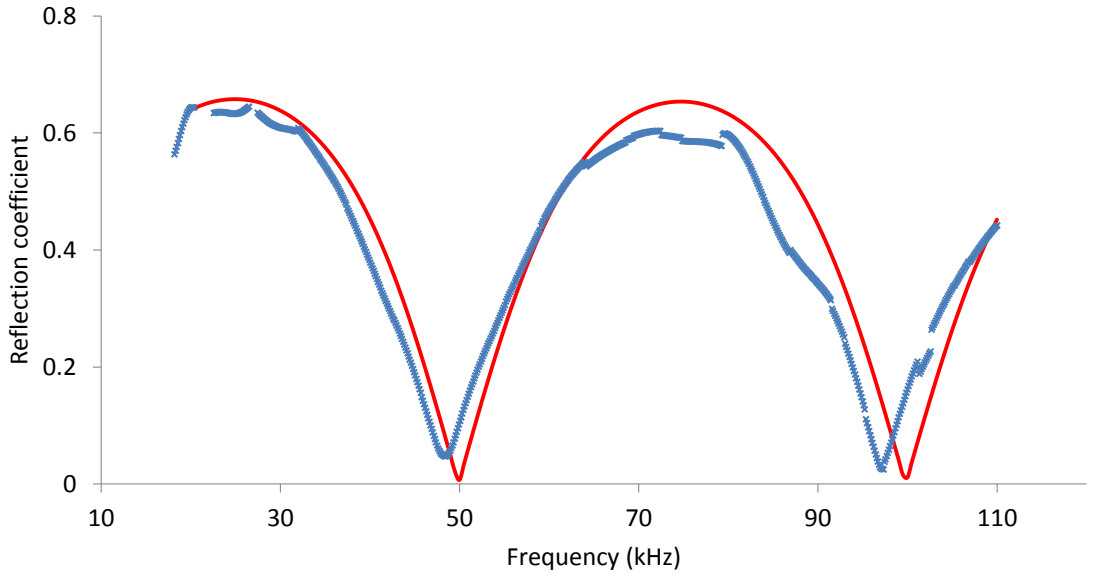

Figure 5.13: Reflection coefficient for a non-uniform defect of length $L_n = 30$ mm with $\gamma = 60°$ and using T(0,1): ×, experiment; ——, prediction.

Figure 5.13 also shows good agreement between numerical predictions and measured data, and the agreement is similar to that seen for the shorter defect in Fig. 5.12. This demonstrates that the hybrid method of Kirby et al [69] is capable of providing accurate predictions.

Longitudinal mode

Predictions generated by the mode matching technique for longitudinal modes is reported by Kirby et al. [70] and these are first compared here against experimental measurements for uniform defects. The geometry of the defects for the longitudinal mode are the same as those studied for the torsional mode T(0,1) in the previous section.

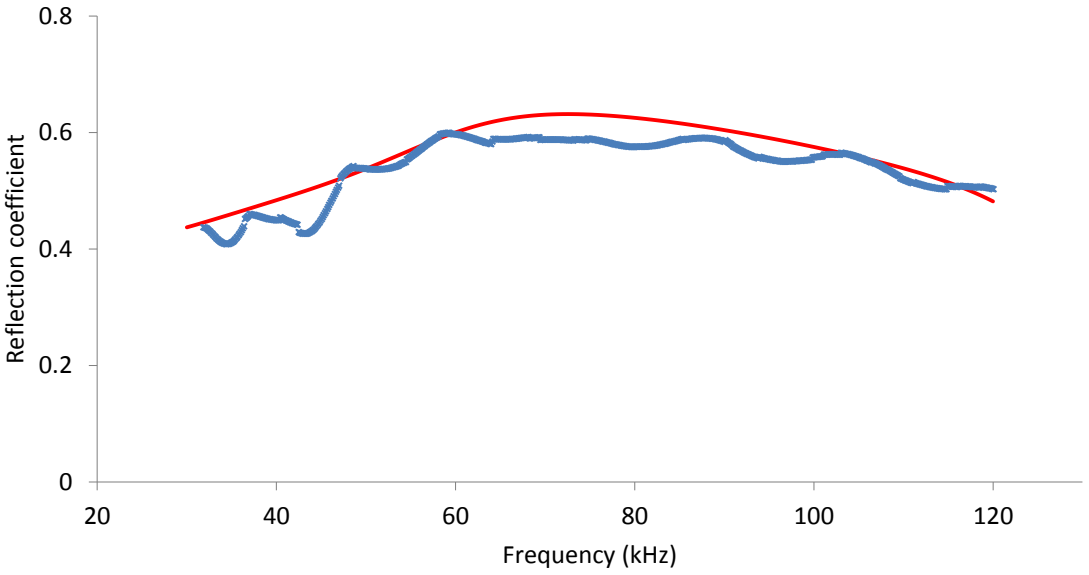

Figure 5.14: Reflection coefficient for a uniform defect of length $L_n = 15$ mm using L(0,2): ×, experiment; ——, prediction.

It is evident in Fig. 5.14 that good agreement between prediction and measurement is observed for the longitudinal mode across a relatively wide frequency range. It is also interesting to note that the maximum RC value is almost the same as the one measured in Figure 5.10, where T(0,1) was used. The position of the first RC minimum and maximum does, however, appear at a higher frequency and this is because the phase speed of L(0,2) is higher than T(0,1).

A comparison between prediction and measurement for a uniform defect with $L_n = 30$mm is shown in Fig. 5.15. It is seen that a comparison between the two is generally good over a wide frequency range. At lower frequencies oscillation in the experimental data is likely to reflect a problem with the experimental equipment, such as the sensitivity of the Teletest transducers at low frequencies, as well as contamination from L(0,1). The deviation at high frequencies is most likely to be caused by the losses in the system not accounted for in the model, such as those discussed earlier.

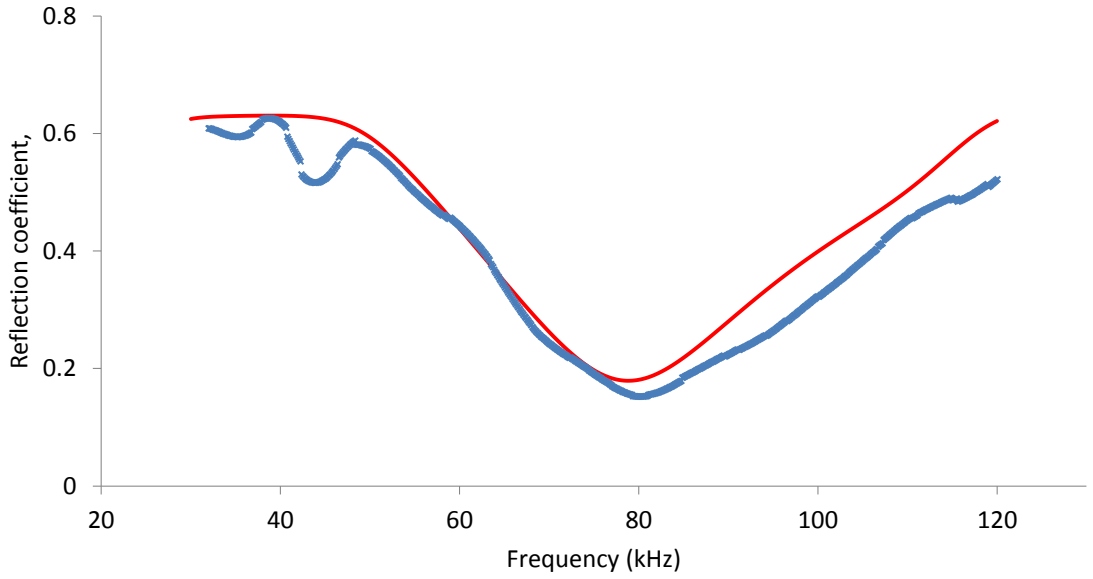

Figure 5.15: Reflection coefficient for a uniform defect of length $L_n = 30$ mm using L(0,2): ×, experiment; ——, prediction.

In Fig. 5.15 it is seen that increasing the length of the defect from 15 mm to 30 mm changes the RC spectra significantly. The position of the RC minimum and maximum is seen to shift to a lower frequency. A similar situation was also observed for T(0,1) in Figs. 5.10 and 5.11. It is interesting also to note that the RC minimum value is not close to zero for L(0,2), as it was for T(0,1). This is because T(0,1) is a planar wave with displacement in the circumferential direction only. For L(0,2) displacement is in both the axial and radial directions and so the mode is no longer planar. This means that the outgoing and reflected waves can no longer perfectly interfere with one another and so the minimum is no longer zero for L(0,2).

In Figs. 5.14 and 5.15 good agreement between prediction and experiment is observed for the RC of L(0,2) across the frequency range of interest. In common with T(0,1) the validity of the theoretical model is also tested here by comparing prediction against measurement for a tapered defect. The defect's geometry is the same as the geometry used for the torsional mode presented in Figs. 5.12 and 5.13. A comparison between experiment and prediction for a tapered defect is shown in Figs. 5.16 and 5.17 for defects with $L_n =$

15 mm, and $L_n = 30$ mm, respectively. The other dimensions of the tapered defect are common with the geometry used for T(0,1), see for example Fig. 5.7.

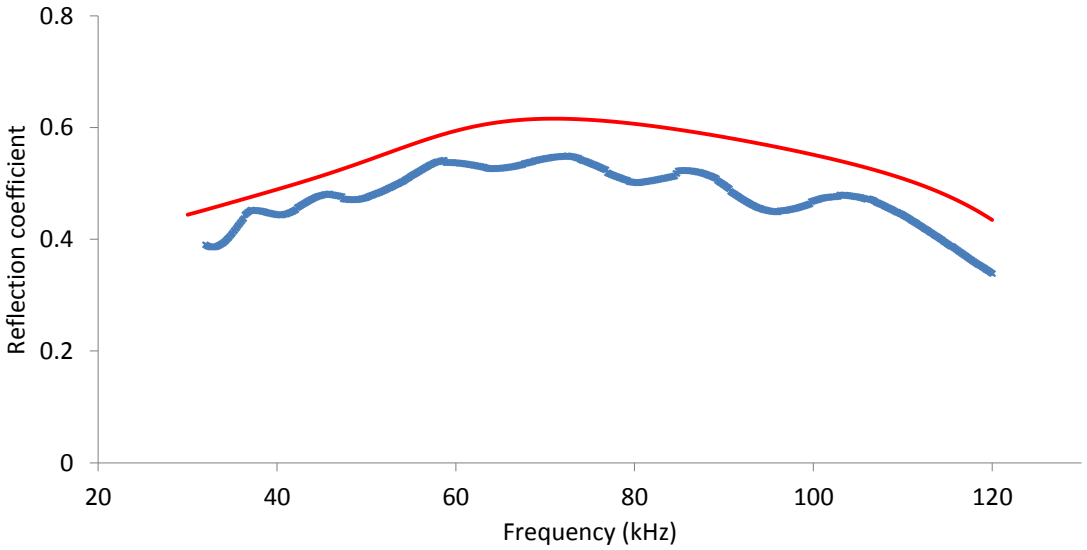

Figure 5.16: Reflection coefficient for a non-uniform defect of length $L_n = 15$ mm with $\gamma = 60°$ and using L(0,2): ×, experiment; ——, prediction.

Figure 5.16 shows a comparison between prediction and measurement for a tapered defect with $L_n = 15$ mm and $\gamma = 60^o$. It is seen that prediction and measurement generally agree with one another, although the predictions are slightly lower and this is likely to be caused by losses in the system not accounted for by the theoretical model, as well as a lack of efficiency in the coupling for the Teletest ring which will be partially contaminated by the L(0,1) mode.

In Fig. 5.17 prediction and measurement are compared for the reflection coefficient of a tapered defect with length $L_n = 30$ mm and a taper angle of $\gamma = 60^o$. Again, good agreement between the two sets of data is observed and this is seen to be an improvement when compared to Fig. 5.16. Therefore, it is possible that any discrepancies between prediction and experiment are simply a result of experimental error.

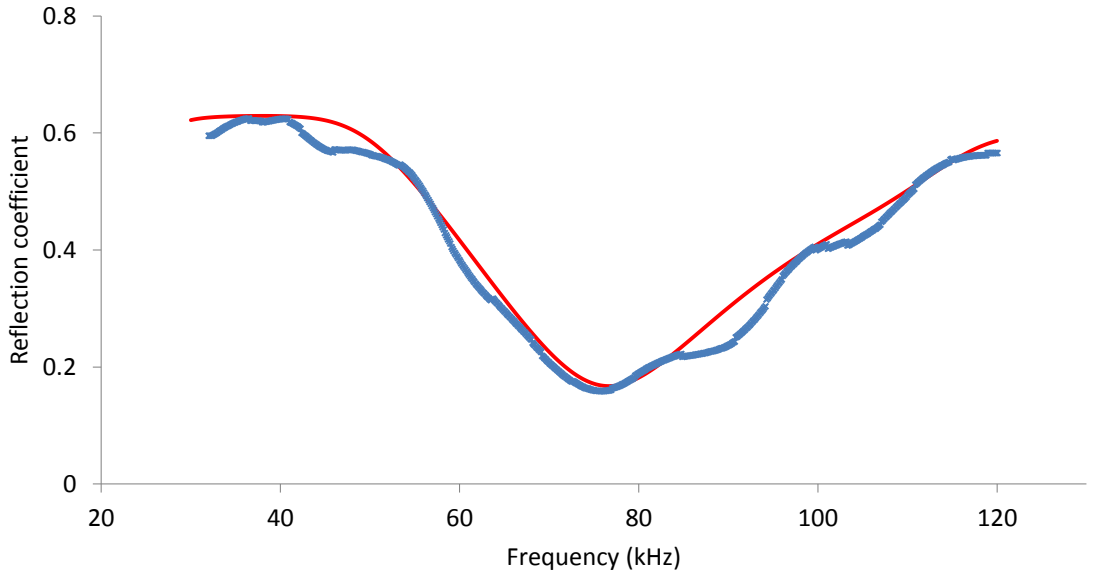

Figure 5.17: Reflection coefficient for a non-uniform defect of length $L_n = 30$ mm with $\gamma = 60°$ and using L(0,2): ×, experiment; ——, prediction.

The data for the tapered defect in Fig. 5.17, and the square defect in Fig. 5.15, follow the same shape as one another, but the presence of the taper shifts the RC minimum towards a lower frequency, as was observed previously for T(0,1). It is interesting also to note the strong influence that the length of a chamfered defect has on the RC of L(0,2).

It is evident from the data presented here that good agreement between prediction and measurement is observed for L(0,2) across the frequency range of interest. This serves to validate the numerical predictions used to calculate reflection coefficients in the absence of a coating material, reported in [70] for L(0,2). This shows that the mode matching and hybrid numerical methods used by Kirby et al. [69, 70] provide accurate predictions for the reflection coefficients of T(0,1) and L(0,2) for uniform and non-uniform axisymmetric discontinuities in an uncoated pipe. The results also show that the detectability of a defect with a specific geometry depends simultaneously on the guided wave mode type and the test frequency, which proves the need for theoretical methods which can predict the optimum parameters for LRUT in pipelines. The next section deals with guided wave reflection coefficients from axisymmetric defects located in a pipe coated with bitumen.

This section also shows how the method for coating material characterisation described in Section 5.1 can be used for the determination of the bulk acoustic properties of the coating material.

5.4 Coated pipe

In the previous section a theoretical method was validated for the relatively simple problem of an uncoated pipe. For a coated pipe additional difficulties are associated with finding appropriate values for $\tilde{c}_c, \alpha_c, \tilde{a}_c$ and $\tilde{\alpha}_L$, which are the acoustic properties of the viscoelastic material. There are also uncertainties associated with the coupling between the pipe wall and the coating material because in the theoretical model this is assumed to be perfect, but in reality this is not always the case.

The presence of a viscoelastic coating material is likely to significantly reduce the amplitude of a signal propagating in a coated pipe. In order to investigate how the presence of a coating material affects the reflection coefficients measured in the previous section, and how accurately they can be predicted, a set of additional experiments were undertaken for a coated pipe which follow the same methodology as for an uncoated pipe. The geometry of the defects investigated is the same as the one reported for an uncoated pipe, but in this case the area before and after the defect was covered with a 1.5 mm thick bitumen material called Bituthene 4000. The length of the coated area is shown in Fig. 5.5, and more information about the coating material may be found in Section 5.2. The experimental data for a coated pipe were collected and processed in the same way as for the uncoated pipe in the previous section. The only difference is that the monitoring ring with transducers for detecting the transmitted and reflected pulse was moved 1 m away from the end of the bitumen coating, as shown in Figure 5.5. This is to ensure that the measurement of reflected signals is not contaminated by evanescent modes scattered by the coating material.

Torsional mode

The reflection of the torsional mode in a coated pipe is investigated first. This is because the torsional mode is a less complicated problem from a modelling point of view when compared to a longitudinal mode. This means that only the shear acoustic properties α_c and $\tilde{c}_c$ are needed, and any errors associated with the accuracy of the longitudinal properties $\tilde{\alpha}_c$ and $\tilde{\alpha}_L$ will not affect the numerical predictions.

In Fig. 5.18 a comparison between measurements carried out here and two sets of theoretical predictions for a coated pipe with a uniform defect of length $L_n = 15$ mm are presented. The theoretical predictions were generated using code from the mode matching method reported by Kirby et al. in [69]. The first set of theoretical predictions is based on values for the acoustic properties of a bitumen material reported by Barshinger and Rose in [20]. The data from Barshinger and Rose is $\alpha_c = 0.24 \times 10^{-3}$ s/m and $\tilde{c}_c = 750$ m/s. Comparison between measurement and prediction for a coated pipe using the data of Barshinger and Rose shows significant deviation in Fig. 5.18. It is obvious that at low frequencies the theoretical predictions show much higher values for the reflection coefficient, and at higher frequencies the reflection coefficient seems almost to disappear. The discrepancies described are likely to be the result of differences between the properties quoted by Barshinger and Rose and the actual properties of the material studied. This is because measurements for an uncoated pipe with the same defect geometry, shown in Fig 5.10, provide accurate correlation with predictions. This suggests there are problems with the values for a coating reported by Barshinger and Rose [20], at least in characterising the type of bitumen material used in this study.

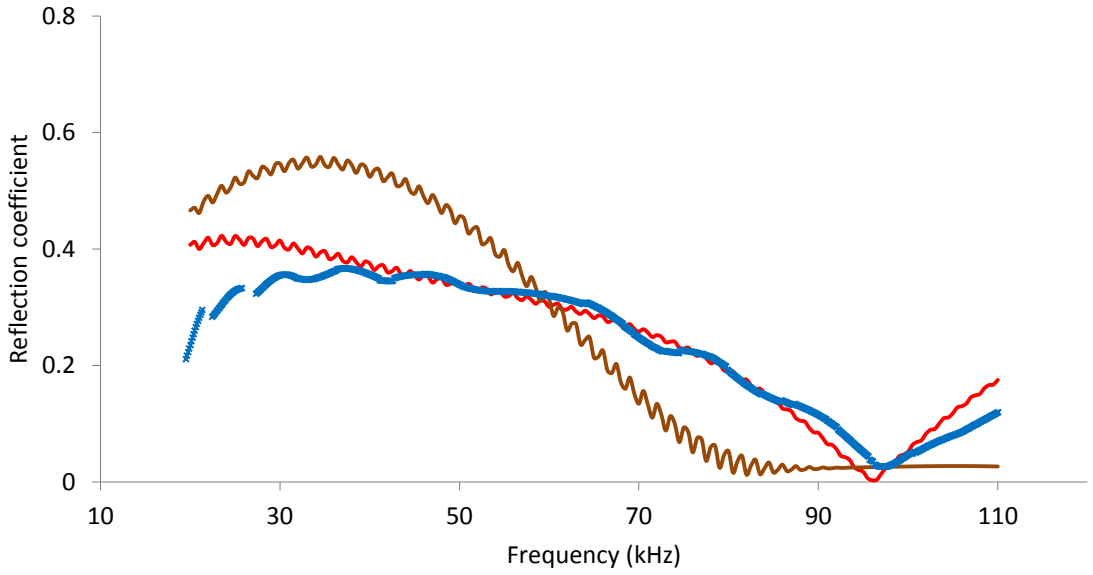

Figure 5.18: Reflection coefficient for a uniform defect of length $L_n = 15$ mm in a coated pipe using T(0,1): ×, experiment; ——, prediction with new values; ——, prediction using values from [20].

The difference between prediction and measurement when using the data of Barshinger and Rose show that it is not possible to use one set of values for all types of bitumen material. To overcome this the method identified in section 5.1 is used in order to obtain new values for α_c and $\tilde{c}_c$. To do this, the experimental data shown in Fig. 5.18 is used as the input for the method described in Fig. 5.1. After a few iterations a value for the shear attenuation constant of $\alpha_c = 3.9 \times 10^{-3}$ s/m was obtained, and in Fig. 5.18 it is seen that this provides a much better agreement between measurement and prediction. The shear velocity value $\tilde{c}_c$ was also kept constant during this iteration because parametric studies showed that the shear attenuation constant α_c has the dominant effect on the predictions presented in Fig. 5.18. In Fig. 5.18 it is shown that it is possible to obtain good agreement between prediction and measurement if the appropriate shear properties are chosen. It is interesting to see that a much higher value for α_c than the one reported by Barshinger and Rose is appropriate for the bitumen material used in this study.

The oscillations seen in the theoretical predictions shown in Fig. 5.18 are caused by internal reflections within the coated section. The wavelength and amplitude of these oscillations is largely dictated by the length of the coating, L_c. Increasing the length of the coated section decreases the wavelength and amplitude of the oscillations observed. This effect can be observed in the theoretical predictions presented later. The amplitude of these oscillations is relatively small compared to the overall signal amplitude and it is not expected to be present in the experimental data.

In Figure 5.19 the measured reflection coefficient of a uniform defect with length $L_n = 30$ mm is compared against two sets of predictions. The first set of numerical predictions is based on the values reported by Barshinger and Rose [20], and the second set of predictions is based on the new values of α_c and $\tilde{c}_c$ obtained in the previous set of experiments. The first set of predictions, based on the values reported by Barshinger and Rose, show predictions that are much higher than measured values at low frequency, and much lower at higher frequencies. This behaviour is similar to that observed in Fig. 5.18. This confirms that the values reported by Barshinger and Rose are most likely to be inappropriate for the bitumen material used in this study. However, this also shows that the reflection coefficient is very sensitive to values of the shear attenuation and that it is important to find accurate values for this property. The sensitivity of guided wave propagation to values of shear attenuation were also observed by Simonetti [14], Rose [15], and Kirby et al. [69, 70]. The second set of numerical predictions, based on the new values of $\alpha_c = 3.9 \times 10^{-3}$ s/m and $\tilde{c}_c = 750$ m/s calculated previously, agree much better with measurement. The good agreement in Fig. 5.19 between measurement and prediction based on these new values implies that the values of α_c and $\tilde{c}_c$ arrived at previously are successful in capturing the acoustic behaviour of the coating material. This will be further investigated by comparing numerical predictions based on these new values against measurements for tapered defects.

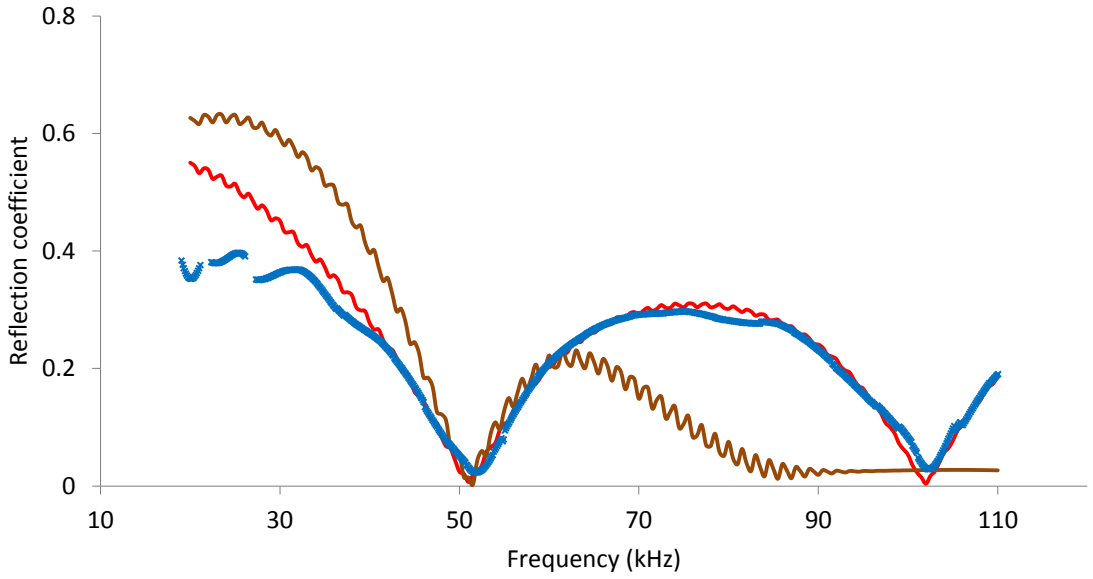

Figure 5.19: Reflection coefficient for a uniform defect of length $L_n = 30$ mm in a coated pipe using T(0,1): ×, experiment; ——, prediction with new values; ——, prediction using values from [20].

In order to further investigate the accuracy of the hybrid model for a coated pipe, a tapered defect identical to that reported for an uncoated pipe in Fig. 5.12 is studied here. Figure 5.20 shows a comparison between measurement and two sets of predictions for a tapered defect with $L_n = 15\text{mm}$ and $\gamma = 60^o$. The mismatch between measurement and a first set of predictions based on the values reported by Barshinger and Rose [20] is similar to that observed in Figs. 5.18 and 5.19. The second set of predictions based on the new values of α_c and $\tilde{c}_c$ agree much better with the measured data. Comparison with reflection coefficients for an uncoated pipe with the same defect geometry shown in Fig. 5.12, shows that the presence of a coating material lowers the value of the reflection coefficient. This clearly demonstrates that the presence of coating material makes it difficult to locate defects.

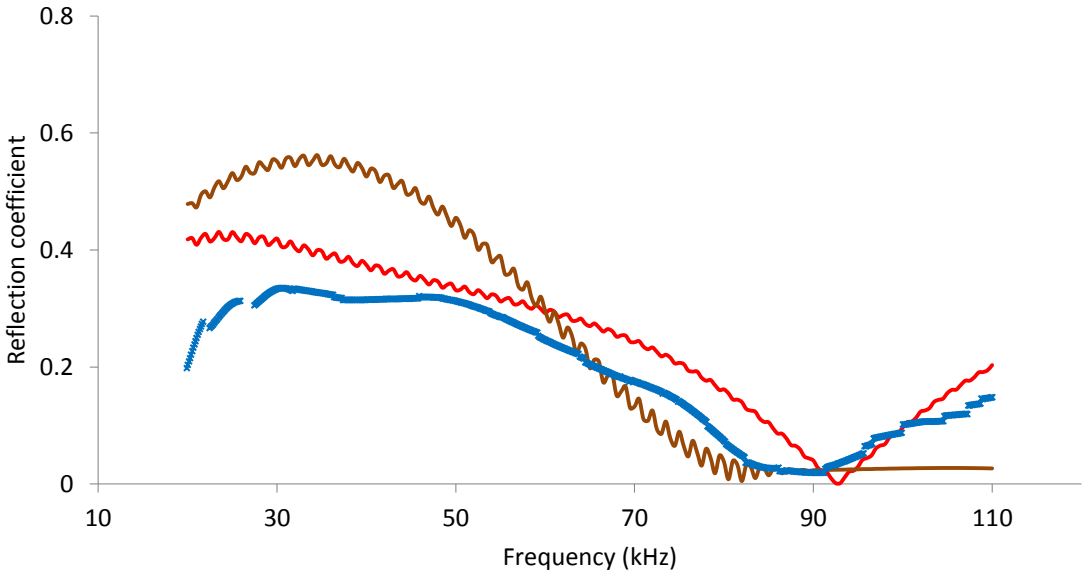

Figure 5.20: Reflection coefficient for a tapered defect of length $L_n = 15$ mm and $\gamma = 60°$ in a coated pipe using T(0,1): ×, experiment; ——, prediction with new values; ——, prediction using values from [20].

Further validation of the predictions for torsional modes is presented in Fig. 5.21 by comparing measurement against numerical predictions for a tapered defect with $L_n = 30$ mm and $\gamma = 60^{o}$. The first set of data based on the shear properties reported by Barshinger and Rose do not agree with the measured data. A similar mismatch observed in the previously presented data serves to reinforce the need for more appropriate values to be found for α_c and $\tilde{c}_c$. The second set of numerical predictions based on the new shear acoustic properties gives the best match between measurement and experiment in Fig. 5.18 and agrees much better with the measurements in Fig. 5.21. However, in Fig. 5.21 the predicted values are generally higher than measurement and this may be attributed to errors associated with the lower signal to noise ratio for a measured pipe, as well as additional losses in the system present in the pipe and in possible areas of incomplete coupling between the bitumen material and the pipe.

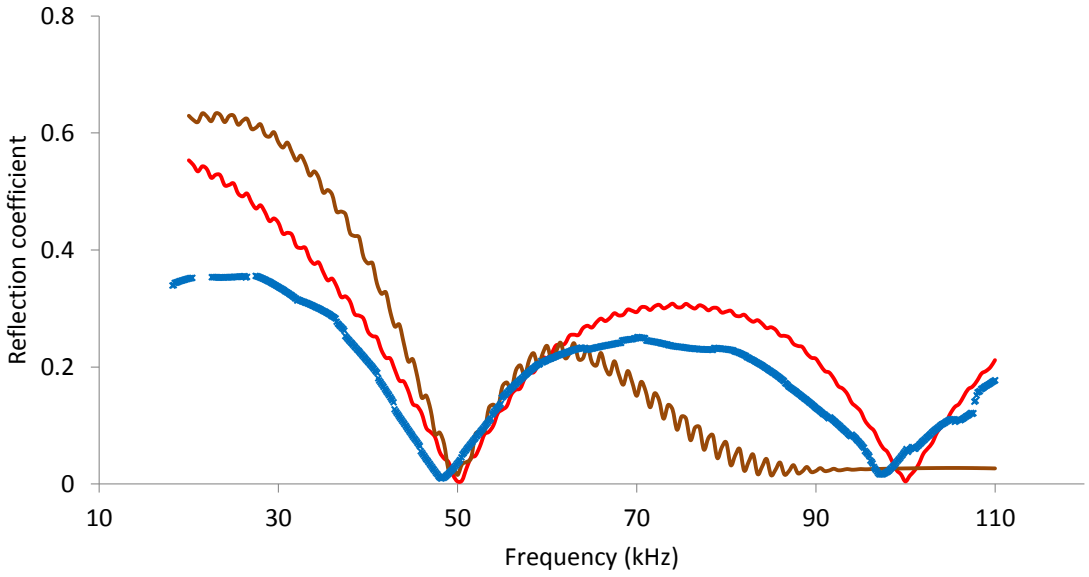

Figure 5.21: Reflection coefficient for a tapered defect of length $L_n = 30$ mm and $\gamma = 60°$ in a coated pipe using T(0,1): ×, experiment; ——, prediction with new values; ——, prediction using values from [20].

The data for T(0,1) presented in these figures shows that a bitumen coating material may significantly reduce the amplitude of a signal reflected back from a defect. The measurements and predictions for T(0,1) show that the reflection coefficients of defects with specific geometry in coated pipes can be predicted with good accuracy provided the right shear acoustic properties α_c and $\tilde{c}_c$ are obtained for the coating material. It was demonstrated that these properties could be derived from experimentally measured reflection coefficient data using the iterative method described in Section 5.1. In this case the values were derived from a single set of experimental data, but the accuracy of the method could be improved if the values α_c and $\tilde{c}_c$ are derived and averaged from more experimental data sets. Of course the validity of these values requires further investigation and one possibility is to use these same values to investigate a comparison between prediction and experiment for L(0,2). This approach is described in the next section, which examines the reflection coefficients of L(0,2) for coated pipes.

The reflection coefficient amplitude in a coated pipe depends simultaneously on the energy reflected from the defect and the attenuation of the signal propagating in the coated section

of the pipe. According to Simonetti, [14] the frequency where the first attenuation maximum occurs for both longitudinal and torsional modes is proportional to the ratio between the shear velocity and the thickness of the coating. The guided wave attenuation predictions for a pipe coated with 0.15 mm thick bitumen material reported in [20] shows that the attenuation maximum occurs at around 1 MHz. This means that if we use the values for the coating material reported in [20], the frequency where the first attenuation maximum should occur for the pipe coated with 1.5 mm thick bitumen material should be at around 100 kHz. This explains the strong influence of the of the bulk shear attenuation constant above 60 kHz. The increased reflection coefficient above 60 kHz when the shear attenuation constant is increased from $\alpha_c = 0.24 \times 10^{-3}\,\mathrm{s/m}$ to $\alpha_c = 3.9 \times 10^{-3}\,\mathrm{s/m}$ can be explained with decreased guided wave attenuation as result of the increased bulk shear attenuation constant. This dependence also corresponds with the findings reported by Simonetti in, [14].

Longitudinal mode

The reflection coefficients for longitudinal modes in a coated pipe are much more difficult to achieve from a modelling point of view. This is because the theoretical predictions for longitudinal modes in a coated pipe require two coupled equations to be solved, as well as knowledge of both the shear and longitudinal properties of the coating material. The parametric studies conducted in the previous section dealing with the torsional mode showed that the shear properties of the coating material have a significant influence on the torsional mode reflection coefficient. One possibility to understand which acoustic properties will give better correlation between measurement and prediction for longitudinal modes is to generate one set of predictions with the bulk shear and longitudinal acoustic properties suggested by Barshinger and Rose [20], and another set of theoretical predictions where the new shear value $\alpha_c = 3.9 \times 10^{-3}\,\mathrm{s/m}$ is used.

Figure 5.22 shows a comparison between the measured and predicted reflection coefficient using L(0,2) for a uniform defect with $L_n = 15\,\mathrm{mm}$. The geometry of the uniform defect is shown in Figure 5.6. The numerical predictions are generated using the mode matching method reported by Kirby et al. [70]. The correlation between the first set of theoretical

predictions based on the acoustic properties suggested by Barshinger and Rose [20] and the measured reflection coefficient is generally not good. The mismatch between these two sets of data is similar to the mismatch for the same defect geometry for T(0,1) in Fig. 5.18. At low frequencies the predicted reflection coefficient is much lower than that measured, and at higher frequencies the predicted reflection coefficient rapidly decreases almost to zero. The second set of numerical predictions based on the longitudinal properties reported by Barshinger and Rose in [20] and the new shear properties obtained here using T(0,1) shows good agreement between prediction and measurement. The minimal mismatch at certain frequencies between the second set of numerical predictions and measurements can be attributed to the flexural components which cannot be completely suppressed at some frequencies.

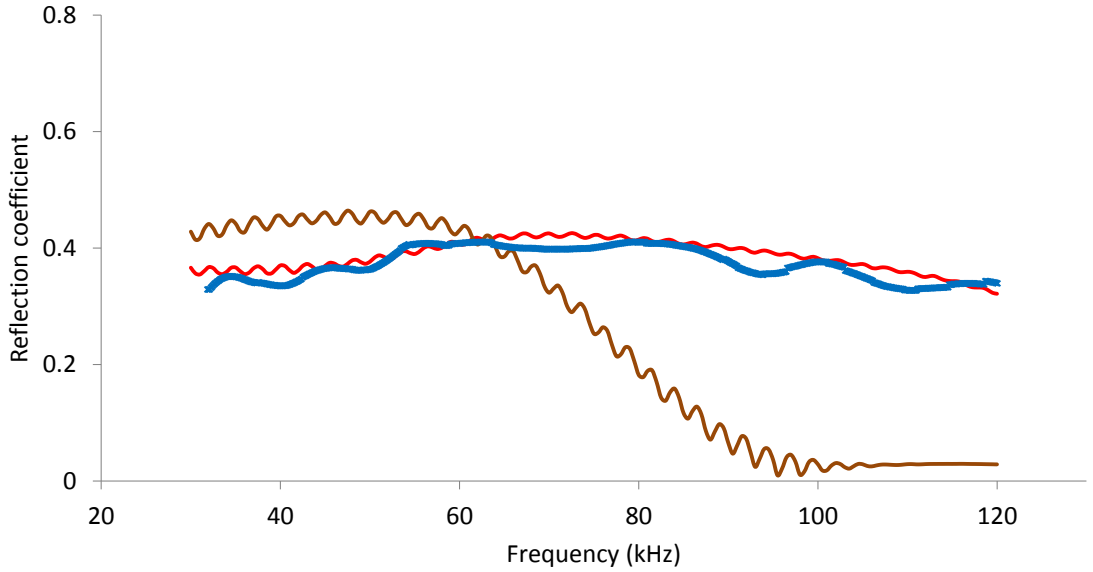

Figure 5.22: Reflection coefficient for a uniform defect of length $L_n = 15$ mm in a coated pipe using L(0,2): ×, experiment; ——, prediction with new values; ——, prediction using values from [20].

Further validation of the coating properties is shown in Fig. 5.23 by comparing RC measurements against predictions for a uniform defect with $L_n = 30$ mm. The geometry of the defect is shown in Fig. 5.6. The first set of numerical predictions based on the values provided by Barshinger and Rose again do agree with measurement. The second set of

numerical predictions based on the longitudinal properties of the bitumen material suggested by Barshinger and Rose and the new shear properties obtained in the previous section again agree well with the measurements. This shows that it is the shear properties of Barshinger and Rose in [20] that causes discrepancies between prediction and measurement for this bitumen material, and these shear properties are the most difficult to measure accurately. The sharp drop at around 45 kHz can be attributed to the presence of flexural components. The measured values are also generally below the second set of numerical predictions because of the additional losses in the system not accounted for in the model, including losses in the steel pipe and scattering/inefficiencies in the Teletest measuring ring.

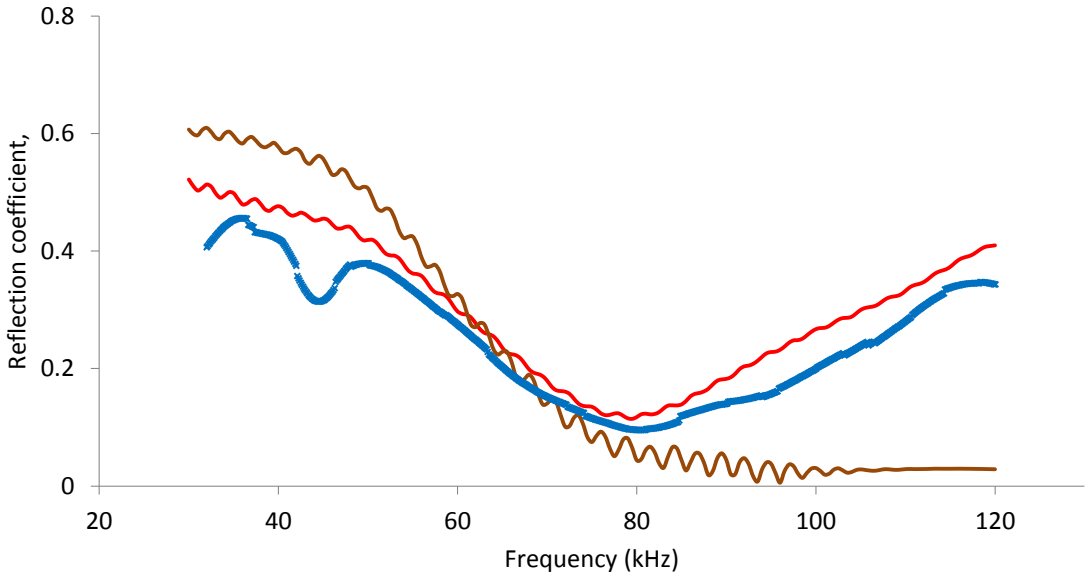

Figure 5.23: Reflection coefficient for a uniform defect of length $L_n = 30$ mm in a coated pipe using L(0,2): ×, experiment; ——, prediction with new values; ——, prediction using values from [20].

The data presented in Figs. 5.22 and 5.23 show that the theoretical method can generate accurate predictions for longitudinal modes if the right shear acoustic properties of the coating material are used.

Finally, the numerical method is validated by comparing prediction and measurement for a tapered defect using longitudinal modes. Figures 5.24 and 5.25 show comparison between measurement and two sets of numerical predictions for a tapered defect with $L_n = 15$ mm and $\gamma = 60^o$, and $L_n = 30$ mm and $\gamma = 60^o$, respectively.

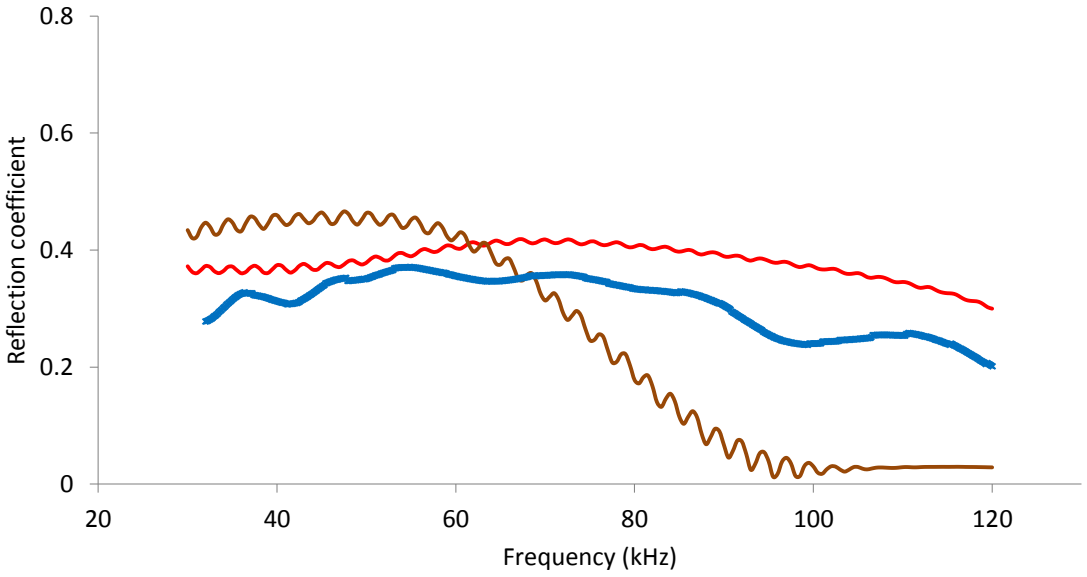

Figure 5.24: Reflection coefficient for a tapered defect of length $L_n = 15$ mm and $\gamma = 60°$ in a coated pipe using L(0,2): ×, experiment; ——, prediction with new values; ——, prediction using values from [20].

In common with the uniform defect, the first set of numerical predictions is generated by using the coating material properties reported by Barshinger and Rose [20], and the second set of numerical predictions are generated by changing only the shear attenuation constant with the shear attenuation constant obtained with the iterative method described in Section 5.1. A comparison between the first set of numerical predictions and the measured reflection coefficients in Figs. 5.24 and 5.25 shows that the numerical predictions generated using the coating properties suggested by Barshinger and Rose give much higher reflection coefficients at low frequencies, and predictions that seem to varnish almost to zero at higher frequencies. Again, the second set of numerical predictions seem to agree much better with the experimental measurements.

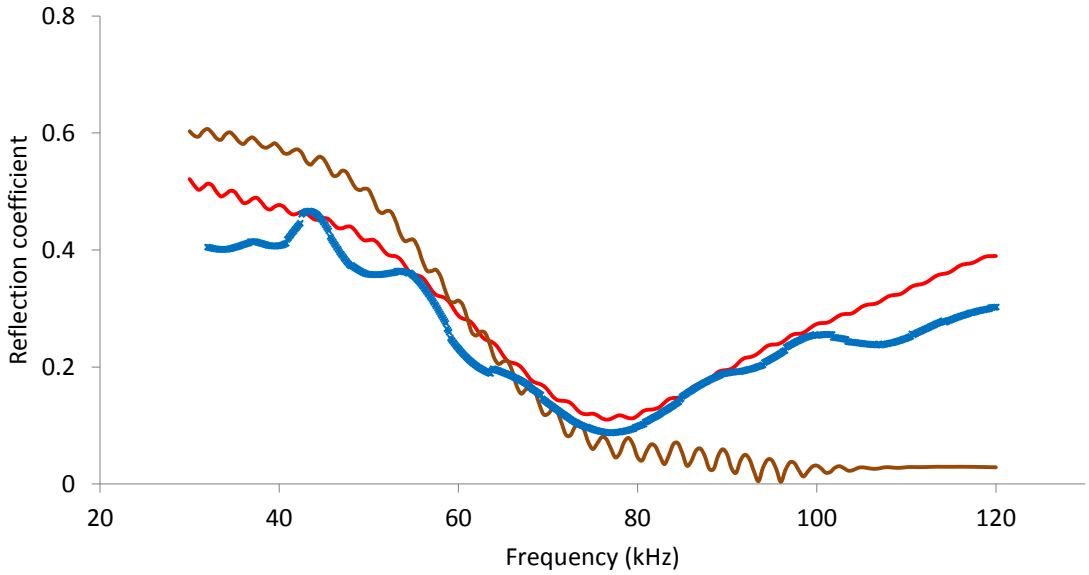

Figure 5.25: Reflection coefficient for a tapered defect of length $L_n = 30$ mm and $\gamma = 60°$ in a coated pipe using L(0,2): ×, experiment; ——, prediction with new values; ——, prediction using values from [20].

The value for the bulk longitudinal properties of the coating material used for the numerical predictions for L(0,2) were kept the same as the values reported by Rose and Barshinger in [20]. This was done because the second part of the method reported in Section 5.2 dealing with the bulk longitudinal properties of the coating material showed that changing the bulk longitudinal properties does not seem to affect the L(0,2) guided wave mode reflection coefficient. This means that the sensitivity of the predictions to the longitudinal properties was much less than the shear properties and so it was not found necessary to identify new values.

5.5 Summary

The data for L(0,2) and T(0,1) for uncoated and coated pipes shows the strong influence of the defect geometry and the presence of viscoelastic coating material on the reflection

coefficients. The accurate determination of where the reflection coefficient in a coated pipe takes on a maximum value depends not only on the defect geometry but also on the bulk properties of the coating material. It is shown that values for the bulk properties of the coating material that give accurate numerical predictions can be determined from the measurement of reflection coefficients and using the iterative method described earlier. The data also shows that at some frequencies the reflection coefficient of L(0,2) is higher than the reflection coefficient of T(0,1). This observation corresponds with the findings reported by other researchers in [16], and this is because L(0,2) has lower levels of attenuation when compared to T(0,1) over the frequency range of interest. The numerical predictions calculated with two different bulk shear attenuation constants demonstrates the important role that the bulk shear attenuation constant plays in both the torsional T(0,1) and longitudinal L(0,2) behaviour. In contrast, the longitudinal acoustic properties do not seem to have such a significant effect on L(0,2). Of course, this should not be accepted as a general rule for all guided waves problems, however it appears that for coated pipes the shear properties are dominant and this chapter shows how these may be obtained by comparing prediction and measurement.

Chapter 6

Practical application of the findings

Introduction

The data for the reflection coefficients of T(0,1) and L(0,2) presented in Chapter 5 show that the amplitude of a guided wave in a coated pipe is reduced because of the attenuation caused by the presence of a viscoelastic coating material. The objectives in this chapter are the accurate prediction of guided wave attenuation using the bitumen coating materials investigated in the previous chapters and:

- To compare T(0,1) and L(0,2) predictions against experimental data for a 3 inch Schedule 40 pipe coated with Bituthene 4000.
- To investigate how accurately the attenuation of T(0,1) and L(0,2) propagating in a 6 inch Schedule 40 pipe coated with Bitustik 4000 can be predicted using the bulk acoustic properties determined in Chapter 3.
- To determine the bulk acoustic properties of a coating material from guided wave attenuation data.
- To investigate the temperature dependence of the bulk acoustic properties of Bitustik 4000 using the new iterative trial and error method developed in the previous section, and the data measured for the attenuation of T(0,1) and L(0,2).

6.1 Bituthene 4000 – Guided wave attenuation

Further validation of the SAFE method for torsional and longitudinal modes proposed by Kirby et al. [69, 70], and the bulk acoustic properties of Bituthene 4000 derived in Chapter 5, is achieved by comparing predicted and measured values for attenuation. The attenuation measurements for a coated section of the pipe presented in the following figures are

calculated from the reflection coefficient measurements for a coated pipe presented in Chapter 5. This was done at each frequency using Eq. (6.1):

$$A_n = [20\log_{10}(\Lambda_{un}/\Lambda_c)]/2L_c\,, \tag{6.1}$$

where A_n is the attenuation for the coated section of the pipe in dB/m, Λ_{un} and Λ_c are the reflection coefficients for uncoated and coated pipes, respectively, and L_c is the length of the coated section of the pipe.

Figure 6.1 shows a comparison between experimentally derived attenuation spectrum and two sets of SAFE predictions for T(0,1). The first set of numerical predictions is based on the acoustic properties suggested by Barshinger and Rose in [20] and it is clear that this set of numerical predictions do not correlate well with the experimental measurements. They predict relatively low values of attenuation (a few dB/m) up to 60 kHz and then steeply increasing attenuation after 70 kHz.

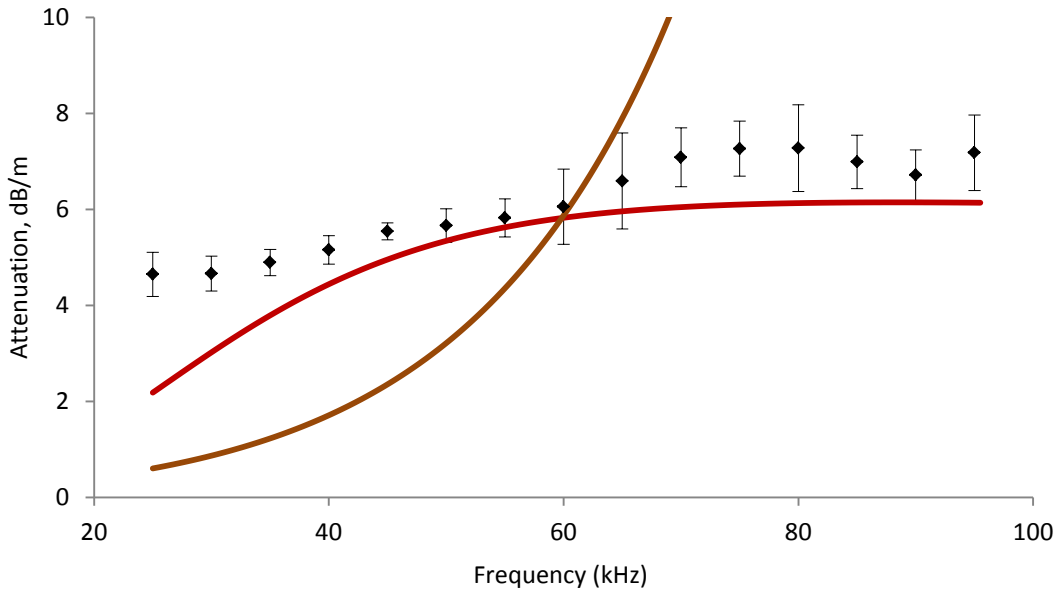

Figure 6.1: Attenuation of T(0,1) for a pipe coated with Bituthene 4000. ♦, experiment; ——, prediction with new values; ——, prediction using values from [20].

Figure 6.1 indicates that the shear acoustic properties reported by Barshinger and Rose [20] are not appropriate for the current bitumen material, and the very high values of attenuation

at higher frequencies show why the predicted reflection coefficient was vanishing almost to zero. The second set of theoretical predictions is based on the new value for the shear attenuation obtained in Chapter 5 of $\alpha_c = 3.9 \times 10^{-3}\,\mathrm{s/m}$. The numerical predictions based on the new value of the bulk shear constant agree well with experimentally determined values for attenuation, and this further demonstrates the validity of the SAFE predictions for T(0,1) and the new bulk shear attenuation constant obtained in Chapter 5. However, the correlation in Fig. 6.1 is not as good as the correlation for reflection coefficients observed in Chapter 5 and this is most likely because the guided wave attenuation was calculated from two sets of experimental data.

Figure 6.2 shows a comparison between experiment and prediction for the attenuation of L(0,2). This figure again shows that the predictions generated using the new material properties show much better agreement with measurement than those obtained using the data of Barshinger and Rose [20].

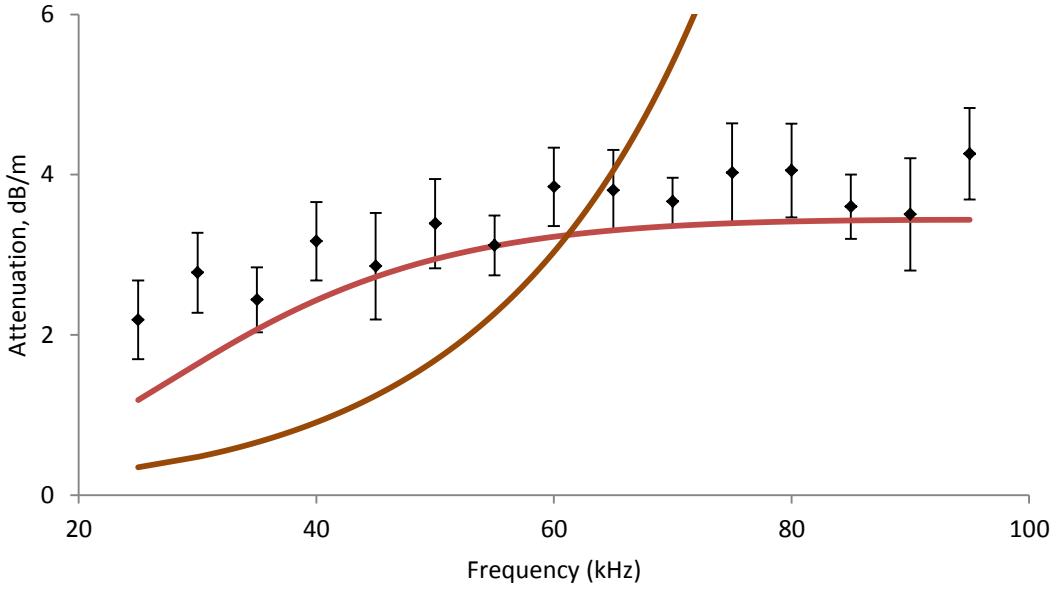

Figure 6.2: Attenuation of L(0,2) for a pipe coated with Bituthene 4000. ♦, experiment; ——, prediction with new values; ——, prediction using values from [20].

The SAFE predictions based on the new shear attenuation data obtained previously also show good agreement with experimental measurement and this serves to further validate the shear and longitudinal properties obtained for Bituthene 4000 in Chapter 5.

The data presented in this section demonstrates how important it is to obtain accurate values for the bulk acoustic properties of a coating material when attempting to reproduce the actual dynamic behaviour of a viscoelastic material when it is applied as a coating on a pipe. The data presented in Figs. 6.1 and 6.2 show a strong dependence between the value for the bulk shear property of Bituthene 4000 and the attenuation of T(0,1) and L(0,2). In addition, the relatively large scatter in the experimental data presented in Figs. 6.1 and 6.2 shows that for the attenuation measurements there is likely to be an increase in experimental errors associated with undertaking two sets of reflection coefficient measurements.

6.2 Bitustik 4000 – Guided wave attenuation

The objective in this section is to investigate how accurately the attenuation of T(0,1) and L(0,2) may be predicted using the values of the shear bulk acoustic properties measured independently for Bitustik 4000 in Chapter 3. This is achieved by comparing prediction against measurement for the attenuation of T(0,1) and L(0,2) at 20ºC in a 6 inch Schedule 40 pipe, coated with 1.25 mm thick Bitustik 4000. The numerical predictions are again generated using the SAFE method [69, 70], and Table 6.1 summarises those values measured in Chapter 3.

	$\tilde{a}_c$	α_L	$\tilde{c}_c$	α_c	Density	r	Source
Material	m/s	s/m	m/s	s/m	kg/m3	mm	-
Mild steel	5960	0	3260	0	7800	77.03-84.14	[79]
Bitustik 4000	1855	1.15 x 10-6	338	994 x 10-6	990	84.14-85.39	Ch. 3

Table 6.1: Acoustic properties and geometry used for numerical predictions.

Figure 6.3 shows a comparison between predictions of attenuation using the SAFE method and based on the input parameters shown in Table 6.1, and the measured attenuation for T(0,1) at 20ºC. This exercise is then repeated in Fig. 6.4 for L(0,2).

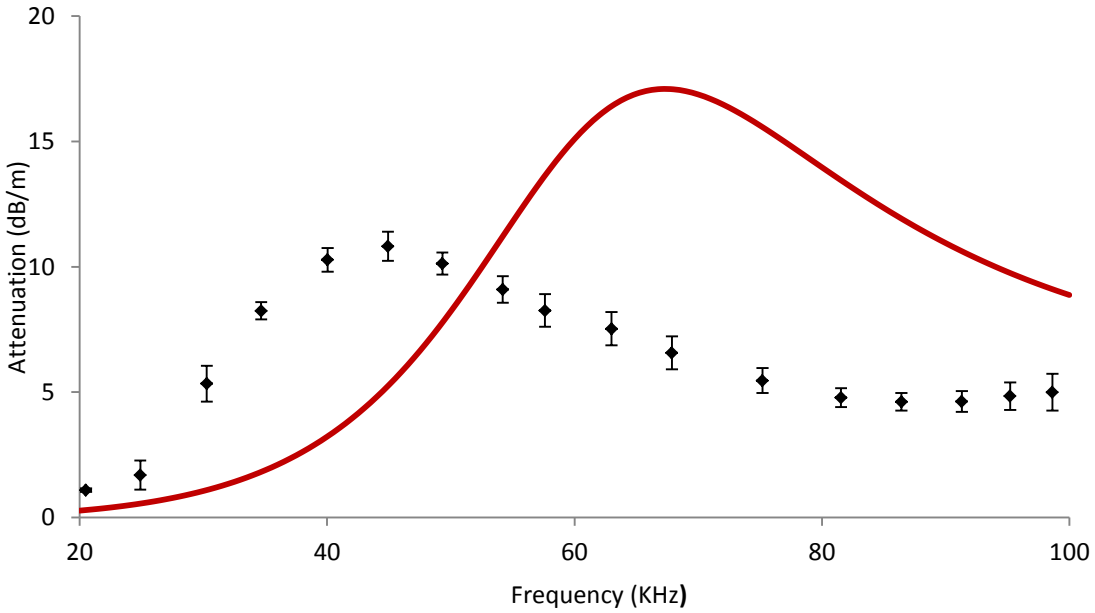

Figure 6.3: Attenuation of T(0,1) for a pipe coated with Bitustik 4000 at 20ºC. ♦, experiment; ——, prediction based on the bulk properties measured in Chapter 3.

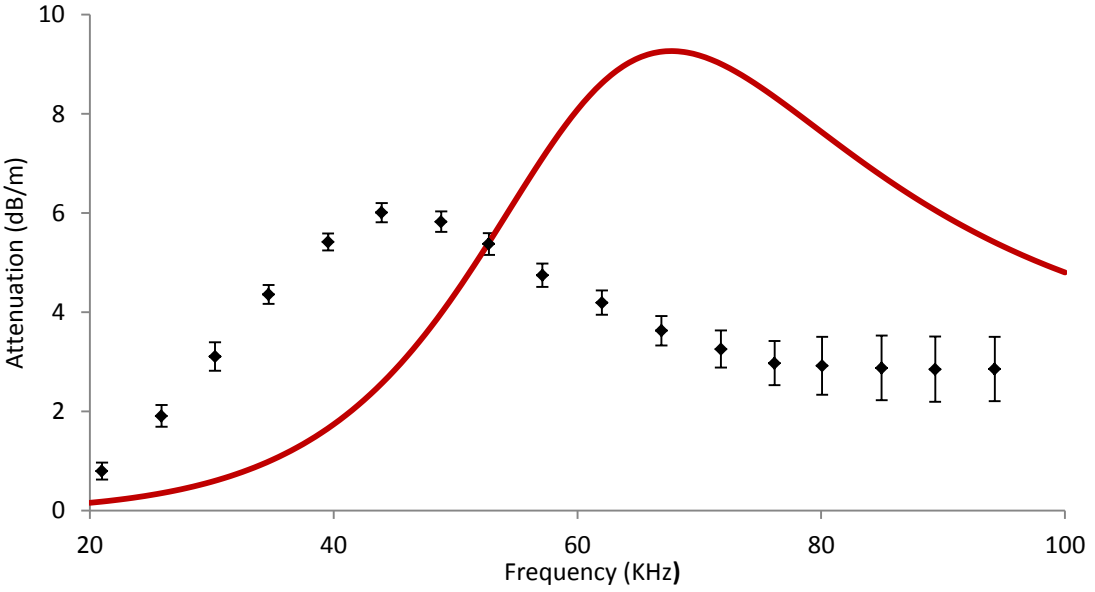

Figure 6.4: Attenuation of L(0,2) for a pipe coated with Bitustik 4000 at 20ºC. ♦, experiment; ——, prediction based on the bulk properties measured in Chapter 3.

It is seen in Figs. 6.3 and 6.4 that the correlation between measurement and prediction is poor for both modes. This mismatch is likely to be caused by inherent problems and inaccuracies associated with the direct measurement of the shear acoustic properties and the extrapolation of data to low frequencies. One possible way of overcoming these inaccuracies is to try to obtain new values for the bulk acoustic properties of Bitustik 4000 using an iterative method similar to that introduced in the previous chapter, but this time using data for attenuation. This is discussed in the next section.

6.3 Method for acoustic characterisation of coating material using attenuation

It was demonstrated in Chapter 5 that the reflection coefficients of T(0,1) and L(2,0) depend mostly on the shear properties of the coating material, and good agreement between prediction and experiment may be achieved only by carefully identifying a suitable value for the shear attenuation constant α_c. It was seen that the geometry of the defect also has a strong influence on the values measured for the reflection coefficient. The measurement of attenuation in the previous section shows minima and maxima for the attenuation spectra and these depend only on the thickness and the acoustic properties of the coating material. Therefore, less variables are involved in predicting the attenuation of a guided wave in a coated pipe, when compared to predicting the reflection coefficient, and this means it should be possible to use attenuation measurements to obtain data for the coating material.

Figure 6.5 shows a flow chart describing an iterative method for obtaining the bulk shear acoustic properties of a coating material from measurements of the attenuation of T(0,1) for a coated pipe. Predictions for the attenuation of T(0,1) are based on the SAFE method reported by Kirby et al. [69]. The flow chart shown in Fig. 6.5 implies that bulk shear speed $\tilde{c}_c$ and the attenuation constant α_c may be varied simultaneously. This could be a complication but it is needed because usually the bulk shear speed and attenuation constant are interlinked and change simultaneously.

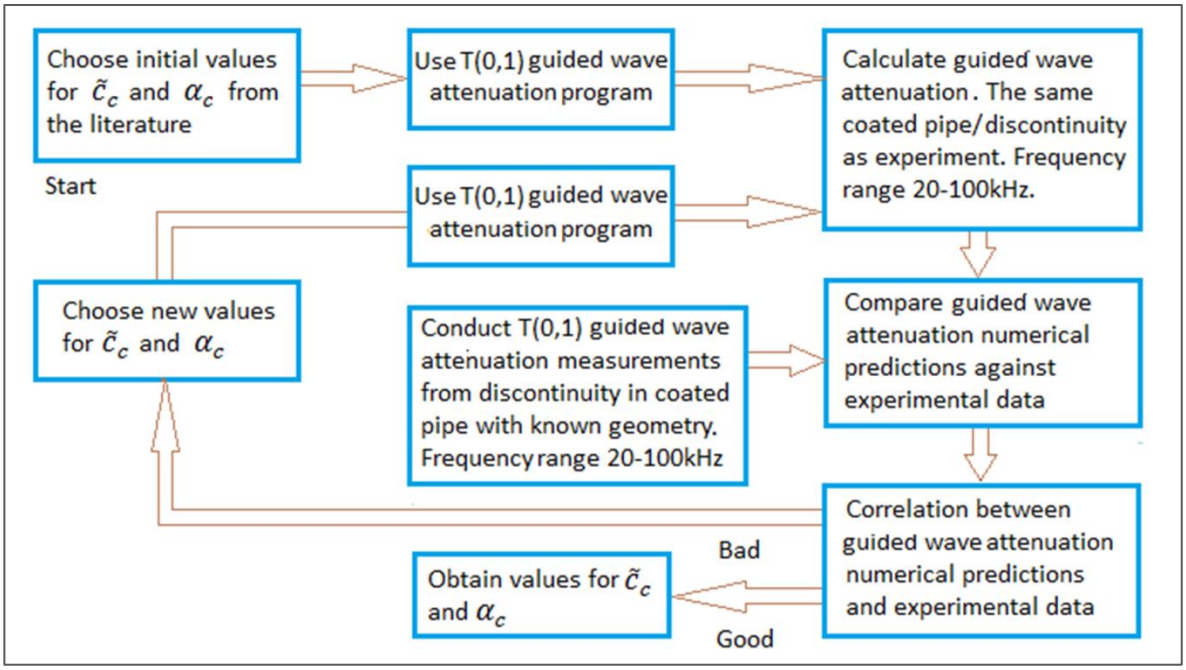

Figure 6.5: Flow chart describing iterative method for determining coating material properties using the attenuation of T(0,1).

To further understand the link between guided wave attenuation and the acoustic properties of the coating for a given model geometry, parametric studies are conducted here by varying the coating properties and observing how the attenuation changes. To do this, the geometry and properties of the pipe are taken from Table 6.1. A range of values for shear speed and attenuation constant are chosen so that $\tilde{c}_c = 200;\ 400;\ 800\ \mathrm{m/s}$ and $\alpha_c = 0.5 \times 10^{-3};\ 1 \times 10^{-3};\ 2 \times 10^{-3};\ 4 \times 10^{-3}\ \mathrm{s/m}$. The results for this parametric study are shown in Figs. 6.6 to 6.8.

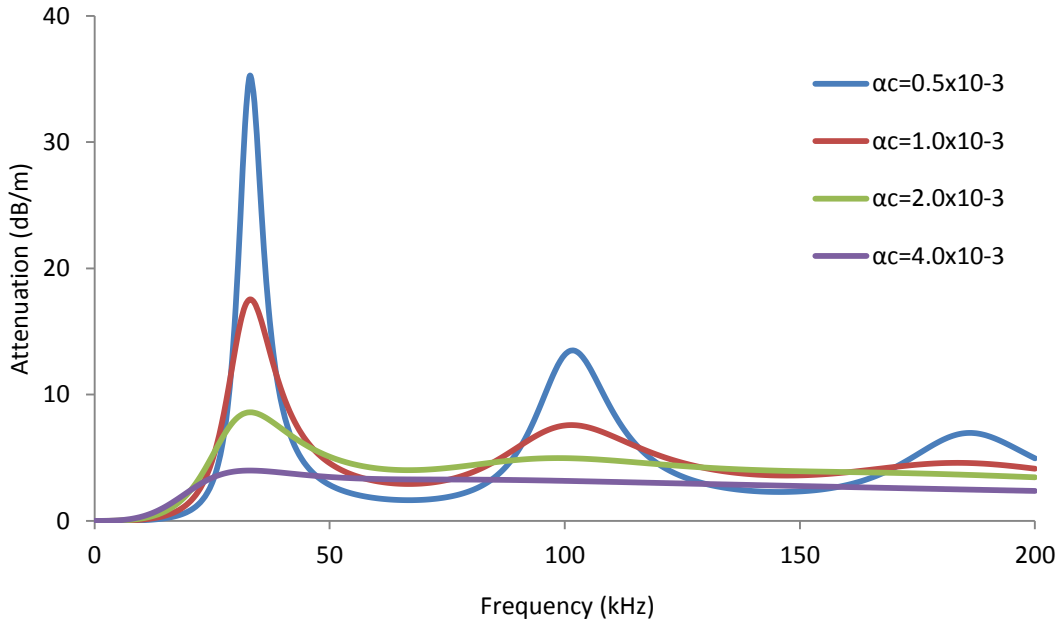

Figure 6.6: Predicted attenuation of T(0,1) with $\tilde{c}_c = 200$ m/s.

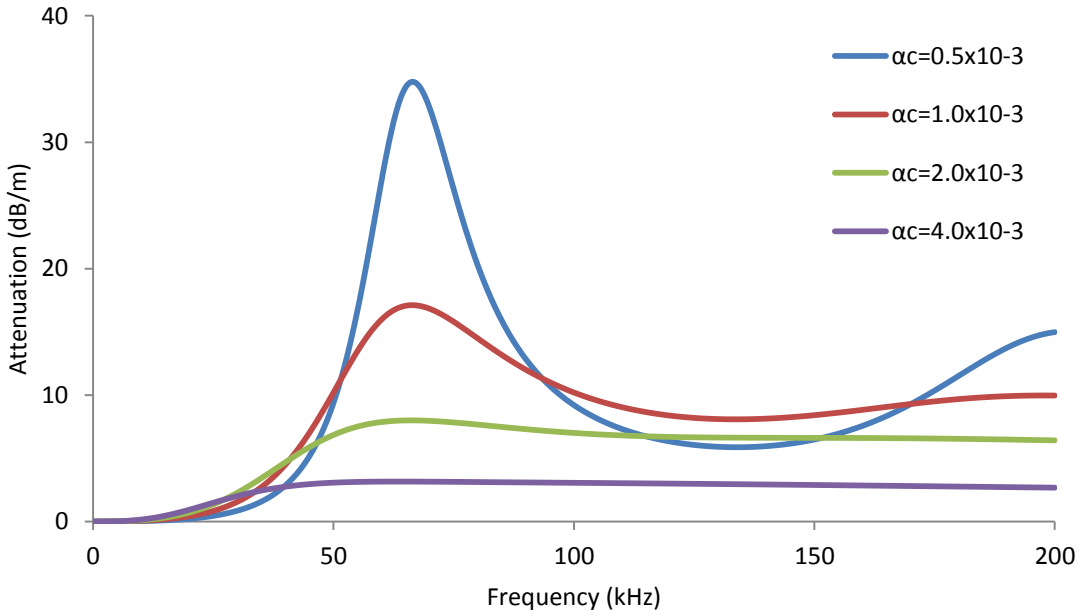

Figure 6.7: Predicted attenuation of T(0,1) with $\tilde{c}_c = 400$ m/s.

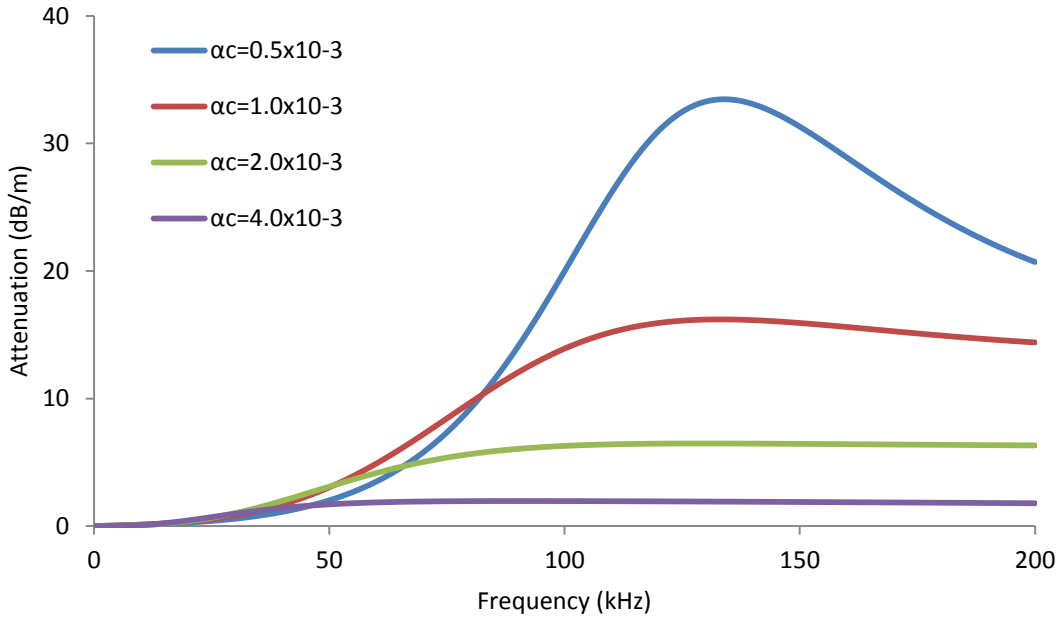

Figure 6.8: Predicted attenuation of T(0,1) with $\tilde{c}_c = 800$ m/s.

The results from the parametric study conducted with the shear properties of the coating material show that the position of the first attenuation peak on the frequency axis strongly depends on the shear speed $\tilde{c}_c$ of the coating material. Increasing the coating material shear speed $\tilde{c}_c$ then leads to an increase in the frequency at which the first attenuation maximum occurs. The coating material shear attenuation constant α_c also plays a significant role, but it mostly influences the magnitude of the attenuation.

New values for the bulk shear properties of the Bitustik 4000 coating are now determined using the method described in Fig. 6.5. In Fig. 6.9 the results from an application of this method using a few iterations are show for the attenuation measured at 20ºC. The new method gives the best correlation between measurement and prediction for values of $\tilde{c}_c = 225$ m/s and $\alpha_c = 1.5 \times 10^{-3}$ s/m.

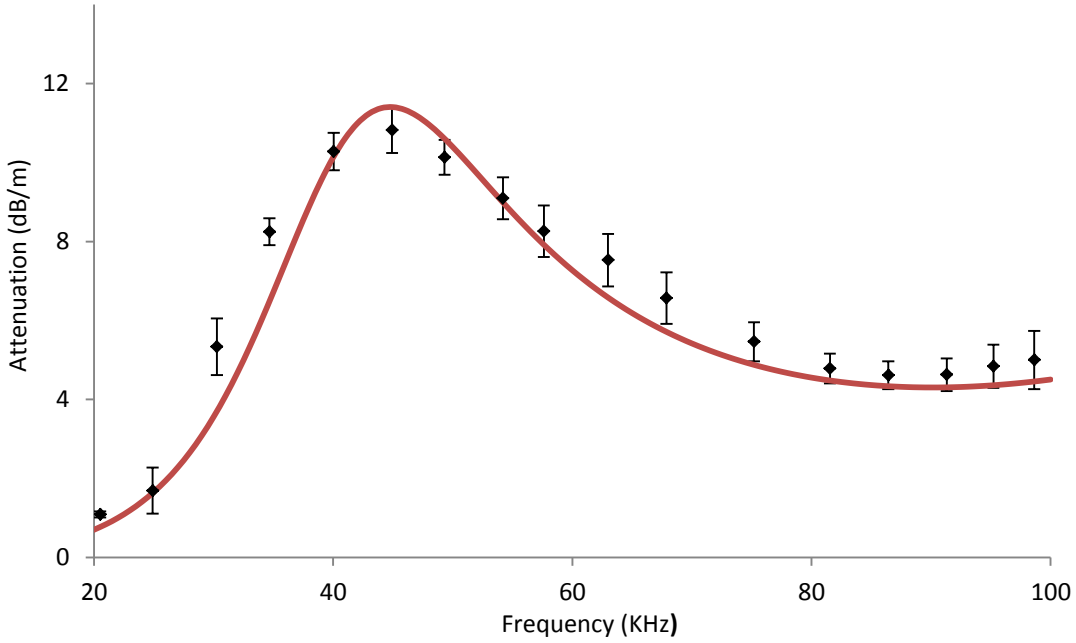

Figure 6.9: Attenuation of T(0,1) for a pipe coated with Bitustik 4000 at 20ºC. ♦, experiment; ——, prediction with $\tilde{c}_c = 225$ m/s and $\alpha_c = 1.5 \times 10^{-3}$s/m.

It is interesting to note that the new value found for the bulk shear speed using the iterative approach is about 33% lower than the direct measured value, and the new shear attenuation constant is about 50% higher. This mismatch is quite significant and it is most likely caused by difficulties with measuring accurately high levels of attenuation using the method in Chapter 3. Once the bulk shear properties of the coating material have been identified using T(0,1) the next step is to check how well these values perform when used for calculating the attenuation of L(0,2). This is achieved by using the iterative method described in Fig. 6.10. The second part of the method derives the longitudinal properties from experimental data measured for the attenuation of L(0,2) and retains the shear bulk properties calculated for T(0,1).

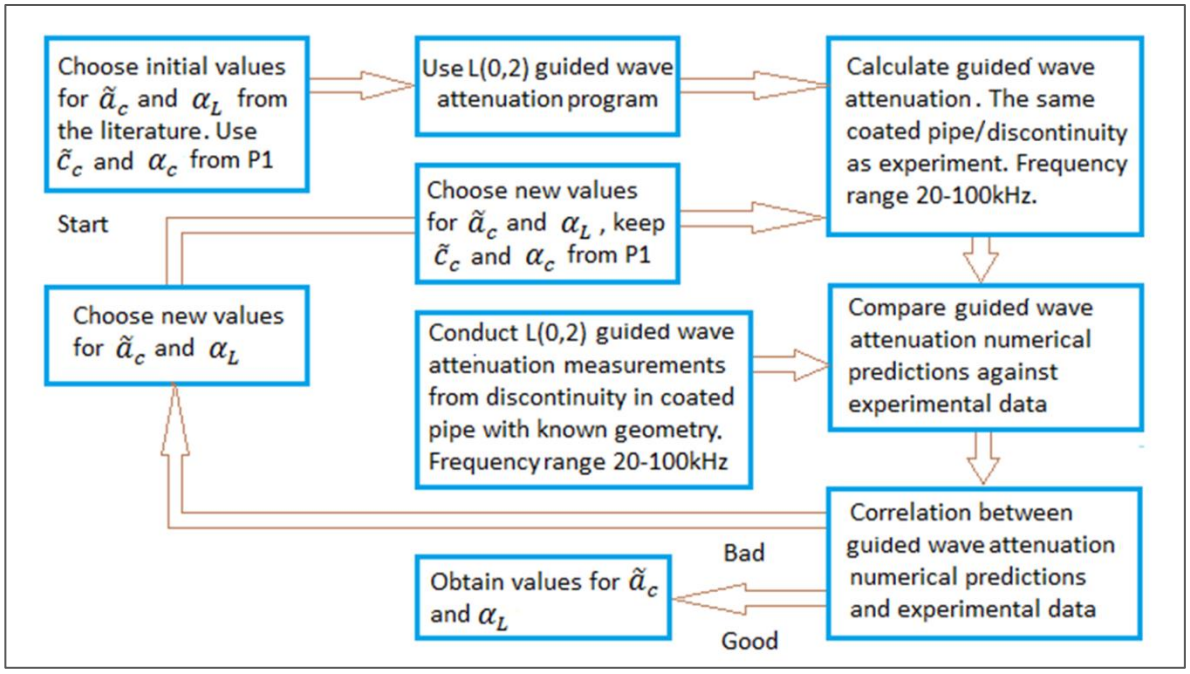

Figure 6.10: Flow chart describing iterative method for determining coating material properties using the attenuation of L(0,2).

The flow chart in Fig. 6.10 suggests that the bulk longitudinal speed $\tilde{\alpha}_c$ and attenuation constant α_L could be changed simultaneously. In order to understand what influence the longitudinal bulk properties of the coating material have on the attenuation spectra of L(0,2) another parametric study is conducted. This time the attenuation spectra of L(0,2) is calculated for different values of the bulk longitudinal acoustic speed C_{Lc}, and the attenuation constant α_{Lc}. The range of values chosen for the parametric study are: $\tilde{\alpha}_c = 900;\ 1800;\ 3600\ \mathrm{m/s}$, and $\alpha_L = 0.1 \times 10^{-6};\ 1 \times;\ 10 \times 10^{-6};\ 100 \times 10^{-6}\ \mathrm{s/m}$. The results of the parametric study are shown in Figs. 6.11, 6.12 and 6.13.

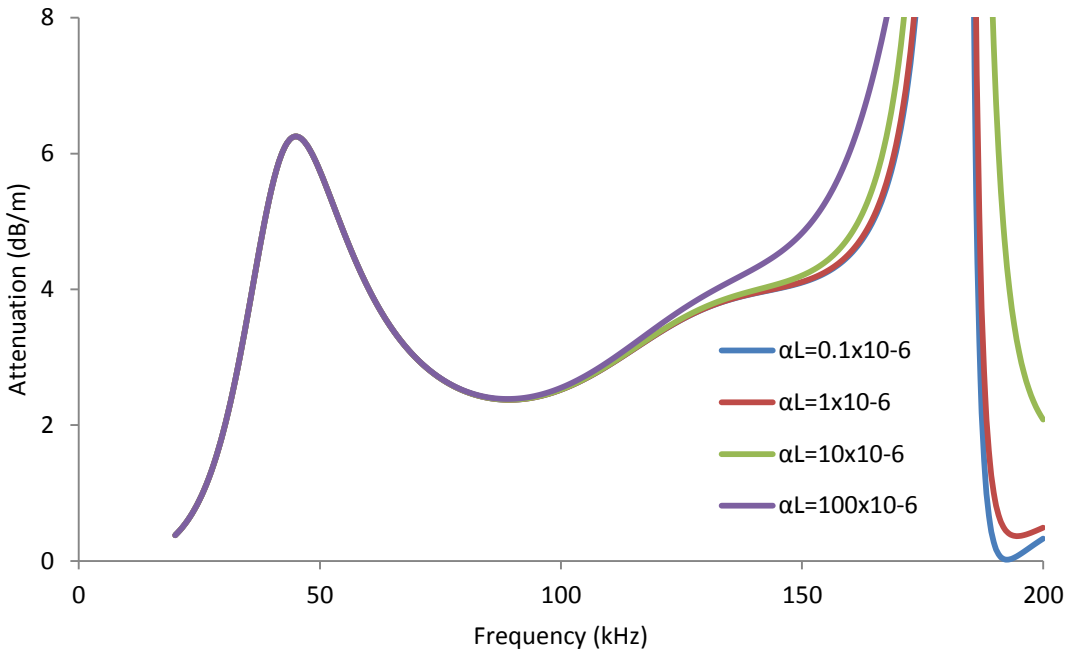

Figure 6.11: Predicted attenuation of L(0,2) with $\tilde{a}_c = 900$ m/s.

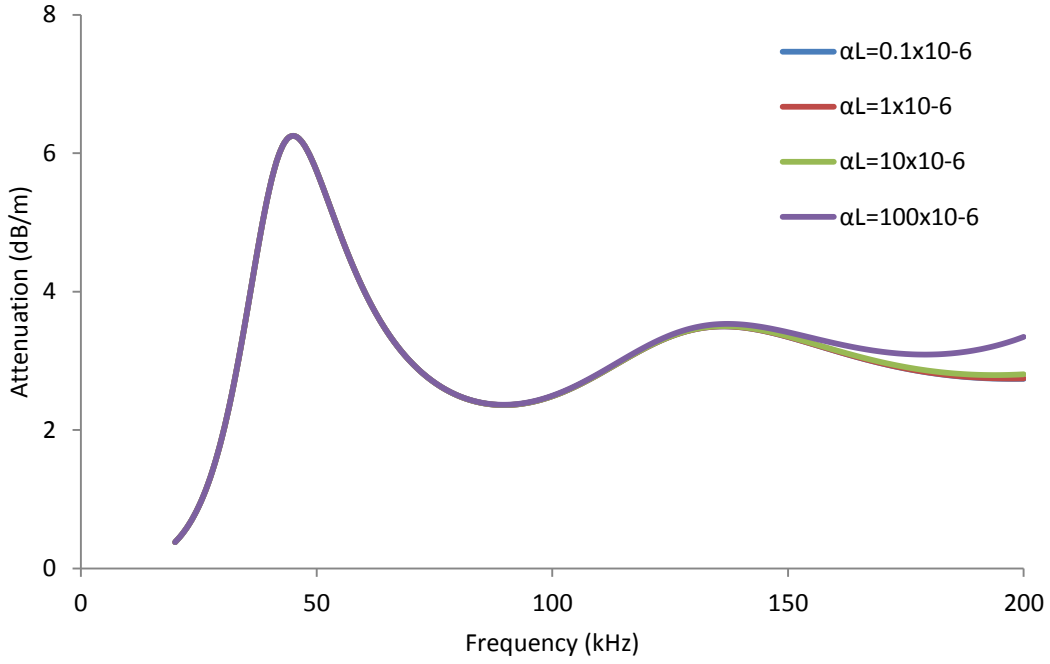

Figure 6.12: Predicted attenuation of L(0,2) with $\tilde{a}_c = 1800$ m/s.

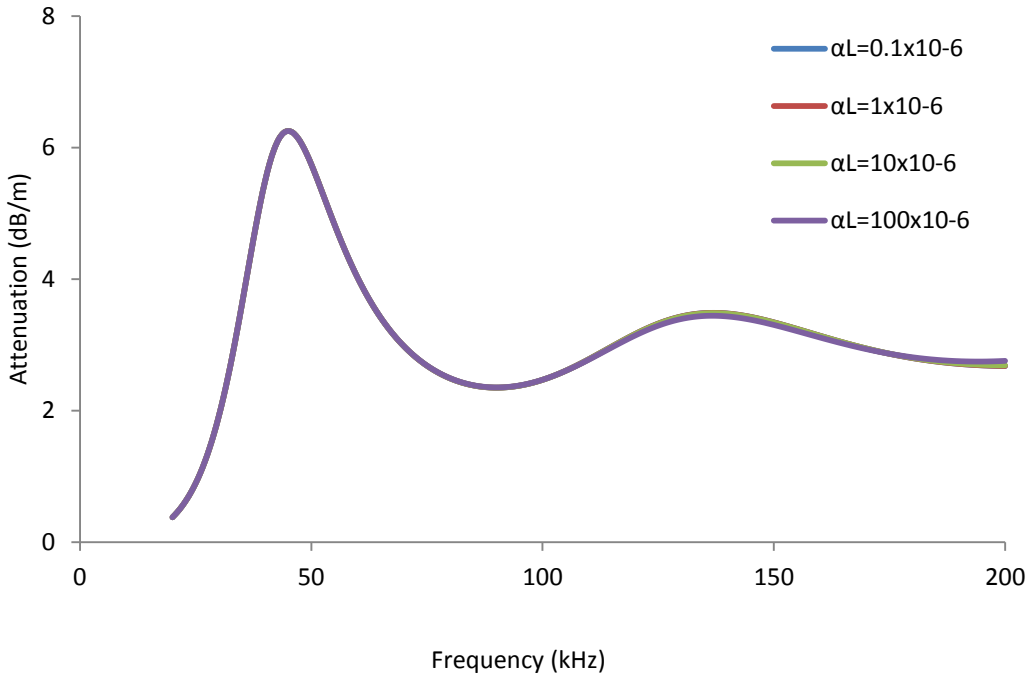

Figure 6.13: Predicted attenuation of L(0,2) with $\tilde{\alpha}_c = 3600$ m/s.

The results in Figs. 6.11 to 6.13 demonstrate that changing the longitudinal properties of the coating material does not significantly affect the attenuation of L(0,2) over the frequency range of interest, with the difference between the plots being less than $\pm 2\%$ below 100 kHz. This means that the values measured in Chapter 3 for the bulk longitudinal acoustic properties may be used here without any influence of the accuracy of the attenuation predictions. Table 6.2 summarises the acoustic properties calculated when using a 6 inch Schedule 40 pipe at 20 ºC for and coated with 1.25 mm Bitustik 4000.

	$\tilde{\alpha}_c$	α_L	$\tilde{c}_c$	α_c	Density	r	Source
Material	m/s	s/m	m/s	s/m	kg/m3	mm	-
Mild steel	5960	0	3260	0	7700	77.05-84.15	[79]
Bitustik 4000	1855	1.15 x 10-6	225	1.5 x 10-3	990	84.15-85.40	Ch. 6

Table 6.2: Acoustic properties obtained from iterative method.

Figure 6.14 shows a comparison between measured values for the attenuation of L(0,2) at 20ºC, and predictions based on the values in Table 6.2.

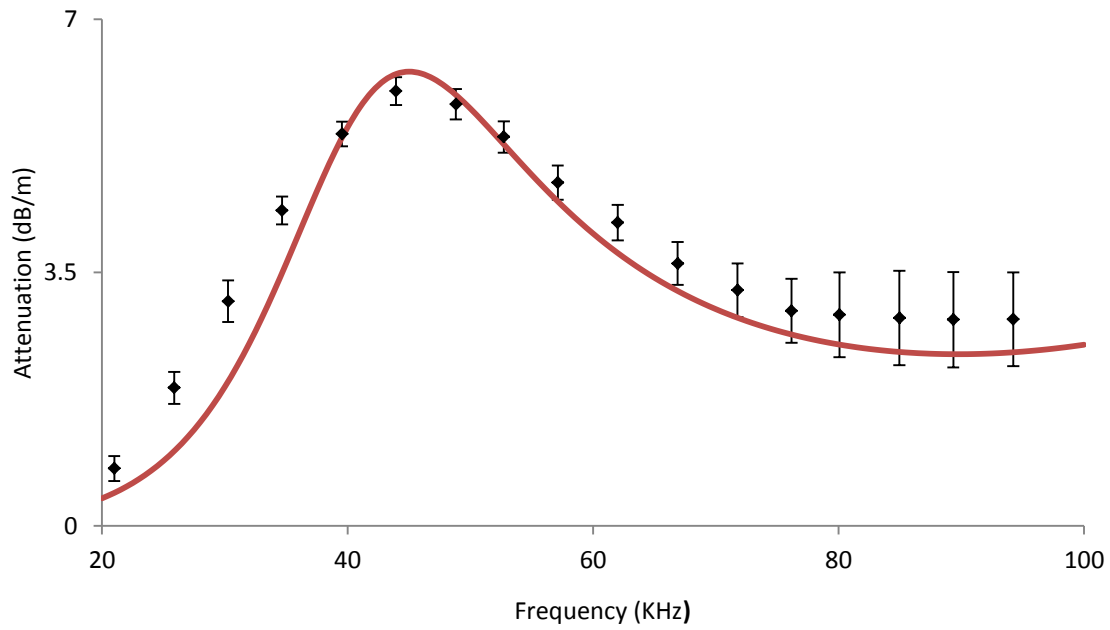

Figure 6.14: Attenuation of L(0,2) for a pipe coated with Bitustik 4000 at 20ºC. ♦, experiment; , prediction based on values in Table 6.2.

The correlation between measurement and prediction for L(0,2) in Fig. 6.14 is much better than the correlation achieved with the directly measured data for the shear acoustic properties shown in Fig. 6.4. Therefore it is seen that the new iterative method for attenuation introduced here may be used to deliver a much better agreement between prediction and measurement. It is also seen that the values obtained independently for T(0,1) also give good agreement when used for L(0,2). Therefore it is demonstrated that the bulk acoustic properties of a viscoelastic coating material may be successfully derived from guided wave attenuation data by using an iterative trial and error technique based on theoretical predictions generated using the SAFE method. The main advantage of the method described in this section, when compared to the experiment-based fitting method for shear attenuation reported by Hua and Rose in [15], is that the method is divided into two parts which deal with the bulk shear and longitudinal properties separately. This provides an independent test for the values chosen for the important shear properties, as well as allowing them to be obtained in a quick and computationally efficient way. The complications associated with the need to change two variables (bulk acoustic speed and attenuation) simultaneously in order to obtain good correlation between prediction and

measurement was also simplified by demonstrating that each variable affects the guided wave attenuation spectra in a different way so that a unique solution can be achieved.

The method's accuracy depends on the accuracy of the measurements for the guided wave attenuation. If the attenuation spectrum does not contain at least one attenuation peak, and the attenuation is steadily increasing with frequency, then unique values for the bulk acoustic speed and attenuation may be difficult to be obtained. This could happen in case of very thin or thick solid coatings, which are outside of the scope of this work. However, the measurement of attenuation in a coating is much easier than reflection coefficient, and so this method is easier to implement in tests on-site such as for the continuous pipelines described in Chapter 4.

6.4 Bitustik 4000 - bulk properties temperature dependence

In this section the acoustic properties of Bitustik 4000 are obtained at different temperatures using iterative trial technique described in Section 6.3. The attenuation of T(0,1) and L(0,2) in Bitustik 4000 were measured in Chapter 4 at 0 ºC, 10 ºC, 20 ºC, 30 ºC and 40 ºC, and this date is used as an input into the iterative method. In Figs. 6.15 to 6.19 a comparison is shown between the experimentally measured attenuation of T(0,1) in a 6 inch Schedule 40 pipe coated with Bitustik 4000, and SAFE method predictions based on best fit values for the bulk shear properties of the material. The bulk shear properties giving best correlation between numerical prediction and experimental measurement are summarised in Table 6.3.

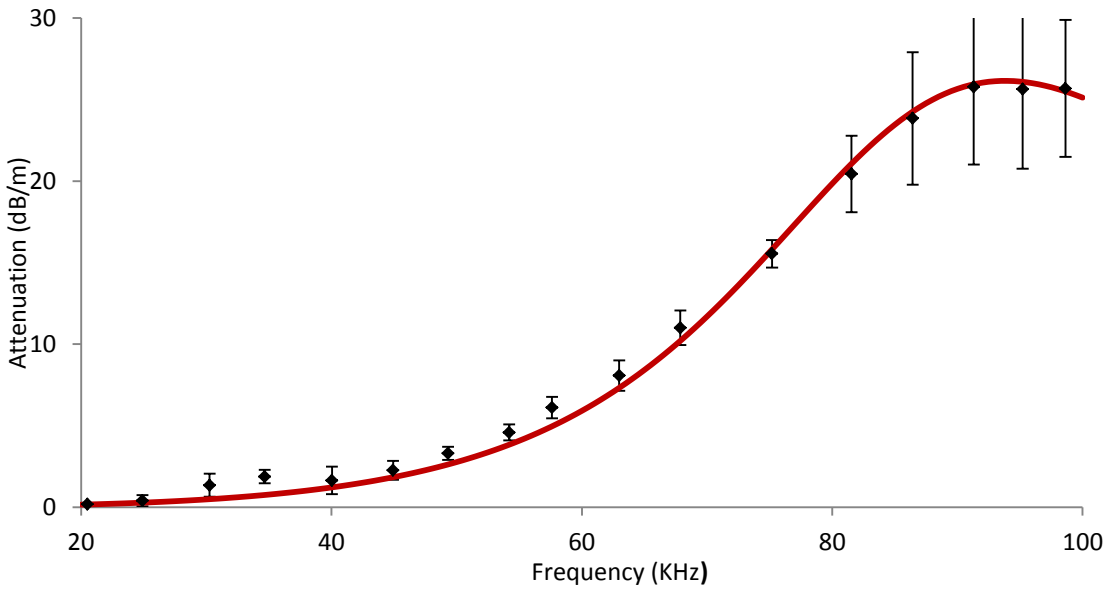

Figure 6.15: Attenuation of T(0,1) for a pipe coated with Bitustik 4000 at 0ºC. ♦, experiment; ——, prediction with $\tilde{c}_c = 470$ m/s and $\alpha_c = 0.65 \times 10^{-3}$s/m.

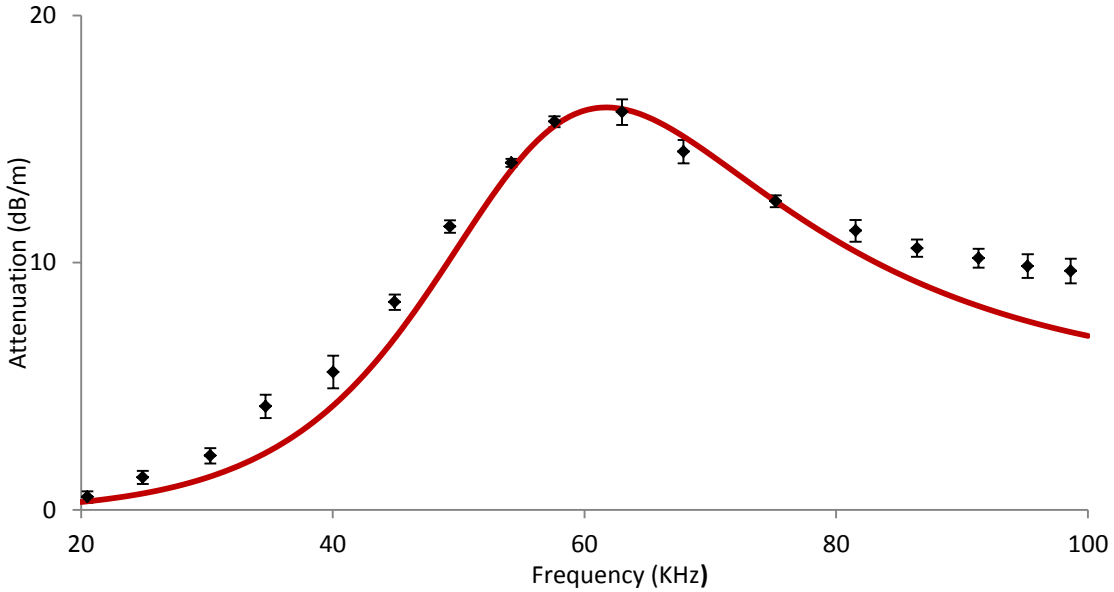

Figure 6.16: Attenuation of T(0,1) for a pipe coated with Bitustik 4000 at 10ºC. ♦, experiment; ——, prediction with $\tilde{c}_c = 310$ m/s and $\alpha_c = 1.05 \times 10^{-3}$s/m.

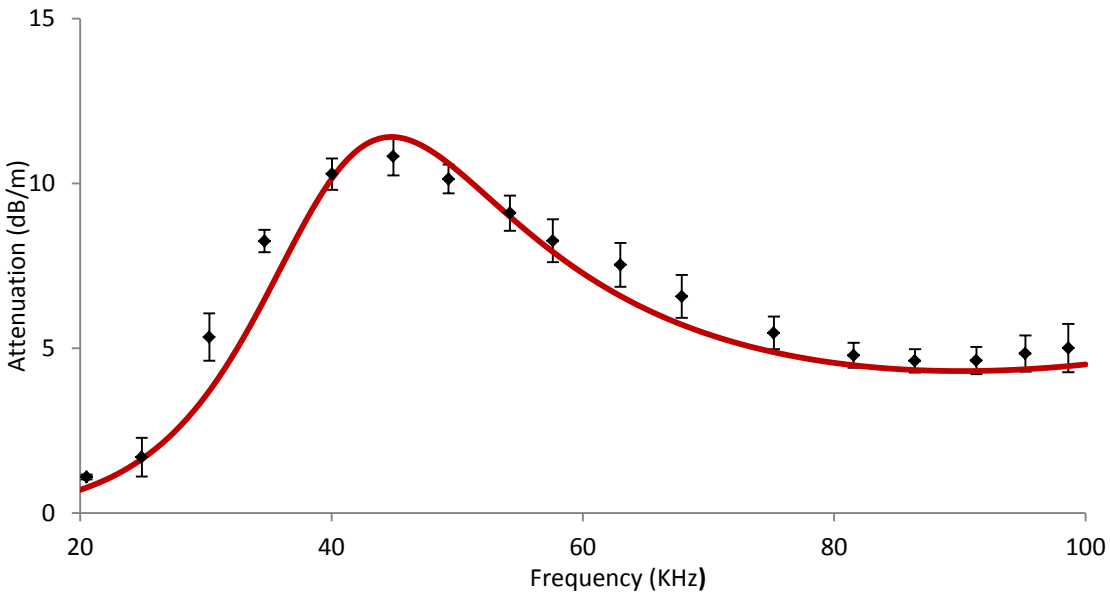

Figure 6.17: Attenuation of T(0,1) for a pipe coated with Bitustik 4000 at 20ºC. ♦, experiment; ——, prediction with $\tilde{c}_c = 225$ m/s and $\alpha_c = 1.5 \times 10^{-3}$s/m .

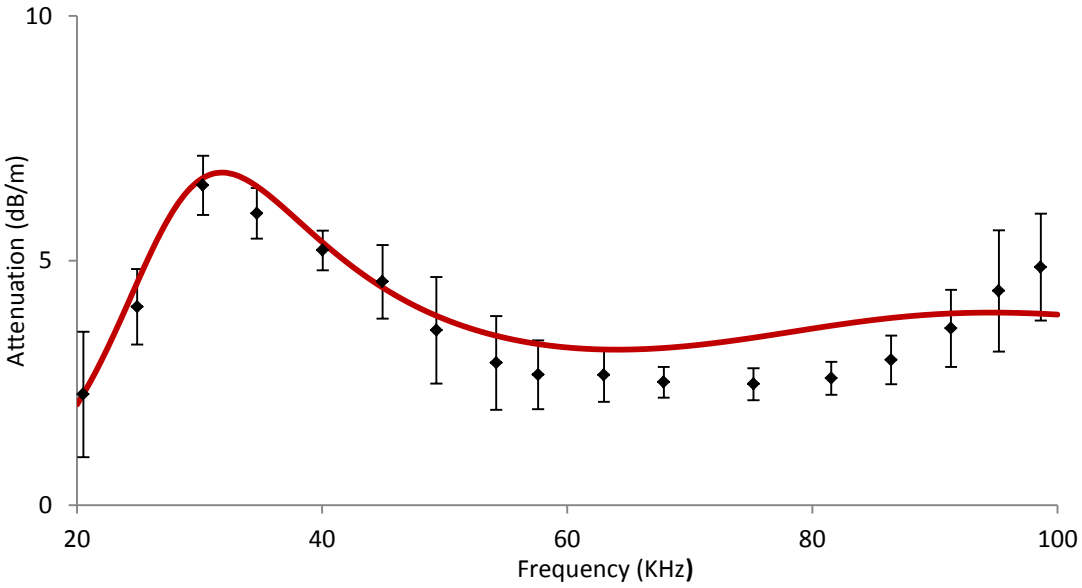

Figure 6.18: Attenuation of T(0,1) for a pipe coated with Bitustik 4000 at 30ºC. ♦, experiment; ——, prediction with $\tilde{c}_c = 160$ m/s and $\alpha_c = 2.5 \times 10^{-3}$s/m .

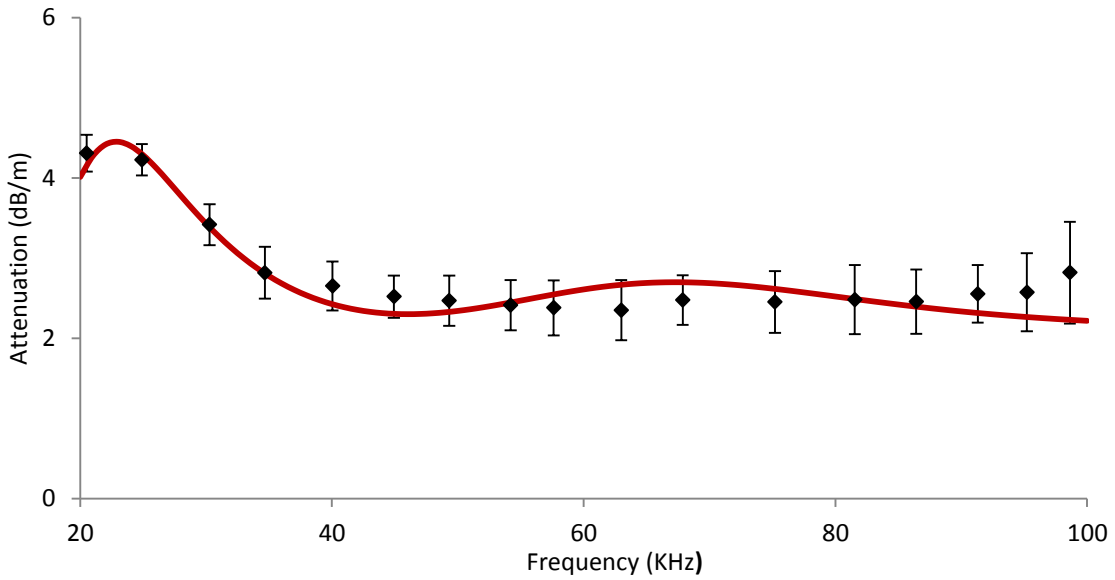

Figure 6.19: Attenuation of T(0,1) for a pipe coated with Bitustik 4000 at 40ºC. ♦, experiment; ——, prediction with $\tilde{c}_c = 115\ m/s$ and $\alpha_c = 3.8 \times 10^{-3}$s/m.

	Temp.	$\tilde{a}_c$	α_L	$\tilde{c}_c$	α_c	Density	r
Material	ºC	m/s	s/m	m/s	s/m	kg/m3	mm
Mild steel	-	5960	0	3260	0	7700	77.05-84.15
Bitustik 4000	0	1855	1.15 x 10-6	470	0.65 x 10-3	990	84.15-85.40
Bitustik 4000	10	1855	1.15 x 10-6	310	1.05 x 10-3	990	84.15-85.40
Bitustik 4000	20	1855	1.15 x 10-6	225	1.5 x 10-3	990	84.15-85.40
Bitustik 4000	30	1855	1.15 x 10-6	160	2.5 x 10-3	990	84.15-85.40
Bitustik 4000	40	1855	1.15 x 10-6	115	3.8 x 10-3	990	84.15-85.40

Table 6.3: Acoustic properties and geometry for numerical predictions at specific temperatures.

It was noted in the previous section that the attenuation of L(0,2) is mostly influenced by the shear properties of the coating material. Accordingly the second part of the iterative method dealing with the bulk longitudinal properties of the coating material uses the longitudinal properties determined in Chapter 4. The validity of the new bulk shear properties for Bitustik 4000 calculated using T(0,1) for different temperatures are now examined by comparing SAFE predictions using this data against measurement for L(0,2). The results are shown in Figs. 6.20 to 6.24.

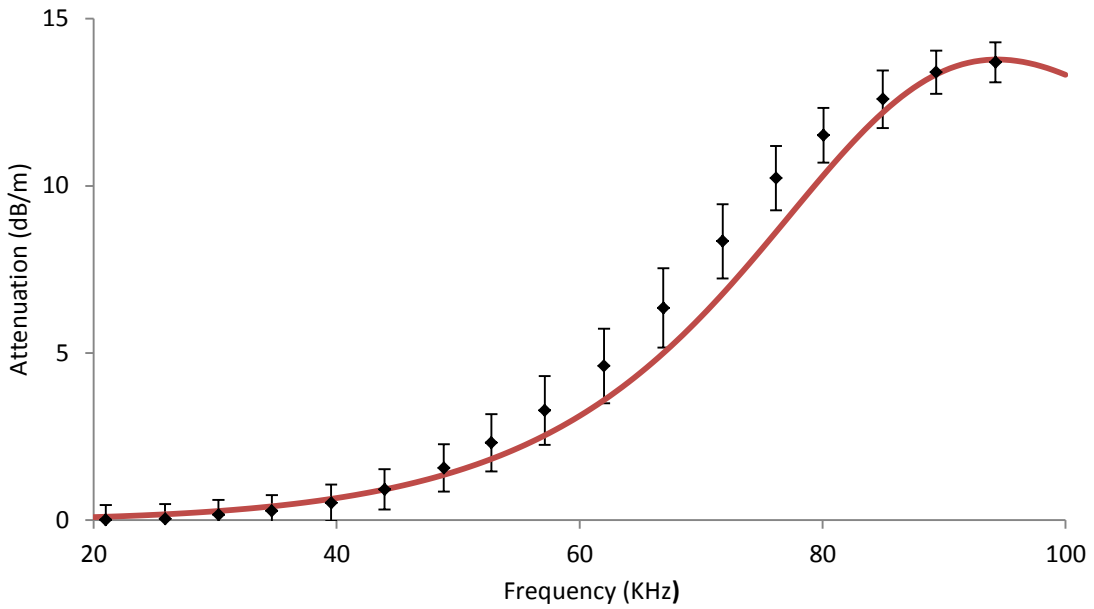

Figure 6.20: Attenuation of L(0,2) for a pipe coated with Bitustik 4000 at 0ºC. ♦, experiment; ——, $\tilde{c}_c = 470$ m/s and $\alpha_c = 0.65 \times 10^{-3}$s/m.

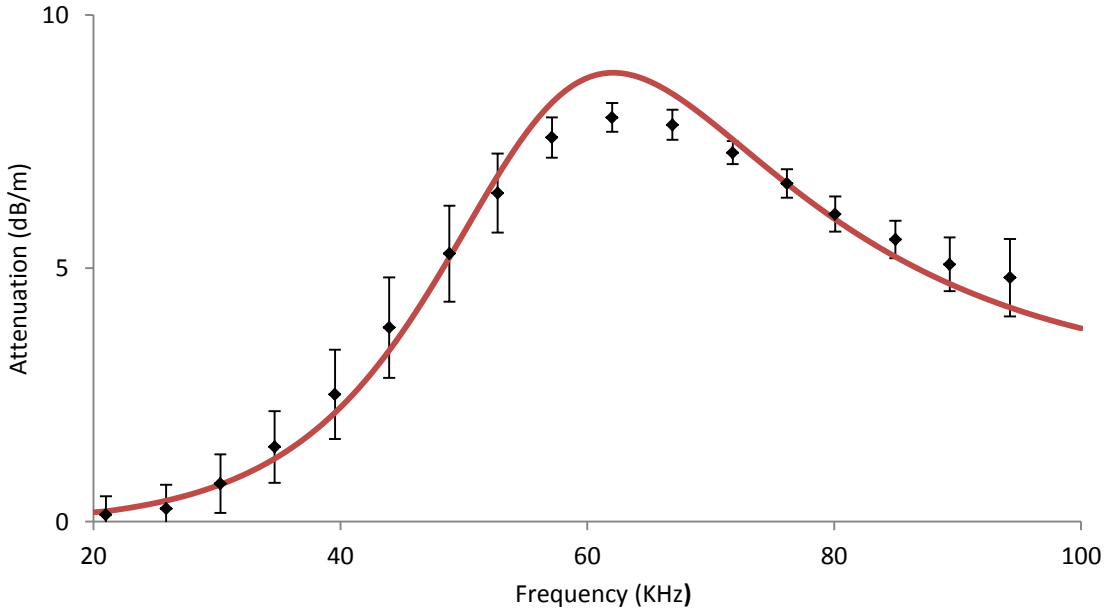

Figure 6.21: Attenuation of L(0,2) for a pipe coated with Bitustik 4000 at 10ºC. ♦, experiment; ——, $\tilde{c}_c = 310$ m/s and $\alpha_c = 1.05 \times 10^{-3}$s/m.

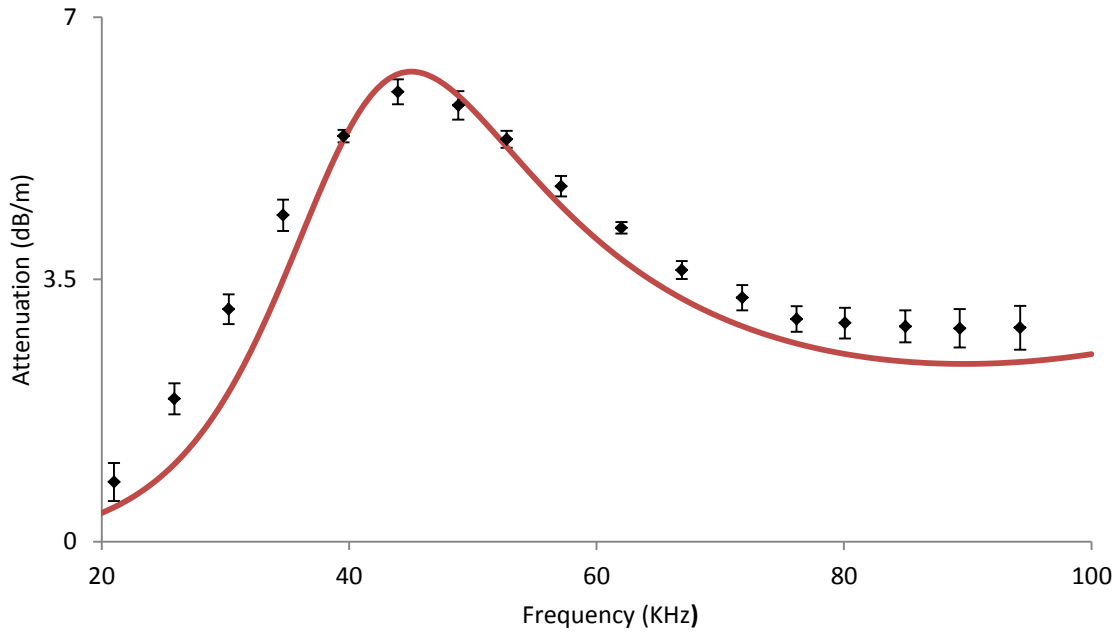

Figure 6.22: Attenuation of L(0,2) for a pipe coated with Bitustik 4000 at 20ºC. ♦, experiment; ——, $\tilde{c}_c = 225$ m/s and $\alpha_c = 1.5 \times 10^{-3}$s/m.

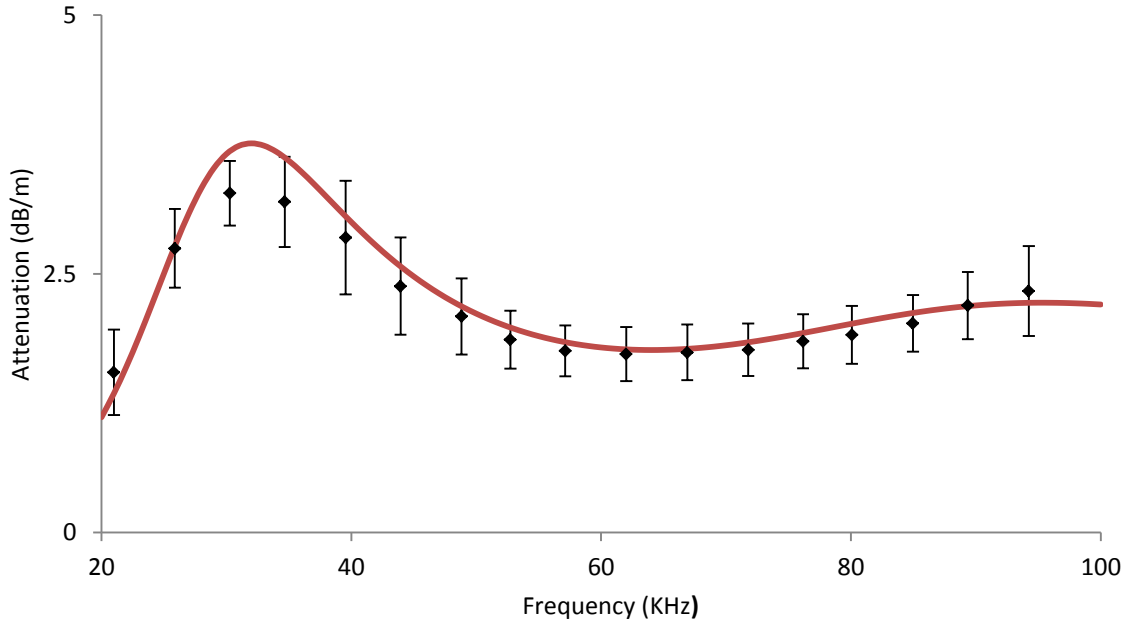

Figure 6.23: Attenuation of L(0,2) for a pipe coated with Bitustik 4000 at 30ºC. ♦, experiment; ——, $\tilde{c}_c = 160$ m/s and $\alpha_c = 2.5 \times 10^{-3}$s/m.

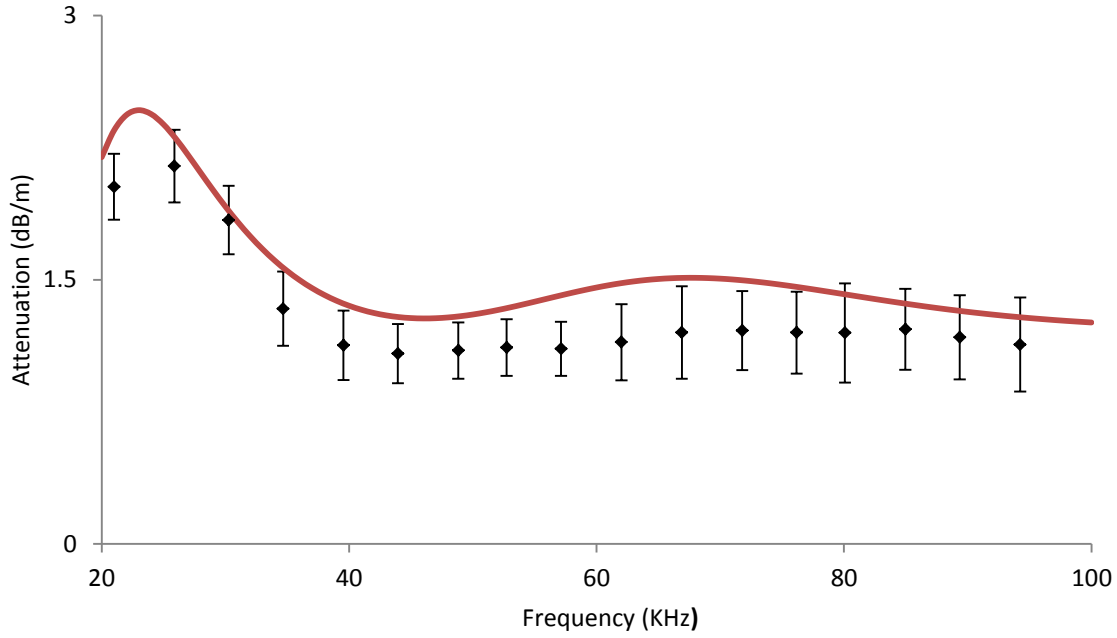

Figure 6.24: Attenuation of L(0,2) for a pipe coated with Bitustik 4000 at 40ºC. ♦, experiment; ——, $\tilde{c}_c = 115$ m/s and $\alpha_c = 3.8 \times 10^{-3}$s/m.

The agreement between prediction and experiment in Figs. 6.20 to 6.24 is generally very good. This serves to validate the values for the bulk acoustic properties obtained at specific temperatures using the iterative method described in Section 6.3. The results presented in this section also demonstrate the significant effect that temperature has on the bulk acoustic properties and guided wave attenuation.

A summary of the temperature dependence of the bulk shear acoustic properties for Bitustik 4000 is presented in Figs. 6.25 and 6.26.

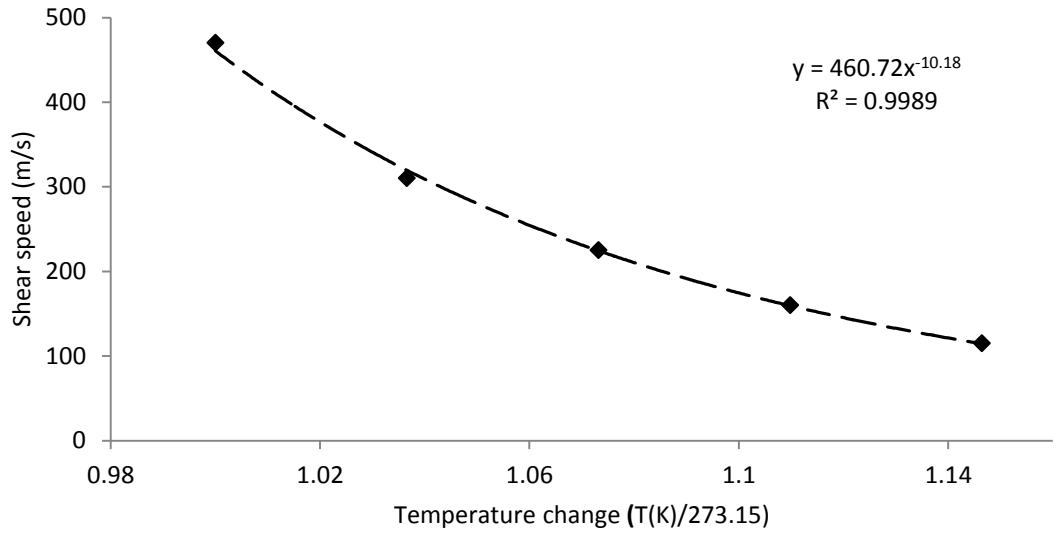

Figure 6.25: Dependence of bulk shear speed on temperature for Bitustik 4000: ♦, experiment; ——, curve fit.

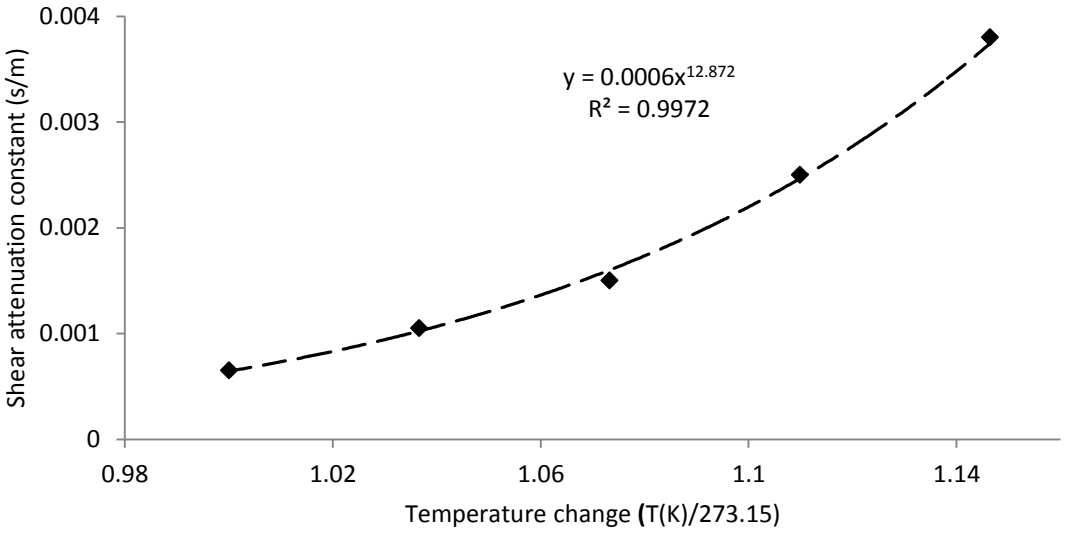

Figure 6.26: Dependence of the bulk shear attenuation on temperature for Bitustik 4000: ♦, experiment; ——, curve fit.

The coefficients describing the temperature dependence of the bulk shear speed and attenuation constant were obtained by fitting a power law through the data, which gives

$$C_{Sc}(t) = 460.72\left[\frac{T(K)}{273.15}\right]^{-10.18} \quad (6.2)$$

$$\alpha_{Sc}(t) = 0.0006\left[\frac{T(K)}{273.15}\right]^{12.87} \quad (6.3)$$

The data presented show the significant influence that temperature has on the bulk acoustic properties of Bitustik 4000. Relatively small temperature variations cause significant changes in the coating material bulk acoustic properties. It is difficult to compare the bulk acoustic properties for the coating material studied in this section with data in the literature because the temperature dependence of bitumen has not been widely studies. However, the temperature dependence of the attenuation spectra corresponds well with the data reported in [71] for pipes coated with epoxy, and polyethylene based coating materials. This study also implies that the bulk acoustic properties of these materials are temperature dependent.

6.5 Summary

A new method for obtaining the bulk acoustic properties from guided wave attenuation data has been successfully applied in the analysis of the temperature dependence of the bulk acoustic properties of Bitustik 4000. The temperature dependence of the shear bulk properties is derived in a temperature range from 0 ºC to 40 ºC and it is demonstrated that relatively small temperature variations have a significant effect on the bulk acoustic properties of a bitumen based coating material. An iterative method was used based on varying the material properties in a SAFE model until good agreement was achieved between measured and predicted values for T(0,1) and L(0,2) at individual temperatures. It was also demonstrated that the shear bulk properties derived from the attenuation spectra of T(0,1) can be successfully used to predict the attenuation of L(0,2) in a frequency range typical for LRUT. The method proposed here is based on attenuation and so it could also be measured on-site using those methods developed in Chapter 4. This makes the method suitable for the practical application of LRUT in coated pipes situated in the field.

7. Conclusions and future work

This thesis investigates experimental methods for studying guided wave propagation in coated pipes and the problems associated with their practical application for on-site use. To obtain a better understanding of the behaviour of wave propagation in coated pipes it is necessary to determine the bulk acoustic properties of the viscoelastic coatings. Current methods for doing this in the literature work only for relatively thin and lightly attenuative coating materials, or at frequencies much higher than those used in LRUT. This is because these methods rely on traditional independent ultrasonic measurement techniques that cannot be performed accurately at low ultrasonic frequencies, especially for the shear properties. This thesis presents two new methods for obtaining the bulk properties of a coating material based on experimental measurements taken on a pipe coated with the material of interest. The first method derives the bulk properties of the coating material from guided wave reflection coefficient data measured from a discontinuity located in a coated pipe. The second method derives the coating material bulk properties from guided wave attenuation data. Each method works by successively changing the bulk acoustic properties of the viscoelastic material in a theoretical model until predictions and measurement agree for data obtained for both T(0,1) and L(0,2) modes. This then permits the deduction of material properties over a wide frequency range and it is shown that by using this method it is possible to obtain good agreement between prediction and measurement over a number of independent tests. Both methods measure the coating material acoustic properties while the material is applied on the pipe and take into account the coupling between the pipe wall and coating material, and how exactly the coating material is deformed . The methods are used to measure the bulk acoustic properties of two highly viscoelastic bitumen based coating materials. The results obtained show that the bulk acoustic properties of bitumen based coating materials can vary significantly even if they look similar in appearance. Results also indicate that the data for the shear properties measured here is very different to that found using more traditional methods in the literature. The method is also capable of deriving the bulk properties of coating materials from attenuation data and this method was used to measure the bulk acoustic properties of a

bitumen based material at different temperatures. This has generated new data for the dependence on temperature of the shear acoustic properties of a viscoelastic material.

The methods developed here and the data obtained for the bulk acoustic properties of viscoelastic materials will enable the future use of this data in theoretical models, which can then be used to develop a much better understanding of the way in which sound waves propagate in coated pipes. This will then enable an investigation into more efficient methods for studying coated pipelines with the aim of extending the measurements and improving the sensitivity of the method when inspecting a pipe. The data obtained is also for the bulk acoustic properties and so the results obtained here are applicable in other areas associated with the acoustic characterisation of viscoelastic materials, guided wave propagation characteristics and NDT. The future development and application of the findings reported in this work are:

- The method for obtaining the bulk acoustic properties of coating materials from guided wave attenuation data may be further developed and integrated into the LRUT equipment software. This will allow the method to be used for on-site measurements.
- The methods for the acoustic characterization of coating materials developed in this work can be used to investigate the variations of the coating material bulk acoustic properties caused by non-uniformity, bonding levels, aging and temperature changes.
- The data on the bulk acoustic properties of bitumen derived in this work have been used to study reflection coefficients from axisymmetric discontinuities located in a coated pipe. One future application of the data is as an input into numerical modules suitable for studying reflection coefficients from non-axisymmetric three dimensional discontinuities located in a coated pipe.
- The method for independent measurement of bulk shear acoustic properties could be used for characterization of other types of semisolid materials if they can be formed into a waveguide. Of course it should be noted that this method measures the shear bulk acoustic properties of the coating material and does not take into account the coupling between the base and the coating material when applied.

8. References

1. Estimated Natural Gas Pipeline Mileage in the Lower 48 States, Close of 2008. http://www.eia.gov/pub/oil_gas/natural_gas/analysis_publications/ngpipeline/mileage.html, last viewed 10/9/14.
2. A. Antaki, *Piping and Pipeline Engineering*, CRC Press, (2003).
3. M. Berndt, *Non-Destructive Methods for Geothermal Piping*, Energy Resources Division, Brookhaven National Laboratory, Upton New York, 11973 (2001).
4. D. Alleyne, A. Lank, P. Mudge, M. Lowe, P. Cawley. Guided Wave Inspection of Chemical Plant Pipework, Proceedings of SPIE - The International Society for Optical Engineering, 2947 (1996) 177-188.
5. P. Cawley, Practical Long Range Guided Wave Inspection – Applications to Pipes and Rails, National Seminar of ISNT, Chennai, (2002).
6. P. Cawley, Practical Guided Wave Inspection and Applications to Structural Health Monitoring, 5th Australian Congress on Applied Mechanics, Brisbane, Australia, (2007).
7. BS 9690-1: Non-Destructive Testing, Guided Wave Testing, General Guidance and Principles, (2011).
8. BS 9690-2: Non-Destructive Testing, Guided Wave Testing, Basic Requirements for Guided Wave Testing of Pipes, Pipelines and Structural Tubulars, (2011).
9. M. Lowe, P. Cawley, Long Range Guided Wave Inspection Usage – Current Commercial Capabilities and Research Directions, (2009). http://www3.imperial.ac.uk/pls/portallive/docs/1/55745699.PDF, last viewed 10/9/14.
10. P. Mudge, P. Catton, Monitoring of Engineering Assets Using Ultrasonic Guided Waves, Proceeding of the 9th European Conference on Non-Destructive Testing, Berlin, Germany, (2006).
11. P. Mudge, Practical Enhancement Achievable in Long Range Ultrasonic Testing by Exploiting the Properties of Guided Waves. The 16th World Conference of Non-Destructive Testing, Montreal, Canada, (2004).
12. P. Catton, *Long Range Ultrasonic Guided Waves for the Quantitative Inspection of Pipelines*, Brunel University EngD Thesis, (2009).

13. J. Barshinger, J. Rose, Ultrasonic Guided Wave Propagation in Pipes with Viscoelastic Coatings, Journal of Pressure Vessel Technology, 124 (2002) 303-310.
14. F. Simonetti, *Sound Propagation in Lossless Waveguides Coated with Attenuative Materials*, PhD Thesis, Imperial College of Science Technology and Medicine, (2004).
15. J. Rose, J. Hua, Guided Wave Inspection Penetration Power in Viscoelastic Coated Pipes, Insight, 52 (2010) 195-200.
16. J. Van Velsor, *In Situ Analysis of Viscoelastic Coatings on Hollow Cylinders for Enhanced Guided Wave Inspection*, The Pennsylvania State University PhD Thesis, USA, (2006).
17. J. Rose, *Ultrasonic Waves in Solid Media*, Cambridge University Press, New York, (1999).
18. B. Auld, *Acoustic Fields and Waves in Solids, vol. 2*. New York: Wiley, (1973).
19. K. F. Graff, *Wave Motion in Elastic Solids*, New York, Dover, (1991).
20. J. Barshinger, J. Rose, Guided Wave Propagation in an Elastic Hollow Cylinder Coated with a Viscoelastic Material, IEEE Transactions on Ultrasonics, Ferroelectrics, and Frequency Control, 51 (2004) 1547–1556.
21. B. Pavlakovic and M. Lowe, Disperse: A System for Generating Dispersion Curves. User's Manual, (2000), http://www.me.ic.ac.uk/dynamics/ndt, last visited 10/9/14.
22. J. Barshinger, J. Rose, M. Avioli, Guided Wave Resonance Tuning for Pipe Inspection, Journal of Pressure Vessel Technology, 124 (2002) 303–310.
23. J. Barshinger, *Guided Wave Propagation in Pipes with Viscoelastic Coatings*, The Pennsylvania State University PhD Thesis, (2002).
24. T. Hayasashi, W. Song, J. Rose. Guided Wave Dispersion Curves for a Bar with an Arbitrary Cross Section, a Rod and Rail example. Ultrasonics, 41 (2003) 175-183.
25. F. Seco, J. Martin, A. Jimenez, J. Pons, L. Calderon, R. Ceres, PCDISP: A Tool for the Simulation of Wave Propagation in Cylindrical Waveguides, Proceedings of the Ninth International Congress on Sound and Vibration, Orlando, FL, (2002).
26. R. Lakes, *Viscoelastic Materials*, Cambridge University Press, (2009).
27. D. Bland, *The Theory of Linear Viscoelasticity*, Pergamon Press, London, (1960).

28. Y. Wang, C. Shen, L. Zhu, F. Sun, Guided Waves Mode Discrimination in Pipes NDT Based on the Matching Pursuit Method, Journal of Analytical Sciences, Methods and Instrumentation, 2 (2012) 149-155.
29. P. Shull, *Nondestructive Evaluation: Theory, Techniques, and Applications*, CRC Press, (2005).
30. Hanning Window Function, http://uk.mathworks.com/help/signal/ref/hann.html, last viewed 10/9/14.
31. D. Alleyne, T. Vogt, P. Cawley, The Choice of Torsional or Longitudinal Excitation in Guided Wave Pipe Inspection, Insight, 51 (2009) 373–377.
32. A. Chaston, *Development of a Transducer to be Used in Long Range Ultrasonic Testing*, Cardiff University EngD Thesis, (2008).
33. D. Alleyne, P Cawley, The Excitation of Lamb Waves in Pipes Using Dry Coupled Piezoelectric Transducers, Journal of Nondestructive Evaluation, 15 (1996) 11-20.
34. H. Kwun, S. Kim, and G. Light, Long-Range Guided Wave Inspection of Structures Using the Magnetostrictive Sensor, Journal of the Korean Society for Nondestructive Testing 21 (2001) 383–390.
35. LRUT equipment Teletest Focus®, www.plantintegrity.co.uk, last viewed 10/9/14.
36. LRUT equipment Wavemaker G4, www.guided-ultrasonics.com, last viewed 10/9/14.
37. LRUT equipment MsSR-3030, www.mkckorea.com/english.htm, last viewed 10/9/14.
38. LRUT equipment UltraWave LRT, www.olympus-ims.com/en/ultrawave/, last viewed 10/9/14.
39. J. Li, J. Rose, Natural Beam Focusing of Non-Axisymmetric Guided Waves in Large-Diameter Pipes, Ultrasonics, 44 (2006) 35–45.
40. J. Rose, J. Mu, Y. Cho, Recent Advances on Guided Waves in Pipe Inspection, 17th World Conference on Nondestructive Testing, Shanghai, China, (2008).
41. J. Mu, J. L. Rose, Long Range Pipe Imaging with a Guided Wave Focal Scan, Materials Evaluation, 66 (2008) 663-666.
42. J. L. Rose, J. Mu, J. Hua, Ultrasonic Guided Wave Phased Array Inspection of Coated and Buried Pipe (part 2: Experiment), www.ndt.net/article/jrc-nde2009/papers/72.pdf, last viewed 10/9/14.

43. A. Demma, P. Cawley, M. Lowe, A. Roosenbrand, The Reflection of the Fundamental Torsional Mode from Cracks and Notches in Pipes, Journal of the Acoustical Society of America, 114 (2003) 611-625.
44. M. Lowe, D. Alleyne, P. Cawley, The Mode Conversion of a Guided Wave by a Part-Circumferential Notch in a Pipe. Journal of Applied Mechanics, 65 (1998) 649-656.
45. D. Alleyne, M. Lowe, The Reflection of Guided Waves from Circumferential Notches in Pipes. Journal of Applied Mechanics, 65 (1998) 635-641.
46. H. Kwun, S. Kim, M. Choi, S. Walker, Torsional Guided Wave Attenuation in Coal Tar Enamel Coated, Buried Piping, Nondestructive Testing and Evaluation International, 37 (2004) 663–665.
47. J. L. Rose, J. Mu, J. Hua, Ultrasonic Guided Wave Phased Array Inspection of Coated and Buried Pipe (part 1:Theory), Pennsylvania State University, USA; www.ndt.net/article/jrc-nde2009/papers/71.pdf, last viewed 10/9/14.
48. F. Simonetti, P. Cawley, A Guided Wave Technique for the Characterisation of Highly Attenuative Viscoelastic Materials, Journal of the Acoustical Society of America, 114 (2003) 158-165.
49. F. Simonetti, P. Cawley, Ultrasonic Interferometry for the Measurement of Shear Velocity and Attenuation in Viscoelastic Solids, Journal of the Acoustical Society of America, 115 (2004) 157-164.
50. P. Cawley, M. Lowe, F. Simonetti, C. Chevalier, A. Roosenbrand, The Variation of the Reflection Coefficient of Extensional Guided Waves in Pipes From Defects as a Function of Defect Depth, Axial Extent, Circumferential Extent and Frequency, Journal of Mechanical Engineering Science, 216 (2002) 1131-1143.
51. R. Carandente, J. Ma, P. Cawley, The Scattering of the Fundamental Torsional Mode from Axi-Symmetric Defects with Varying Depth Profile in Pipes, Journal of the Acoustical Society of America, 127 (2010) 3440–3448.
52. P. Cawley, M. Lowe, F. Simonetti, The Reflection Coefficient of Extensional Guided Waves in Pipes as Function of Defect Size and Frequency. 8th ECNDT, Barcelona, (2002).
53. W. Luo, *Ultrasonic Guided Waves and Wave Scattering in Viscoelastic Coated Hollow Cylinders*, The Pennsylvania State University PhD Thesis, (2005).

54. M. Lowe, Matrix Techniques for Modelling Ultrasonic Waves in Multi Layered Media, IEEE Transactions on Ultrasonics, Ferroelectrics and Frequency Control, 42 (1995) 525-542.
55. F. Simonetti, P. Cawley , On the Nature of Shear Horizontal Wave Propagation in Elastic Plates Coated with Viscoelastic Materials, Proceedings of the Royal Society, 460 (2004) 2197-2221.
56. F. Simonetti, Lamb Wave Propagation in Elastic Plates Coated with Viscoelastic Materials, Journal of the Acoustical Society of America, 115 (2004) 2041-2053.
57. F. Simonetti, P. Cawley, M. Lowe, Long Range Inspection of Lossy Bilayers, American Institute of Physics, 700 (2004) 222-229.
58. Q. Mohammad, Attenuation Properties of Viscoelastic Material, Pure and Applied Geophysics, 131 (1998) 703-713.
59. R. D. Borcherdt, *Viscoelastic Waves in Layered Media*, Cambridge University Press, (2009).
60. M. A. Meyers, K. K. Chawla, *Mechanical Behaviour of Materials*, Cambridge University Press, (2009).
61. H. D. Benedetto, B. Delaporte, C. Sauzeat, Three Dimensional Linear Behaviour of Bituminous Materials: Experiments and Modelling, International Journal of Geomechanics, 7 (2007) 149.
62. W. Luo, J. L. Rose, Phased Array Focusing with Longitudinal Guided Waves in a Viscoelastic Coated Hollow Cylinder, Journal of the Acoustical Society of America, 121 (2006) 1945-1955.
63. ABAQUS, http://www.3ds.com/products-services/simulia/products/abaqus/, last viewed 10/9/14.
64. A. Nayfeh, F. Pai, *Linear and Nonlinear Structural Mechanics*, John Wiley & Sons, Inc, (2004).
65. O. Zienkiewicz, R. Taylor, *The Finite Element Method*, Butterworth-Heinemann, (2000).
66. R. Cook, D. Malkus, *Concepts and Applications of Finite Element Analysis*, John Wiley & Sons, Inc, (2001).

67. J. Mu and J. Rose, Guided Wave Propagation and Mode Differentiation in Hollow Cylinders with Viscoelastic Coatings, Journal of the Acoustical Society of America, 124 (2008) 866-874.
68. Z. Sun, *Phased Array Focusing Wave Mechanics in Tubular Structures*, The Pennsylvania State University PhD Thesis, (2004).
69. R. Kirby, Z. Zlatev, P. Mudge, On The Scattering of Torsional Elastic Waves From Axisymmetric Defects in Coated Pipes, Journal of Sound and Vibration, 331 (2012) 3989 - 4004.
70. R. Kirby, Z. Zlatev, P. Mudge, On the Scattering of Longitudinal Elastic Waves From Axisymmetric Defects in Coated Pipes, Journal of Sound and Vibration, 332 (2013) 5040-5058.
71. C. Cobb, H. Kwun, L. Caseres, G. Janega, Torsional Guided Wave Attenuation in Piping From Coating, Temperature, and Large Area Corrosion, NDT & E International, 47 (2012) 163–170.
72. H. Kwun, S. Kim, G. Light, The Magnetostrictive Sensor Technology for Long Range Guided Wave Testing and Monitoring of Structures, Materials Evaluation, 61 (2003) 80–84.
73. R. E. Challis, G. P. Wilkinson, R J Freemantle, Errors and Uncertainties in the Ultrasonic Pulse Echo Reflectometry Method for Measuring Acoustic Impedance, Measurement Science and Technology, 4 (1998) 692.
74. J. Krautkramer, H. Krautkramer, *Ultrasonic Testing of Materials*, Springer-Verlag, (1990).
75. Bitustik 4000 Coating Material, https://grace.com/construction/en-gb/waterproofing/Bitustik-4000, last viewed 10/9/14.
76. R. Kazys, L. Mazeika, R. Raisutis, Prediction of Ultrasonic Waveforms in Highly Attenuating Plastic Materials, Ultragarsas, 3 (2002) 1392-2114.
77. V. Mangulis, Kramers-Kronig or Dispersion Relations in Acoustics, Journal of the Acoustical Society of America, 36 (1964) 211–212.
78. M. O`Donell, E. Jaynes, J. Miller, Kramers-Kroing Relationship Between Ultrasonic Attenuation and Phase Velocity, Journal of the Acoustical Society of America, 69 (1981) 696-701.

79. Tables of Acoustic Properties of Materials, http://www.ondacorp.com/tecref_acoustictable.shtml, last viewed 10/9/14.
80. J. L. Buchanan, Numerical Solution of the Dynamic Moduli of a Viscoelastic Bar, Journal of the Acoustical Society of America, 81 (1978) 1775-1786.
81. E.Ginzel, R.Ginzel, Ultrasonic Properties of a New Low Attenuation Dry Couplant Elastomer, NDTnet, 1 (1996) 2.
82. Acoustic Properties of Rubbers, http://www.ondacorp.com/images/Rubbers.pdf, last viewed 10/9/14.
83. J. Zhu, B. Birgisson, N. Kringos, Polymer Modification of Bitumen: Advances and Challenges, European Polymer Journal, 54 (2014) 18–3.
84. R. Blanc, Transient Wave Propagation Methods for Determining the Viscoelastic Properties of Solids, Journal of Applied Mechanics, 60 (1993) 763–768.
85. H. Waterman, Determination of the Complex Moduli of Viscoelastic Materials with the Ultrasonic Pulse Method (Part I,II), Kolloid-Zeitschrift und Zeitschrift für Polymere, 192 (1963) 1-8.
86. S. L. Garret, Resonant Acoustic Determination of Elastic Moduli, Journal of the Acoustical Society of America, 88 (1990) 210-221.
87. R. D. Adams, J Coppendale, Measurement of the Elastic Moduli of Structural Adhesives by Resonant Bar Technique, Journal of Mechanical Engineering Science, 18 (1976) 149-158.
88. B. G. Ferguson, Calculation of the Loss Tangent for Viscoelastic Materials Using the Triple Bar Composite Resonance Technique, Journal of the Acoustical Society of America, 76 (1984) 1577-1579.
89. Araldite 2011 Adhesive Data Sheet, http://www.go-araldite.com/, last viewed 10/9/14.
90. Polytec Scanning Vibrometers, http://www.polytec.com/us/products/vibration-sensors/scanning-vibrometers/, last viewed 10/9/14.
91. H. Kwun, Method of Detecting Tension Wire Break in Concrete Pole, United States Patent US 6,815,948 B1, (2004).
92. R. Ribichini, F. Cegla, P. Nagy,P. Cawley, Study and Comparison of Different EMAT Configurations for SH Wave Inspection, IEEE Transactions on Ultrasonics, Ferroelectrics, and Frequency Control, 58 (2011) 2571-2581.

93. R. Ribichini, *Modelling of Electromagnetic Acoustic Transducers*, PhD thesis, Imperial College of Science, Technology and Medicine, (2011).
94. F. Bertoncini, G. Giunta, M. Raugi, F. Turcu, Overview and Experimental Evaluation of Magnetostrictive Transducers for Guided Wave Inspection http://www.ndt.net/article/ndtnet/2012/1_Turcu.pdf, last viewed 10/9/14.
95. M. Bailoni1, Y. Wei, L. Norum, Mathematical Modelling and Simulation of Magnetostrictive Materials by Comsol Multiphysics, COMSOL Conference, Hannover (2008).
96. Y. Okawa, R. Murayama, Development of a Movable Inspection Sensor for a Pipe Using an Electromagnetic Acoustic Transducer of the Magnetostriction Effect Type, Japanese Journal of Applied Physics 48 (2009) 07GD07.
97. A. Vinogradov, Method and System for Generating and Receiving Torsional Guided Waves in a Structure, United States Patent US 7,821,258 B2,(2009).
98. Bituthene 4000 Coating Material, https://gcpat.com/construction/en-nz/waterproofing/Bituthene-4000, last viewed 10/9/14.

9. Appendix: Matlab Code

Section 3.2: Spectrogram of signals R1 and T3.

```
fs = 500e6;
yres = 10000;
xres = 300;
olp = round(xres*0.99);

[B1,f1,t1]= specgram(sig1,yres,fs,xres,olp);
power1 = abs(B1);

imagesc(t1, f1, power1);
set(gca,'YDir','normal')
axis([0e-6 3.5e-6 0e6 15e6]);
xlabel(['Time, us']);
ylabel(['Frequency, MHz']);
```

Section 3.3: Fourier transform of $U_{R1(\omega)}$ and $U_{T3(\omega)}$.

```
pk1padd = padarray(pk1, 1000);
pk2padd = padarray(pk2, 1000);

fs = 500e06;
L = size(pk1padd,1);
n = pow2(nextpow2(L));
f = (0:n-1)*(fs/n);

y1 = (fft(pk1padd,n))';
power1 = (y1.*conj(y1)/n)';

y2 = (fft(pk2padd,n))';
power2 = (y2.*conj(y2)/n)';
```

Section 3.9: Spectrogram of signals T_{15} and T_{20}

```
fs = 1e6;
yres = 1024;
xres = round(4000/centre frequency);
olp = round(xres*0.99);

[B1,f1,t1]= specgram(pk1,yres,fs,xres,olp);
power1 = abs(B1);
```

```
[B2,f2,t2]= specgram(pk2,yres,fs,xres,olp);
power2 = abs(B2);

clims = [ 0 1200 ];

subplot(1,2,1), imagesc(t1, f1, power1, clims);
set(gca,'YDir','normal')
axis([0 16e-5 0e6 0.15e6]);
xlabel(['Time, ms']);
ylabel(['Frequency, Hz']);

subplot(1,2,2), imagesc(t2, f2, power2,clims );
set(gca,'YDir','normal');
axis([0 16e-5 0e6 0.15e6]);
xlabel(['Time, ms']);
ylabel(['Frequency, Hz']);
```